Geological Survey of Finland
Water Management Solutions
Espoo

June 28, 2022

GTK/72/03.01/2017

Groundwater flow modelling for an assessment of climate change impacts on groundwater recharge at the Lahti aquifer, southern Finland

Samrit Luoma, Anu Eskelinen, Jaana Jarva, Jarkko Okkonen

RAiNMAN

GEOLOGICAL SURVEY OF FINLAND **DOCUMENTATION PAGE**

Date 31.03.2022 /GTK/72/03.01/2017

Authors
Samrit Luoma, Anu Eskelinen, Jaana Jarva, Jarkko Okkonen

Type of report
GTK Open File Work Report

Commission by
CBC RAINMAN -project and the city of Lahti

Title of report
Groundwater flow modelling for an assessment of climate change impacts on groundwater recharge at the Lahti aquifer, southern Finland

Abstract
Three-dimensional groundwater flow models of the shallow groundwater area in Lahti, southern Finland were developed by the Geological Survey of Finland (GTK) in cooperation with the city of Lahti under the RAINMAN-project to provide the hydrogeological information for the assessment of climate change impacts on groundwater recharge and groundwater resources. In this study, the geological conceptual model was constructed based on the geophysical and hydrologeological data to provide the geological framework for the groundwater flow model. The background reviews and trend analysis were performed for the hydrologic parameters during 1961-2021. The flow model was developed by using the unsaturated zone flow (UZF) coupled with the saturated zone flow MODFLOW-NWT, to simulate the flow from the ground surface through unsaturated zone to the aquifer. Lake infiltration and surface water - groundwater interactions were simulated by using the RIVER package, where the infiltration rate depends on the lakebed conductance and the head differences between lake stage and groundwater level. The UZF input data requires initial infiltration and potential evapotranspiration (PET) data. The snowmelt model was used to calculate the snowmelt and rainfall data based on the temperature and precipitation data with the calibration of the snow-water equivalent data. Initial infiltration was then estimated from the snowmelt and rainfall data and the infiltration capacity, which based on the spatial distributions of land use, runoff, soil type and vegetation. PET was calculated using a temperature-based method after Hamon (1963).

The flow models were performed in 3 phases. First, the steady-state model was made by using the mean climate data during 1961-2020 to provide the initial head for the transient flow model. Second, the daily time step transient flow model of climate data during 2000-2005 was made to evaluate the seasonal variability of groundwater by calibrating with the measured groundwater level during 2002-2004. The calibrated model was used to simulate the potential impacts of climate scenario in phase 3. Temperature and precipitation data from the high-emissions scenario RCP 8.5 from the SMHI for the period 2021-2100 were used for the simulation. The scenario data was performed for the bias correction and calibration with the historic data by using the Delta-change approach. In phase 3, the daily transient flow model was performed for both historic and scenario data from 1979-2100. To evaluate the impacts of climate change, the monthly mean 30-year of the simulation results during the periods 2021-2050 and 2071-2100 were compared with the current condition during the period 1981-2010. At current condition (1981-2010), the annual mean infiltration is 287.9 mm (42% of snowmelt and rainfall), the annual mean recharge is 188.9 mm (27.7 % of snowmelt and rainfall), the annual mean runoff is 312 mm (45.7% of snowmelt and rainfall), and the annual mean lake infiltration is 177.5 mm. The studied Lahti aquifer area is covered by the extensive urban area (51% of the total groundwater area). Impervious surface in the urban area causes the reduction of the infiltration from the snowmelt and rainfall and promote more the surface runoff. Moreover, thick unsaturated zone causes a longer lag time between the infiltration from the soil zone and the groundwater table and a reduction of the recharge. At current condition snowmelt reached the highest value in April, while the highest mean recharge is presented in August.

Under the scenario data, the annual mean temperature is predicted to increase 1.6 and 4.2 ^{o}C during 2021-2050 and 2071-2100, respectively. The highest increase in mean temperature is 6.1 ^{o}C in winter during 2071-2100. The annual mean precipitation is predicted to increase 10.4% and 30.9% during 2021-2050 and 2071-2100, respectively. While

the annual mean snowmelt and rainfall is predicted to increase 26.4% and 60.8% during 2021-2050 and 2071-2100, respectively. The highest increase in the snowmelt is found in winter during 2071-2100 due to the highest increase in temperature in this period. Annual mean infiltration of the scenario data increase 12.8% and 33.7% for the periods 2021-2050 and 2071-2100, respectively, compared with the current condition. The significant changes in infiltration patterns occur in winter and spring in both periods, where snowmelt and infiltration take place earlier in winter. The high infiltration during spring (April) in current condition does not exist in the scenario data. Annual mean recharge of the scenario data increase 10.8% and 30.1% for the periods 2021-2050 and 2071-2100, respectively. The recharge patterns show less seasonal variability over the scenario data. On the opposite, lake infiltrations show slightly decreases (less than 13%) from the current condition. With the recharge increase, groundwater level also increases and reduce the lake infiltration rate. Annual mean runoff shows the similar pattern as the snowmelt and rainfall. At current condition, the highest runoff occurs in spring (April) after the snow melted and the lowest runoff is in winter, where the ground is frozen. Annual mean runoff of the scenario data increase 67.4% and 153.5% for the periods 2021-2050 and 2071-2100, respectively. The most tremendous increase in runoff is found in winter during 2071-2100. The infiltration capacity of the aquifer is limited by the impervious surface in the urban area. With the increase in the snowmelt and rainfall in the scenario data, the large part of the excess water will contribute to the runoff. This could induce more the potential stormwater flood risk from the snowmelt.

At current condition (1981-2010) the inflow and outflow rates in the model domain vary between 32 860 – 37 460 m^3/d with the mean value of 34 357 m^3/d. The annual mean flow rates are predicted to increase 2.4% and 7.4% during 2021-2050 and 2071-2100, respectively. The recharge flux rates vary between 11 190 - 17 080 m^3/d with the mean value of 13 212 m^3/d. The lake infiltration flux rates, which mainly occur in the lakeshore nearby the water intake wells, vary between 12 300 – 12 620 m^3/d with the mean value of 12 432 m^3/d. The mean recharge increases 9.9% and 28.4%, while the mean lake infiltration decreases 4.4% and 12.4% during 2021-2050 and 2071-2100, respectively. The main outflow consists of pumping rate and stream discharge. The mean discharge rate at current condition is 2 330 – 2 380 m^3/d with the mean value of 2 352 m^3/d. The discharge rate is predicted to increase 10% and 27% from present during 2021-2050 and 2071-2100, respectively. The main total inflow is obtained from the recharge and the lake infiltration. At current and over the scenario conditions, the simulation results show that the amount of recharge alone (up to 19 000 m^3/d) is not sufficient to meet with the pumping rate of 24 410 m^3/d. The infiltration and recharge areas should be preserved and incorporated into the future land use planning. Additional investigations are needed for the hydraulic properties of the unsaturated zone flow and detailed groundwater and lake water interactions along the lake infiltration area.

Keywords
groundwater modeling, climate change impacts, groundwater recharge, unsaturated zone flow, lake infiltration

Geographical area	Map sheet
Lahti, Finland	L4422

Report serial	Archive code
GTK Open File Work Report	3/2022

Total pages	Language	Price	Confidentiality
71	English	-	Public

Unit	Project code
Water Management Solutions (VER)	50403–30120

Signature/name	Signature/name
Eeva Käpyaho, Head of the Unit	Samrit Luoma, Senior Scientist

Contents

Documentation page

1 INTRODUCTION

The location of Finland in the boreal climate zone causes four seasons: cold winter, cool spring, short summer, and wet autumn. The groundwater levels increase or decrease according to season changes (Mäkinen et al., 2016). In Finland, the aquifers are shallow and groundwater table is commonly 3 to 5 meters below the ground surface. This makes them sensitive to contamination as well as to climate change impacts (SYKE, 2022). The climate in Finland is characterized by seasonal variation, with snow accumulation in winter and snowmelt during spring. However, with warmer temperatures, there will be less snow accumulation during winter and earlier spring floods caused by snowmelt (Veijalainen et al., 2019). Warmer temperatures may shorten the time when the ground is frozen or even hinder freezing. Thus, groundwater recharge may also take place during winter months. During summer, evapotranspiration is generally higher than in winter and groundwater discharge decreases. The longer growth period due to an earlier spring and longer summer will cause even more evapotranspiration (Veijalainen et al., 2019). This will decrease groundwater recharge in the summer months.

The shallow groundwater in the Lahti area, our case study area, locates in the large surface water catchment area and is partly covered by the extensive urban area. Climate change and human activities have the impacts on the groundwater flow system, recharge, and groundwater resources (Cisneros et al., 2014). For the sustainable groundwater resources and development, land use planning and groundwater protection plans, a comprehensive understanding of the aquifer characteristics, recharge patterns, surface water and groundwater interactions, and groundwater flow system is needed. Climate change with the changes in temperature and precipitation is predicted to increase in this area (Klein & Luoma, 2020). This will have impacts on evapotranspiration, timing of snowmelt and groundwater recharge. The studies in the cold regions reported the significant impacts of climate change on seasonal variability of recharge, as it would occur earlier during winter and early spring (Luoma & Okkonen, 2014; Okkonen & Kløve, 2010; Jyrkama & Sykes, 2007), while small change in recharge is predicted during summer, compared with current condition. Luoma and Okkonen (2014) reported potential decrease in recharge of the shallow groundwater in southern Finland during summer in 2021-2050 and could face the risk of water shortage if the demand of water supply increase at the same time. Moreover, the urbanization could cause the reduction of recharge due to the increase of impervious surface (e.g., asphalt, concrete) from the built areas. The impervious surface could lead more surface runoff and with the high intensity of precipitation, the risk of urban stormwater flooding. The impacts of urbanization, e.g., underground septic or oil storage leakages could cause groundwater more vulnerable to the contaminations on the ground surface.

This study is part of the RAINMAN project (Towards higher adaptive capacity in urban water management) that was conducted under the thematic objective “Environmental protection, climate change mitigation and disasters prevention/management” of the South-East Finland – Russia CBC Programme 2014–2020. The RAINMAN project developed solutions to preserve freshwater resources in changing climatic conditions and enhanced the capacity of cities and municipalities to cope with climate change impacts such as changing recharge patterns of groundwater reservoirs located near built-up areas (Jarva & Klein, 2022). The South-East Finland – Russia CBC Programme 2014–2020 was implemented in the border regions between Finland and Russia under the European Neighbourhood Instrument (ENI). The Programme was funded by the European Union and the Republic of Finland. During the RAINMAN-project, the Geological Survey of Finland (GTK) in cooperation with the city of

Lahti have developed the geological and groundwater flow modeling of the shallow groundwater in the Lahti groundwater area. The models have been used for the assessment of climate change impacts on groundwater recharge and groundwater resources during 2021-2100. This knowledge provides valuable input in respect of the update of groundwater protection plans and water resources management in the future.

This study aimed to evaluate the sensitivity of the groundwater system responds to climate change by assessing the impacts of climate change variability on groundwater recharge, groundwater level, lake infiltration and groundwater discharge of the shallow glacial aquifer in the Lahti groundwater area by using groundwater flow modeling as an evaluation tool. During this study, the 1D unsaturated zone flow (UZF) model (Niswonger et al., 2006) was coupled with the 3D MODFLOW-NWT (Niswonger et al., 2011) for a fully integrated flow modeling of the infiltration from ground surface through unsaturated zone flow to the groundwater table where the groundwater recharge, evapotranspiration, and surface leakage were estimated. Snowmelt and potential evapotranspiration (PET) models were calculated to provide the infiltration data for the model. In the lake area, the interactions of lake and aquifer was assessed via the lakebed infiltration rate by using the RIVER (RIV) package. The groundwater simulation results based on future climate change scenario RCP 8.5 were then compared with the current climate conditions, to evaluate the potential change in groundwater resources in the future.

2 STUDY AREA

2.1 General setting

The study area locates in the Lahti groundwater area (#0439801) in the city of Lahti, southern Finland, at approximately 60° 58” N 25° 38” E and covers an area of 25.556 km^2 (Fig. 1). The shallow aquifer in the study area consists of the porous sands and gravels of the First Salpausselkä (SSI) ice-marginal formation and is bounded by the Lake Vesijärvi in the north and the clay layers in the south. The population in Lahti increased from 94 692 in 1981 to 120 093 in 2021 (Statistics Finland, 2022; City of Lahti, 2022). Land use mainly consists of forest (47%) and urban area (51%), which is the largest urban area that lies above the groundwater area in Finland. Topographic landform is characterized by the east-west oriented ice-marginal formation of the SSI with the prominence delta plateau landform (150-152 m a.s.l.), the sporadic hills and low-lying areas in the south and around the lake shore area (70-90 m a.s.l.) in the north.

The study area belongs to the temperate coniferous-mixed forest climate zone with cold, wet winters (Kottek et al., 2006). The monthly mean temperature and annual mean precipitation measured at the Laune weather station in the south of the study area during the 1991–2020 period was 4.7 ºC and 614 mm, respectively (Jokinen et al., 2021). The mean annual temperature increased 0.2 ºC, while the annual mean precipitation decreased 22 mm compared with the data during 1981-2010 (Pirinen et al. 2012). The lowest daily temperatures are generally recorded in January and February, and the highest during July and August. The lowest temperature was -35.2 ºC (1987) and the highest was 35.0 ºC (2010). While the lowest annual precipitation was 435 mm (1962) and the highest was 878 mm (1972).

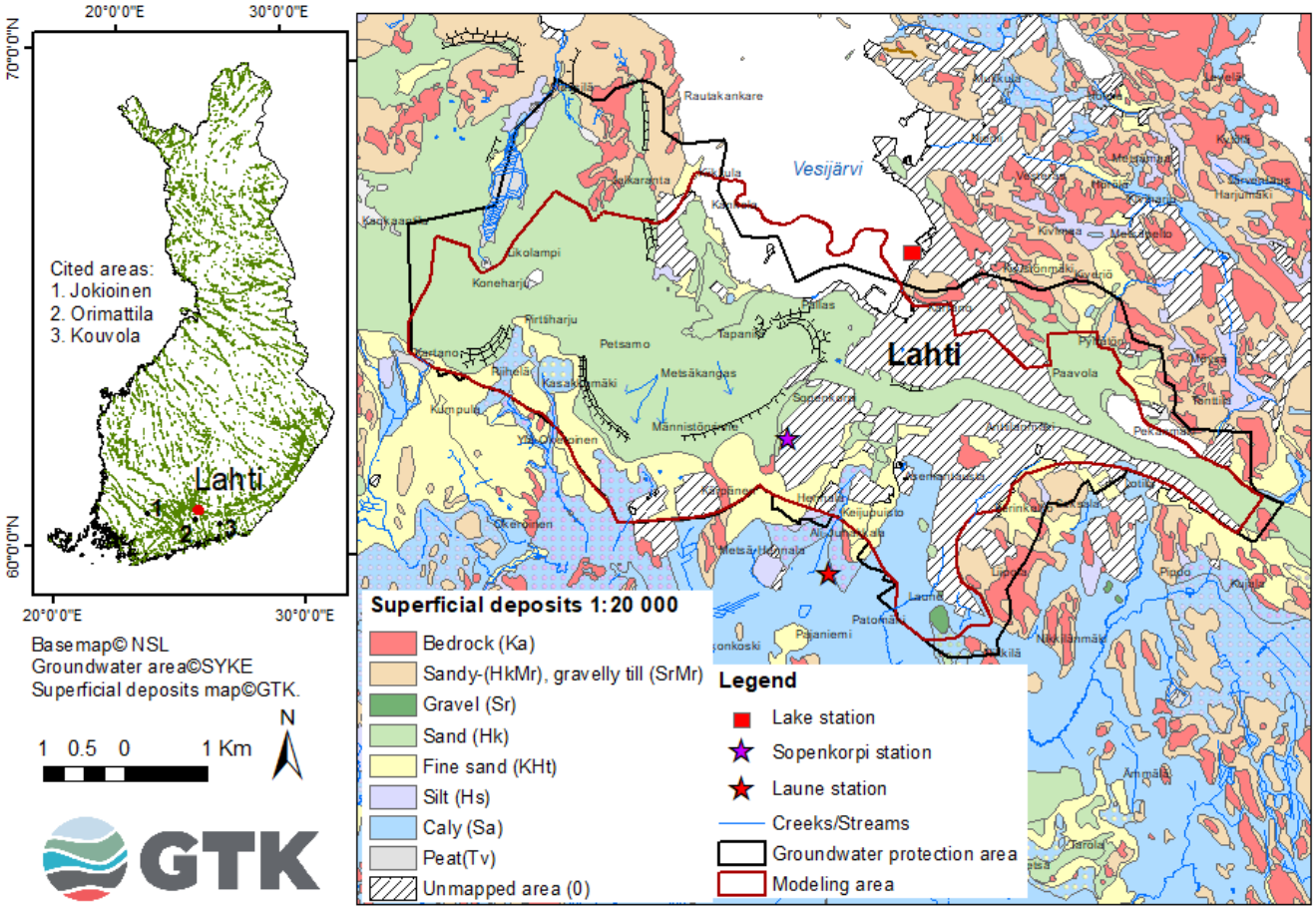

Fig. 1 Location and Quaternary geological deposit map of the study area.

2.2 Geology and hydrogeology

The shallow aquifer in the Lahti area is underlain by the basement of Precambrian crystalline bedrocks and covered by Late Pleistocene and Holocene glacial and post-glacial deposits. The Precambrian bedrock, which mainly consists of granite, quartz diorite and granodiorites, forms a sharp contact with the sedimentary cover, with some rock exposed in the area. The aquifer is accumulated in the First Salpausselkä ice-marginal formation (SSI, Fig. 1), which was formed during the last Weichselian and Holocene deglaciation of the Fennoscandian continental ice sheet (Fyfe, 1990). It was deposited over 217 years throughout the different stages of the Baltic Sea from the Baltic Ice Lake (12 250 – 12 050 BP) over the Yoldia Sea stage (11 590 – 10 800 BP) and the Ancylus Lake (10 800 – 9 000 BP) (Sauramo, 1923; Saarnisto & Saarinen, 2001). The ice-marginal formation consists of till, gravel, sand, and fine-grained sediments. When the ice sheet withdrew from the area, the SSI was successively covered by glaciolacustrine rhythmically alternating (varved) silt and clay, postglacial lacustrine poorly bedded clay, and brackish-water organic-rich mud (Virtasalo et al., 2007; 2014).

The shallow aquifer in the study area is unconfined and partly confined with the thickness up to 115 m and the average thickness of approximately 22 m. Groundwater levels vary spatially and temporally

between 70-119 m a.s.l. (average of 89 m a.s.l. and median of 84 m a.s.l.). The aquifer is characterized by the thick unsaturated zone, up to 50-75 m thick in the delta areas, while the other parts of the aquifer area the unsaturated zone thicknesses vary between 2- 20 m. Thick unsaturated zone causes less responds of groundwater recharge to the temporal variations of the precipitation due to the longer percolation times. In the shallow groundwater area, recharge occurs mainly twice a year during spring (late April-early May) and late autumn (November-early December) from the infiltration of snowmelt and rainfalls, respectively. Based on the stable isotope data and the monitoring data, Lake Vesijärvi recharge to the aquifer in various degrees depends on locations, seasons, and the abstraction rates. High lake infiltration (10-30%) takes place after snowmelt in spring or after heavy summer rain falls. However, the highest infiltration of lake water (up to 90%) takes place in the water intake areas nearby the lake shore.

3 MATERIALS

The geological and groundwater flow models of the shallow groundwater in the study area were constructed by using geological, geophysical, and hydrogeological data that were produced during this study and from the previous studies. Locations of data used for the interpretation are presented in Fig 2. Data produced during this study consists of 5 km of gravimetric survey acquired in August 2019; 56 km of shallow reflection seismic profiles from the Lake Vesijärvi area acquired in June 2018; two wells drilled to confirm the bedrock surface. Details of acquisition, processing and interpretation of gravimetric survey and seismic survey data are presented Valjus (2019) and Hämäläinen (2018), respectively. Intensive data sets from previous studies consist of the gravimetric survey, interpretation of the GPR profiles, drill logs, groundwater levels and background reports obtained from the Geological Survey of Finland (GTK-Lahde database, 2022) and courtesy of the city of Lahti; additional groundwater levels and information of observation boreholes were obtained from the Finnish Environment Institute (SYKE) - POVET database (SYKE, 2020); a LiDAR-based digital elevation model (LiDAR DEM) from the National Land Survey of Finland (NSL, 2021); CORINE land use map from SYKE; and the superficial map of the Quaternary deposits (scale 1:20 000) was obtained from GTK.

The historical weather data include daily precipitation (rainfall and snow), snow thickness and air surface temperatures (daily minimum, maximum, and mean values) during 1961-2021 was obtained from the Finnish Meteorological Institute (FMI) Laune weather station (FMI, 2021). The Laune weather station was located at the edge of the groundwater area. Since August 2018 it was preplaced by the Sopenkorpi weather station, which locates in the city center, 2 km north of the Laune station (Fig. 1). The overlapping data during August 2018-March 2019 from both stations shows insignificant discrepancy with the mean difference temperature of 0.1 ºC and precipitation of 0.083 mm.

The climate scenario data was obtained from the World Data Center for Climate (WDCC, 2017). The selected data was the SMHI-RCA4 regional climate model of the Swedish Meteorological Hydrological Institute (SMHI) with results for the IPCC RCP8.5 emission scenario. The Max Planck Institute for Meteorology Earth System Model provides boundary conditions for the RCA4 model (SMHI, 2017). The data consists of simulated temperature and precipitation during 1981-2100. The scenario data was performed the bias correction and calibration with the measured historical data during 1981-2010. The flow simulation was performed on the daily time step basis, but the assessment of climate change

impact was performed by comparing the monthly mean 30-year simulation results during 2021-2050 and 2071-2100 with the current data during 1981-2010.

The other hydraulic parameters such as lake level and snow-water equivalent were obtained from the SYKE water-database (SYKE, 2021). The daily levels of Lake Vesijärvi were recorded since 1909. The snow-water equivalent data obtained from the Orimattila weather station (18 km SW of Laune) was used for the calibration in the snowmelt model. Evaporation (Pan class A) data during summer 2006-2012 were obtained from the Jokioinen weather station (100 km west of Laune). In addition, the measured runoff data in the study area during 2009-2010 from Valtanen (2015) was used to support the interpretation.

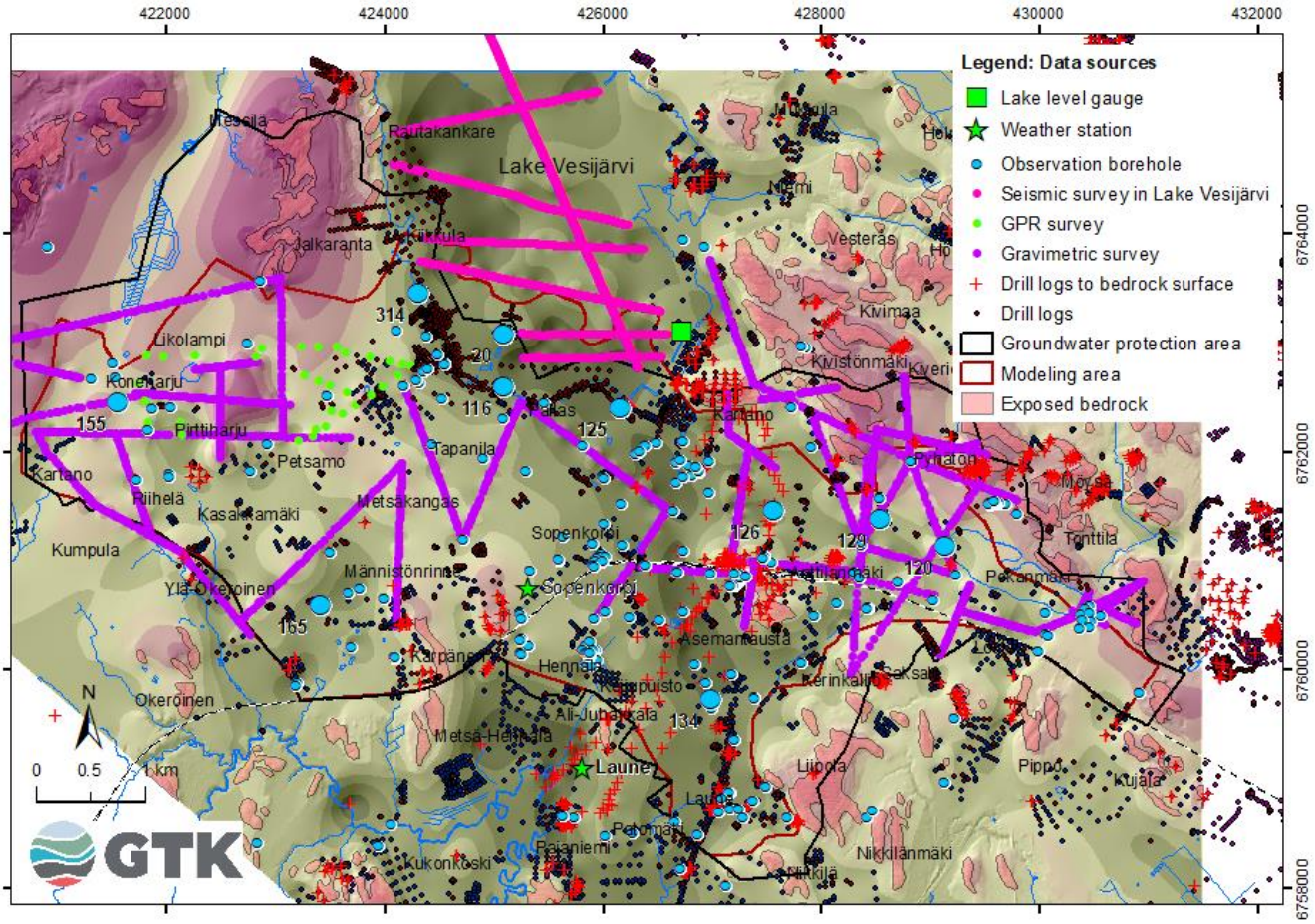

Fig. 2 Locations of data sources presented on the interpolated bedrock surface. Based map © the National Land Survey of Finland. Groundwater protection area © SYKE.

4 METHODOLOGY

In this section the reviews of the current hydrogeological conditions were first presented to provide general information of the study area and the data for the flow modeling. Groundwater flow modeling was then performed in three consecutive simulation processes. First the snowmelt and PET models

were performed to calculate the surface water available for infiltration from the temperature and precipitation input data used in the UZF package. Second, infiltration rate, flow in the unsaturated zone and groundwater recharge were simulated using 1D UZF package coupled with 3D MODFLOW-NWT code. The well calibrated groundwater flow model was then used to evaluate the impact of climate change on groundwater resources in the Lahti area in the final step. The simulated groundwater models under the climate change scenarios RCP 8.5 during the periods 2021-2050 and 2071-2100, were compared with the simulated model from the current data during 1981–2010, to assess the impact of climate change based on those climate scenarios on groundwater resources.

4.1 Analysis of hydrogeological data

4.1.1 Precipitation and temperature

Statistics summary of precipitation, surface air temperature, snow depth, snowmelt and rainfall from snowmelt model, PET and Lake Vesijärvi in the study area during 1961-2021 are presented in Table 1. Fig. 3 presents the annual distributions of precipitation, snowmelt and rainfall, PET, snow depth, temperature, and Lake Vesijärvi during 1961-2021. Detailed calculations of snowmelt and PET models are presented in the following sections.

Trend analysis was performed by using the non-parametric Mann-Kendall test for the trend and the Sen's method for the magnitude of the trend (change of variable per year) (Gilbert, 1987) by using the freeware MAKESENS version 1 from FMI (Salmi et al., 2002) for the annual data of the hydraulic variables such as temperature, precipitation, snow depth, snowmelt and rainfall and PET during 1961-2021. Results of the trend analysis are presented in Table 2. Over the past 60 years, the surface air temperature and PET showed significant increasing trends with the increasing rates of 0.04 ºC and 0.42 mm per year, respectively. While snow depth showed high decreasing trend with the rate of 37.76 cm per year. Precipitation and snowmelts and rainfall showed slightly decreasing trends, while the Lake Vesijärvi showed slightly increasing trend (1.5 mm/yr). However, the level of Lake Vesijärvi is controlled by human action (by adjusting the weir in Vääksy) and it is not fully caused by climate factors.

Table 1 Statistics summary of the climate variables in the Lahti groundwater area during 1961-2021.

Variable	Minimum	Mean	Maximum	Std.Dev.
Daily air temperature (ºC)	-34.4	4.46	35.00	9.69
Precipitation (mm/d)	0	1.72	63.70	3.72
Snow depth (cm/d)	0	10.39	86.00	17.23
Snowmelt and rainfall (mm/d)	0	1.84	66.89	4.19
PET (mm/d)	0.005	0.63	3.02	0.62
Lake Vesijärvi (m a.s.l.)	81.35	81.72	82.18	0.12

Table 2 Summary of trend analysis for the hydrologic variables during 1961-2021.

Variable	Mann-Kendall trend		Sen's slope estimate
	Normalized Test Statistic (Z)	Trend, level of significance	(Q), Change per year
Temperature (ºC)	5.00	Increasing, α = 0.001	0.0399
Precipitation (mm)	-0.80	No significant trend, α > 0.1	-0.6816
Snow depth (cm)	-2.87	Decreasing, α = 0.01	-37.7609
Snowmelt & rainfall (mm)	-0.13	No significant trend, α > 0.1	-0.1196
PET (mm)	4.36	Increasing, α = 0.001	0.4212
Lake Vesijärvi (m)	3.07	Increasing, α = 0.01	0.0015

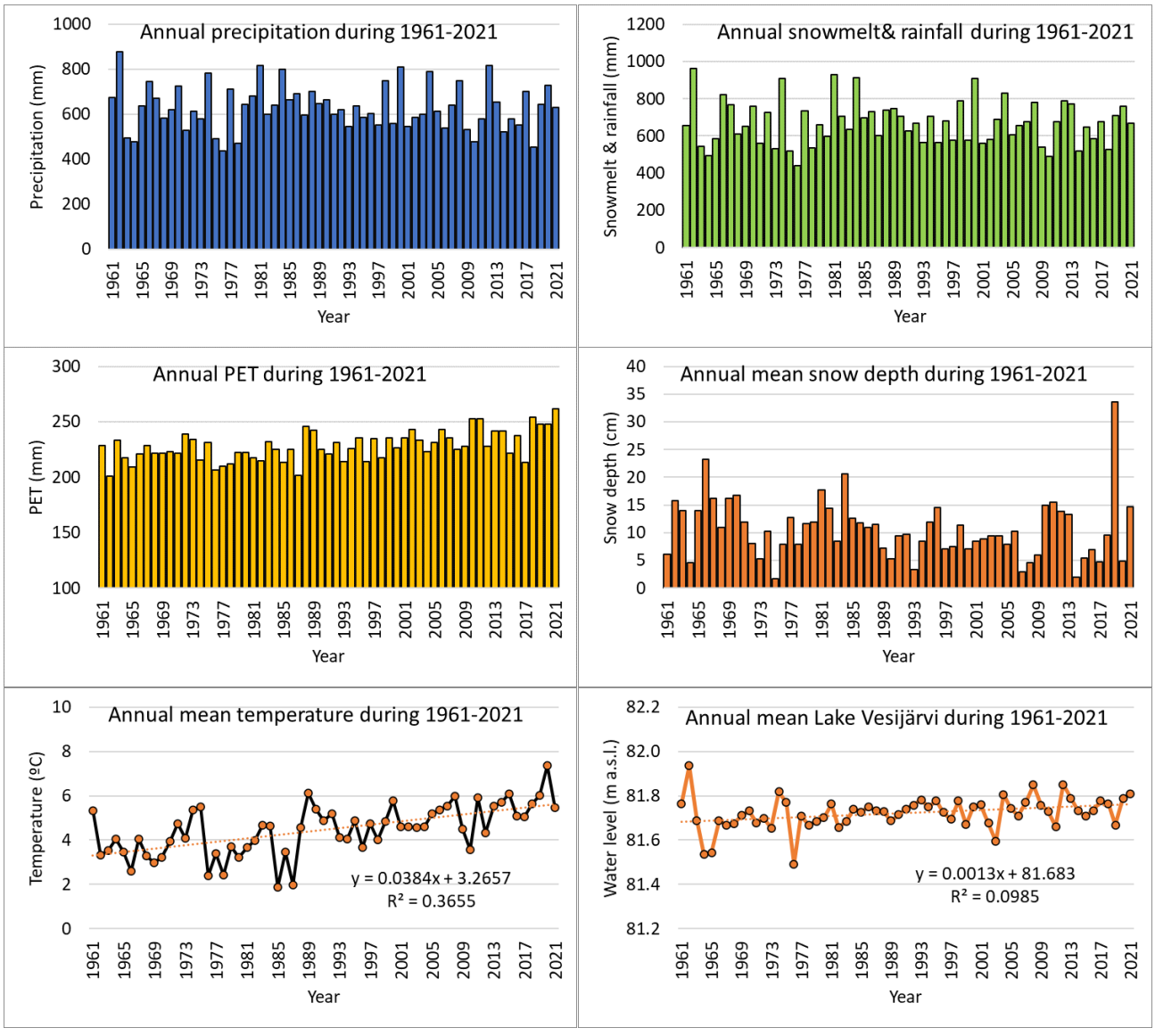

Fig. 3 Annual distributions of precipitation, snowmelt and rainfall, PET, snow depth, temperature, and Lake Vesijärvi during 1961-2021.

4.1.2 Snowmelt model

The water available for infiltration in the UZF model was estimated from the snowmelt model based on two input parameters: daily precipitation and air surface temperature. The measured snow-water equivalent was used as a calibration target. The precipitation was portioned in form of rainfall and snowfall as follows (Vehviläinen, 1992):

$$\text{Snowfall} = C_s F_s P_{tot} \quad (1)$$
$$\text{Rainfall} = C_r F_r P_{tot} \quad (2)$$

Where P_{tot} is the observed precipitation, C_s is a correction-coefficient for snowfall and C_r is the correction coefficient for rainfall. F_r and F_s are fraction of rainfall and snowfall, respectively. F_r and F_s were estimated as follows (Vehviläinen, 1992):

$$F_r = \begin{cases} 0 & if \quad T < T_{\min} \\ \dfrac{T - T_{\min}}{T_{\max} - T_{\min}} & if \quad T_{\min} \le T \le T_{\max} \\ 1 & if \quad T > T_{\max} \end{cases} \quad (3)$$

$$F_s = 1 - F_r \quad (4)$$

The degree day model, that considers freezing of the snowpack, was used to calculate daily snowmelt M_d (Kuusisto, 1984; Vehviläinen, 1992):

$$M_d = \begin{cases} K_m \ (T_a - T_m) & \text{if } T_a > T_m \\ 0 & otherwise \end{cases} \quad (5)$$

$$F_d = \begin{cases} K_f (T_f - T_a)^e & if \ T_a > T_f \\ 0 & otherwise \end{cases} \quad (6)$$

where M_d is the daily snowmelt depth and K_m is the degree day factor. T_a is the daily air temperature and T_m is the temperature at which the snow begins melt. F_d is the rate of freezing in the snowpack, and K_f is the degree day freezing factor, T_f is the threshold temperature for freezing, and *e* is the coefficient indicating the non-linear relationship between refreezing and temperature (Bengtsson, 1982). The liquid water retention capacity of snowpack (WSP) is related to liquid water of ice in the snowpack (WIP) as follows (Vehviläinen, 1992):

$$WSP_{max} = R * WIP \quad (7)$$

where *R* is a retention parameter. Mass balance of the snowpack was calculated as follows:

$$dWSP/dt = P_r + M_d + F_d, \quad WSP \le WSP_{max} \quad (8)$$
$$dWIP/dt = P_s - M_d + F_d \quad (9)$$
$$SWE = WSP + WIP \quad (10)$$

where SWE is the snow water equivalent.

In this study, the snowmelt model was performed in the Microsoft Excel program (Kokkonen et al., 2006). Due to the lack measured snow water equivalent data at the Laune weather station, the snow-water equivalent data were obtained from the Keituri, Orimattila weather station, approximately 18 km SW of the Laune station. The temperature and precipitation data from the Laune station were used to calculate the snow-water equivalent, which was calibrated with the snow-water equivalent data from Keituri station in Orimattila during the period 2013-2020 (Fig. 4) and then was validated during the period 1980-2008 (Fig. 5). The input parameters for the snowmelt model are shown in Table 3. To reduce the calibration parameters, the threshold temperatures T_{min}, $T_{m,}$ T_f and the exponent *e* were set to constant. The calibration parameters were T_{max}, C_s, C_r, K_m, K_f, and R and they were constrained between values found in the literature (e.g., Kuusisto, 1984; Vehviläinen, 1992; Okkonen & Klöve, 2010). The model performance is also evaluated in terms of the Nash – Sutcliffe (1970) efficiency coefficient (*NSE*):

$$NSE = 1 - \frac{\sum_{i=1}^{n}(y_{\text{obs}} - y_{\text{sim}})^2}{\sum_{i=1}^{n}(y_{\text{obs}} - y_{\text{mean obs}})^2} \quad (11)$$

where y_{obs} is the observed SWE value, y_{sim} is the simulated SWE value, $y_{\text{mean obs}}$ is the mean observed SWE value, and *n* is the number of observations. The maximum value of *NSE* is 1 indicating a perfect match between observed and simulated values. The *NSE* value close to 1 indicates a model with more predictive skill, while the negative *NSE* value indicates the observed mean is a better predictor than the model.

In this study, the *NSE* values of the calibration period 2013-2020 and the validation period 1980-2008 were -1.39 and 0.78, respectively. The calibrated parameters were used for the calculation of snowmelt and rainfall data without any further calibration. The input data consists of daily temperature and precipitation during 1961-2020 from the Laune station for the historical data, and during 2021-2100 for the scenario data. Snowmelt and rainfall data obtained from the snowmelt model represents the available water on the ground surface. The spatial distribution of water to be used as an initial infiltration rate (UZF FINF) for UZF and MODFLOW-NWT, will depends on the infiltration capacity of the aquifer area, which varies spatially depending on surface runoff, land use, soil type, and vegetation.

Table. 3 Parameters obtained from calibration of the snowmelt model.

Parameter	Calibrated value
*T*min Snowfall base temperature (°C)	0.064
*T*max Rainfall base temperature (°C)	1.500
Cs Snowfall correction coefficient	1.105
Cr Rainfall correction coefficient	1.050
Kd Degree-day factor (mm/°C per day)	2.384
*T*melt Snowmelt base temperature (°C)	0.064
R Liquid water retention capacity	0.043
Kf Refreezing coefficient (mm/°C per day)	0.050
Tf Refreezing base temperature (°C)	-3.508
e Exponent	0.015

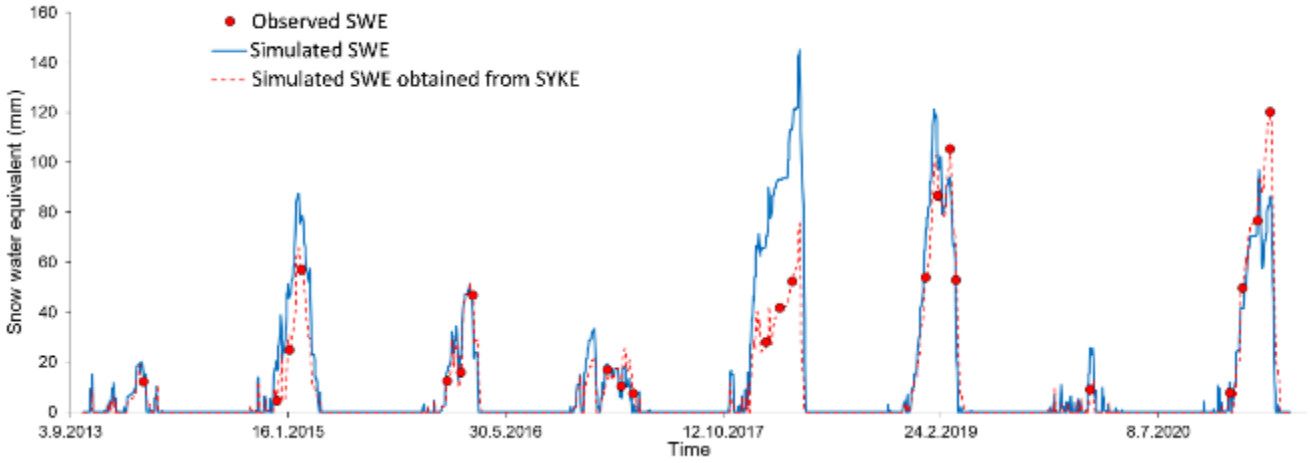

Fig. 4 Comparison between measured and simulated snow water equivalent (SWE) during the calibration period 2013-2020.

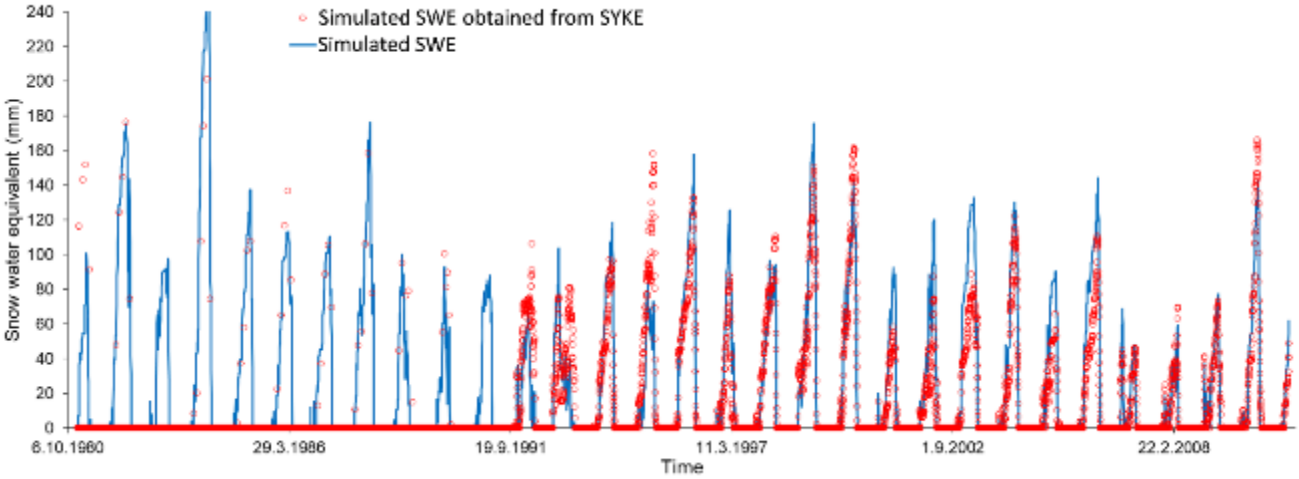

Fig. 5 Comparison between measured and simulated snow water equivalent (SWE) during the validation period 1980-2008.

4.1.3 Evaporation and potential evapotranspiration

Evaporation and evapotranspiration are the climate variables that related directly to temperature and have impacts on the water budget. Evaporation is a transformation of liquid water to water vapor by heat waves, while evapotranspiration (ET) is the combined process of water surface evaporation, soil moisture evaporation, and plant transpiration (Erickson et al., 2013). Increase in evaporation will decrease surface water level (lake, pond) and increase in evapotranspiration will cause the reduction of the soil water content. These parameters could be crucial and are needed for the recharge estimation and stormwater management assessment.

In Finland, generally evaporation from land areas was approximately 40−80 mm and from the larger lakes 80−120 mm. The monthly evaporations measured with a Class-A pan during June 2006-August 2012 at the Jokioinen station vary between 33 and 189 mm. The evaporation sums were approximately 0.8-3.6 times (average of 2.2 times) higher than the sums of rainfalls at the same periods and have a positive correlation with temperature as presented in Fig. 6. Mechanisms and impacts of evaporation and evapotranspiration in the built- and urban areas on hydrogeology and groundwater recharge is still poorly understood. Suomi (2018) monitored the spatial temperature in 8 sites around the city of Lahti. The results of 2 years monitoring indicated a significant increase in temperature during the summer in the city center due to the impacts of urban heating. Evapotranspiration is lower in urban areas due to large coverage of the impervious surfaces and less plants or vegetation. The availability of water for evaporation is also lower in urban areas due to the surface runoff and rainwater is gauged away by sewers (Suomi & Käyhkö, 2012). However, the evaporation rate is expected to be high for the remained water on the urban impervious- and pervious hardened surfaces due to the urban heating. This will reduce the availability of water for the infiltration and consequently the recharge.

For recharge estimation in this study, the potential evapotranspiration (PET) is applied as an input for the UZF model. PET represents the amount of evapotranspiration that is expected over a surface with no limitation of water. In this study PET was predicted after Hamon (1963), which is a temperature-based method and mean daily temperature (T_a) and day length (D) are needed as input parameters.

$$PET = 29.8 * D * \frac{e_a}{T_a+273.2} \quad (12)$$

where e_a is saturation vapor pressure (kPa) at mean daily temperature:

$$e_a = 0.6108 \exp [17.27*T/(T+237.3)] \quad (13)$$

The day length data represented by the duration of sunshine (hour/day) at the Laune weather station is available for only 12 years during 1999-2010 and it may not represent the long-term climate simulation. The data, however, similar with the nearby weather stations: the Ilmala in Jokioinen and the Utti airport in Kouvola. Fig. 7 presents the mean duration of sunshine (hour/day) for each month during 1981-2020 (FMI, 2022) from those stations compared with the data from Laune station in Lahti (1999-2010). The mean duration of sunshine (hour/day) data from Jokioinen was used as an input for the PET model.

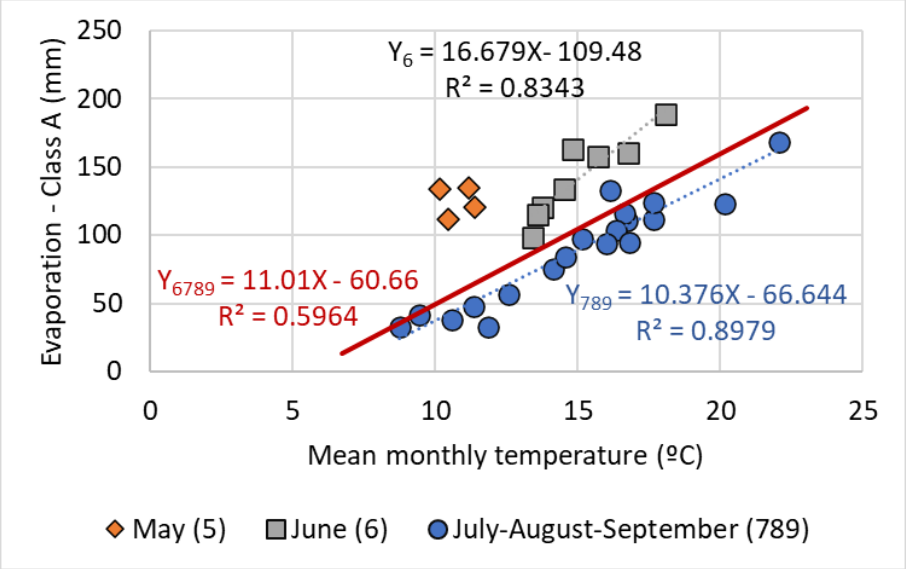

Fig. 6 Correlations between monthly measured evaporation and temperature during June 2006-August 2012 at the Jokioinen station.

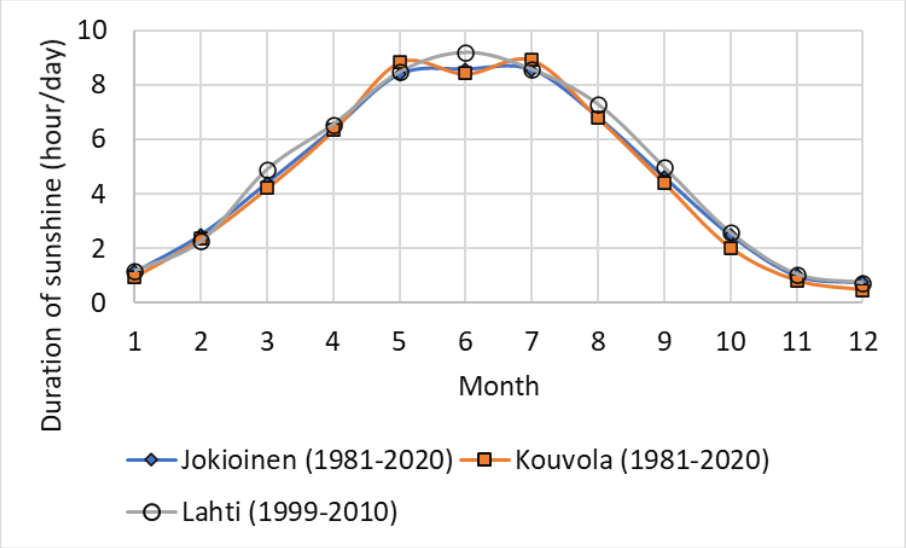

Fig. 7 Mean duration of sunshine (hour/day) for each month during 1981-2020 from the weather stations in the Ilmala, Jokioinen and the Utti airport, Kouvola compared with the Laune station in Lahti (1999-2010).

4.1.4 Lake Vesijärvi

During 1961-2020 the levels of Lake Vesijärvi vary between 81.35-82.18 m a.s.l. with an average of 81.72 m a.s.l. (Fig. 8). Based on the monthly monitoring groundwater levels of the observation boreholes nearby the lakeshore during 2002-2004, the average level of the Lake Vesijärvi is higher than the groundwater levels at approximately 1.91 m at the Jalkaranta (HP314), 2.12 m at the Myllysaari (HP20), and 1.61 m at the Pallas area (HP125). Lake level shows positive correlation with the groundwater levels in the different degree, e.g., in normal condition, lag time between the lake and

the groundwater level is approximately 1 month. The lag time becomes shorter during flooding and high lake levels, e.g., during the summer flood in August 2004, the lag time was only approximately 3-5 days. During that time the cumulative rainfall was 131.6 mm within a 6-consecutive-day. This caused the Lake Vesijärvi rose 0.24 m (82.09 m a.s.l.) and groundwater levels rose 1.05-1.37 m (Fig. 9).

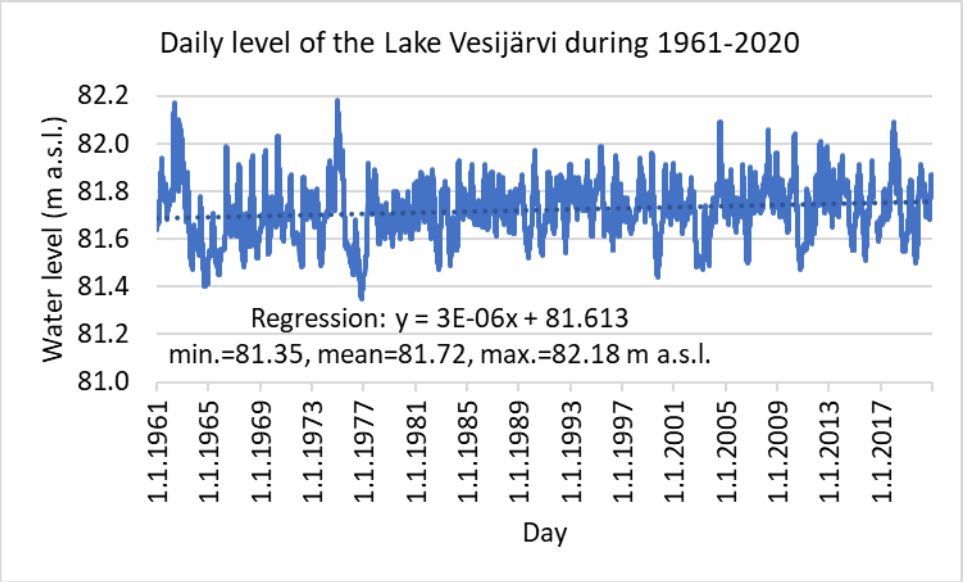

Fig. 8 Daily level and linear regression line of the Lake Vesijärvi during 1961-2020.

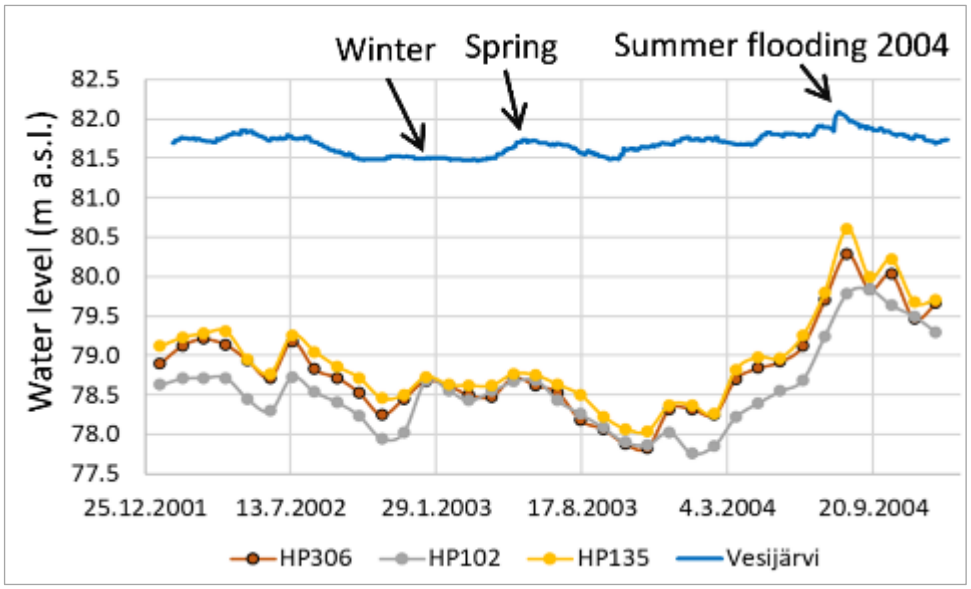

Fig. 9 Monitoring of the Lake Vesijärvi (daily) and groundwater levels (monthly) of the observation boreholes along the lakeshore in the Jalkaranta area during 2002-2004.

4.1.5 Land use

The Lahti groundwater area is characterized by large urban area, which has been extended covered large part of the groundwater recharge area. Based on the CORINE (2018) - land use map, the study area consists of 51% urban and built areas, 38.5% forest and green areas and 2.8% arable land, which is in the discharge area (Fig. 10). Impervious surface materials in the urban area induce more surface runoff and prevent the infiltration of the precipitation cause a reduction of groundwater recharge, e.g., in the commercial areas where the constructions and roads are covered by the concrete or asphalt with impervious of 89%. During the summer with increasing of temperature, the evaporation of the water that remains on the ground will also increase and once the evaporation rate exceeds the precipitation rate, there will be no infiltration into the aquifer.

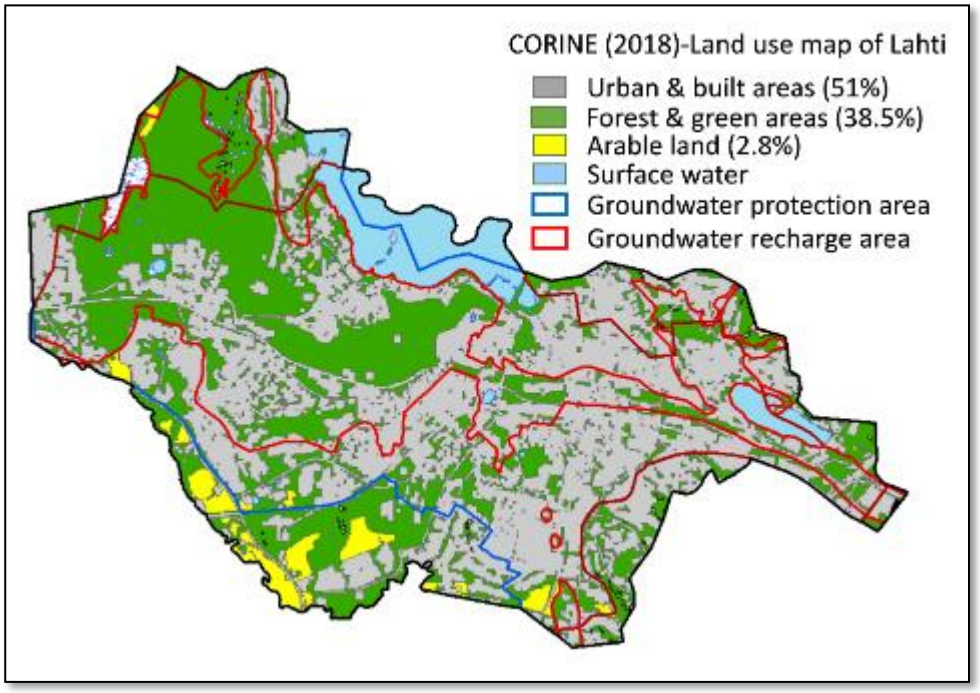

Fig. 10 Land use map of the city of Lahti.

4.1.6 Surface runoff

Runoff take places when snowmelt and rainfall intensity exceed the infiltration capacity of the soil and the degree of slope of the land surface. At the same amount of water available at the surface, the area contains high impervious soil or surface material with high slope, induces more surface runoff. The American Society of Civil Engineers (1970) classified the degree of slope in to three classes: “flat” areas having slope < 2%, “average” with 2–7% and “steep” areas with >7% of slope. Nuottimäki and Jarva (2015) applied four slope classes: <3%, 3–5%, 5–8% and >8% for the qualitative evaluation of the urban flood prone area in Vantaa. Based on the LiDAR-DEM (2m x 2m) data, the slope in the study area vary between 0-71% with 35% of the area contains slope greater than 5% (Fig. 11).

51% of total land use in the study area belongs to urban area that the many parts of the areas are covered by the high impervious surface materials. Valtanen (2015) monitored a two-year (2009-2010) surface runoff in three urban areas in the city of Lahti, that comprised three different impervious materials: High impervious catchment (city center, the built materials of 89% impervious surface, e.g., asphalt, concrete), Intermediate catchment (city center, 62%) and Low catchment (residential, 19%). The surface runoff in urban areas vary between 48-68% of the total precipitations (Table 4). The first study year was characterized by a warm and dry winter and a wet summer, while during the second study year, winter was wet and the summer dry (Valtanen, 2015). The correlation of the runoff data and the snowmelt and rainfall data from snowmelt model calculated from precipitation and temperature at the same period is presented in Fig. 12. Two trends of the runoff were observed in the Low catchment area: 1) high runoff during summer rainfall, which shows similar trend with the other areas, and 2) lower runoff during spring snowmelt.

In this study, no detailed study of surface runoff was performed. Instead, the runoff was estimated from a simple water balance equation as follow:

$$\text{Precipitation} = \text{Recharge} - \text{Evapotranspiration} - \text{Runoff} \quad (14)$$

In this study the daily snowmelt and rainfall, initial infiltration and PET data were used for the calculation as follow:

$$\text{Runoff} = \text{Snowmelt and rainfall} - \text{Infiltration} - \text{PET} \quad (15)$$

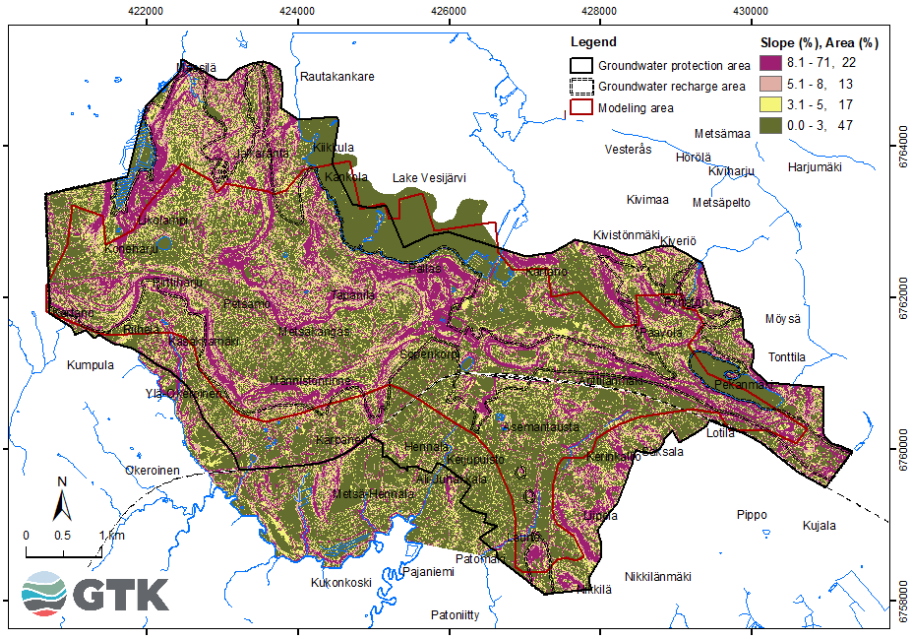

Fig. 11 Slope (%) distribution in the Lahti groundwater area.

Table 4 Surface runoff in three urban areas in the city of Lahti during 2009-2010. Modified from Valtanen (2015).

Impervious area	Runoff during 2009 (%)		Runoff during 2010 (%)	
	June-Nov	Dec-May	June-Nov	Dec-May
High, 89%	68.0	53.0	60.0	33.0
Intermediate, 62%	48.0	48.0	50.0	51.0
Low, 19%	12.0	55.0	8.0	66.0

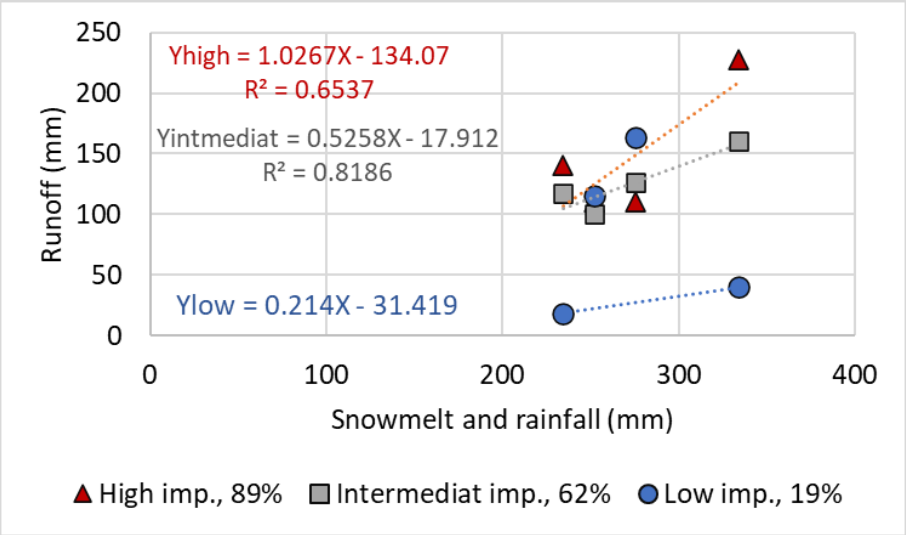

Fig. 12 Correlations between surface runoff and snowmelt and rainfall data during 2009-2010 in three urban areas in the city of Lahti, based on the surface runoff data from Valtanen (2015) and the snowmelt model of precipitation and temperature at the same period.

4.2 Climate change scenario data

The high emission scenario RCP 8.5 of SMHI (SMHI, 2017) was selected for the detailed analysis. The bias-and delta-change corrected version of temperature and precipitation during 2021-2100 were used as the input for the snowmelt and PET models for the flow simulations of the scenarios data. Details of bias correction of the scenario data is presented in Klein & Luoma (2020). Monthly means and changes in temperature, precipitation, snowmelt and rainfall, and PET in Lahti for the period 1981-2010 compared with the scenario data during 2021-2100 are presented in Fig 13. The percentage change was calculated by computing the difference between the scenario and the current values (1981-2010) and compared that difference to the initial value (the value from the current condition) to see much the initial value has changed. The changes of scenario data for the period 2041-2070 are close to the period 2021-2050, therefore, only the simulation results of the scenarios data from the periods 2021-2050 and 2071-2100 were compared with the historic data 1981-2010.

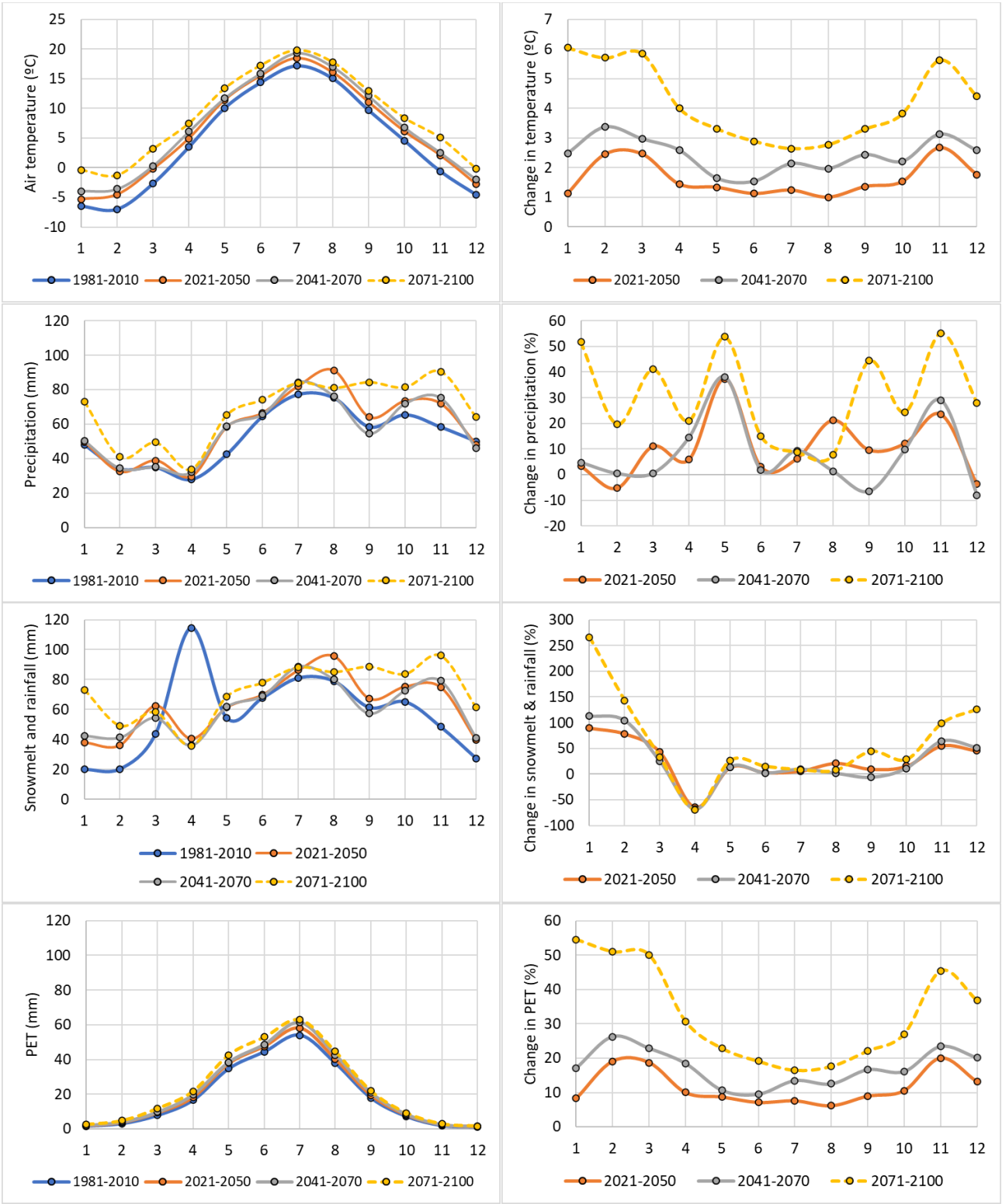

Fig. 13 Monthly means and the differences of temperature, precipitation, snowmelt, and rainfall (from snowmelt model) and PET in Lahti for the period 1981-2010 compared with the scenario data SMHI-RCA4, RCP 8.5 during 2021-2100.

Table 5 Temperature and change in temperature.

Month	Temperature (ºC)				Change in temperature (ºC)		
	FMI	SMHI			SMHI		
	1981-2010	2021-2050	2041-2070	2071-2100	2021-2050	2041-2070	2071-2100
1	-6.4	-5.3	-3.9	-0.4	1.1	2.5	6.1
2	-7.0	-4.5	-3.6	-1.3	2.5	3.4	5.7
3	-2.7	-0.2	0.3	3.2	2.5	3.0	5.9
4	3.5	4.9	6.1	7.5	1.4	2.6	4.0
5	10.1	11.4	11.7	13.4	1.3	1.6	3.3
6	14.4	15.5	15.9	17.3	1.1	1.5	2.9
7	17.2	18.4	19.3	19.8	1.2	2.1	2.6
8	15.1	16.1	17.0	17.8	1.0	2.0	2.8
9	9.7	11.1	12.2	13.0	1.4	2.4	3.3
10	4.6	6.1	6.8	8.4	1.5	2.2	3.8
11	-0.6	2.1	2.6	5.0	2.7	3.1	5.6
12	-4.5	-2.8	-2.0	-0.1	1.8	2.6	4.4
Min.	-7.0	-5.3	-3.9	-1.3	1.0	1.5	2.6
Mean	4.4	6.1	6.9	8.6	1.6	2.4	4.2
Max.	17.2	18.4	19.3	19.8	2.7	3.4	6.1

Table 6 Precipitation and change in precipitation.

Month	Precipitation (mm)				Change in precipitation (%)		
	FMI	SMHI			SMHI		
	1981-2010	2021-2050	2041-2070	2071-2100	2021-2050	2041-2070	2071-2100
1	48.2	49.8	50.5	73.1	3.4	4.8	51.7
2	34.3	32.5	34.4	41.0	-5.2	0.5	19.7
3	35.1	39.0	35.3	49.5	11.1	0.5	41.0
4	28.1	29.7	32.1	34.0	5.9	14.4	21.0
5	42.6	58.5	58.9	65.5	37.4	38.2	53.7
6	64.5	66.6	65.7	74.2	3.2	1.9	15.0
7	77.2	82.1	84.4	84.0	6.3	9.3	8.8
8	75.3	91.3	76.3	81.1	21.3	1.4	7.7
9	58.4	64.1	54.6	84.4	9.7	-6.5	44.4
10	65.5	73.5	71.9	81.4	12.2	9.8	24.3
11	58.4	72.1	75.3	90.6	23.5	29.0	55.3
12	50.1	48.3	46.1	64.2	-3.7	-7.9	28.1
Min.	28.1	29.7	32.1	34.0	-5.2	-7.9	7.7
Mean	53.1	58.9	57.1	68.6	10.4	7.9	30.9
Max.	77.2	91.3	84.4	90.6	37.4	38.2	55.3
Sum	637.5	707.4	685.5	822.8			

Table 7 Snowmelt and rainfall and change in snowmelt and rainfall.

Month	Snowmelt & rainfall (mm)				Change in snowmelt & rainfall (%)		
	FMI	SMHI			SMHI		
	1981-2010	2021-2050	2041-2070	2071-2100	2021-2050	2041-2070	2071-2100
1	20.0	37.9	42.5	73.1	89.8	112.7	266.0
2	20.2	36.2	41.3	49.2	78.7	103.9	143.0
3	43.6	62.5	54.5	58.2	43.4	24.9	33.5
4	114.7	40.4	36.1	35.7	-64.7	-68.5	-68.9
5	54.2	61.5	61.8	68.8	13.3	14.0	26.8
6	67.7	69.9	69.0	77.9	3.2	1.9	15.0
7	81.1	86.2	88.6	88.2	6.3	9.3	8.8
8	79.0	95.8	80.1	85.1	21.3	1.4	7.7
9	61.4	67.3	57.3	88.6	9.7	-6.5	44.4
10	65.1	75.3	72.5	83.7	15.6	11.3	28.5
11	48.4	75.0	79.2	96.1	55.1	63.8	98.6
12	27.2	39.6	41.2	61.5	45.6	51.4	125.8
Min.	20.0	36.2	36.1	35.7	-64.7	-68.5	-68.9
Mean	56.9	62.3	60.4	72.2	26.4	26.6	60.8
Max.	114.7	95.8	88.6	96.1	89.8	112.7	266.0
Sum	682.7	747.8	724.2	866.1			

Table 8 PET and change in PET.

Month	PET (mm)				Change in PET (%)		
	FMI	SMHI			SMHI		
	1981-2010	2021-2050	2041-2070	2071-2100	2021-2050	2041-2070	2071-2100
1	1.7	1.8	2.0	2.6	8.3	17.1	54.6
2	3.2	3.8	4.0	4.8	19.1	26.3	51.0
3	7.9	9.4	9.7	11.9	18.7	22.9	50.1
4	16.7	18.3	19.7	21.8	10.0	18.5	30.8
5	34.7	37.8	38.4	42.7	8.7	10.7	22.9
6	44.4	47.6	48.7	52.9	7.2	9.5	19.1
7	54.0	58.2	61.3	63.0	7.6	13.5	16.5
8	37.9	40.3	42.7	44.6	6.2	12.5	17.6
9	17.9	19.5	20.9	21.9	9.0	16.7	22.2
10	7.3	8.0	8.4	9.2	10.6	16.1	27.1
11	2.0	2.5	2.5	3.0	20.0	23.4	45.5
12	1.2	1.4	1.5	1.7	13.2	20.1	36.9
Min.	1.2	1.4	1.5	1.7	6.2	9.5	16.5
Mean	19.1	20.7	21.7	23.3	11.5	17.3	32.9
Max.	54.0	58.2	61.3	63.0	20.0	26.3	54.6
Sum	229.0	248.5	259.9	280.0			

4.3 Geological and conceptual models

4.3.1 Geological model

Geological and hydrogeological of the aquifer were identified to provide the geological framework for the groundwater flow model. The geological model of the Late Pleistocene and Holocene deposits of the shallow groundwater area in Lahti was constructed under the Geographic Information System (GIS) platform by using ArcGIS/ArcMap version 10.6.1 for 2D spatial analysis and the stratigraphic module in the Groundwater Modeling Software (GMS) version 10.4 for 3D interpretation and visualization. The Late Pleistocene and Holocene deposits sharply overlie the crystalline Precambrian bedrock. In this study, the bedrock surface topography was identified throughout the study area as shown in Fig. 14. The bedrock surface topography varies between -34 and 180 m a.s.l. with the average elevation of 85 m a.s.l. High elevations of the bedrock topography are in the east, the west and the north-west, where the bedrock surface is sporadically exposed. Low elevations of the bedrock topography lie in the middle of the study area in the NNW-SSE direction across the SSI from the Lake Vesijärvi in the north to the Renkomäki groundwater area in the south. The thickness of the Pleistocene and Holocene deposits, obtained from the subtraction between LiDAR-DEM and bedrock surface topography, varies between less than 1 m to 115 m with an average of 22 m. The thickest sedimentary cover is found in the E-W trending following the SSI area, and in the NNW-SSE direction in the bedrock depression areas. Thickness of the coarse-grained sediments (sand, gravel, and coarse-grained till) is presented in Fig. 15. The aquifer is characterized by a very thick unsaturated zone. Based on the mean groundwater levels during 2002-2004 the unsaturated zone thickness varies between 0-75 m (Fig. 16) and the saturated zone thickness varies approximately between 0-60 m (Fig. 17). Very thick saturated zones (60-120 m) of the fine-grained sediments locate in the Lake Vesijärvi, east of Rautakankare and in the Metsä-Hennala, south of the study area also presented in Fig 17.

In the Lake Vesijärvi area, the aquifer is extended approximately 300-900 m into the Lake Vesijärvi, with the thicknesses vary between 0-60 m. The porous aquifer media was draped and bounded by thick glaciolacustrine rhythmite (silt and clay layers) and post-glacial lacustrine clay and mud. The thicknesses of fine-grained layer at the modeling also vary between 0-60 m, where it is thin of absent at the lakeshore area.

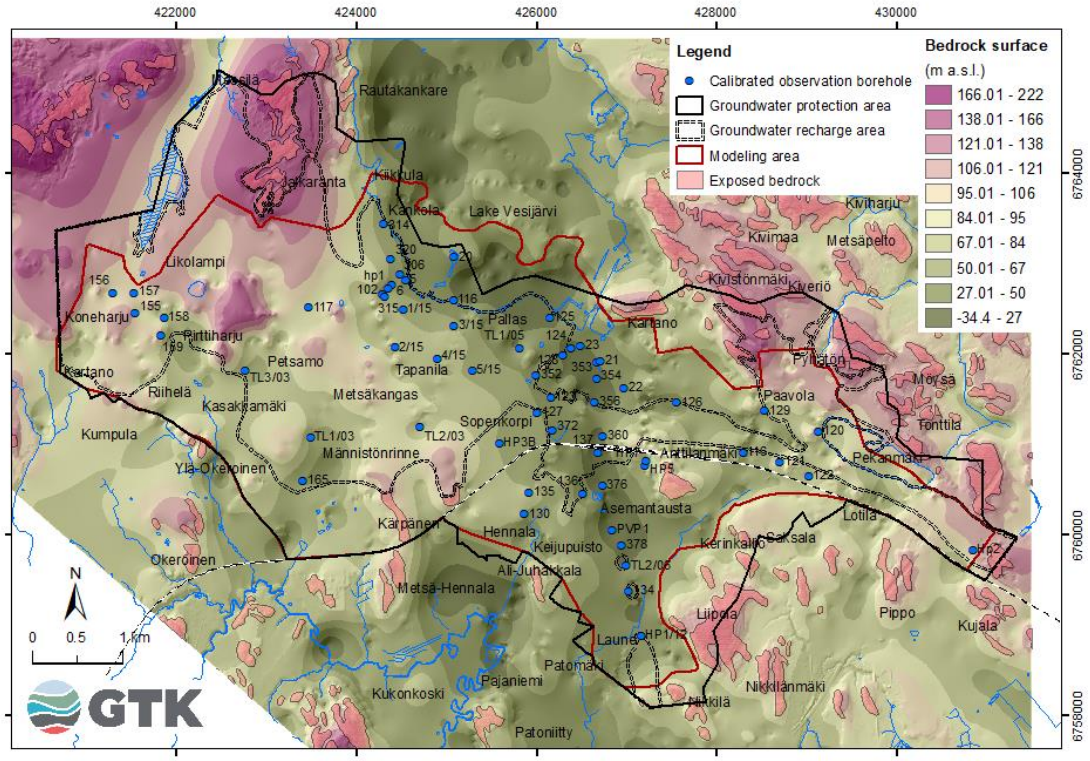

Fig. 14 Bedrock topography map of the study area.

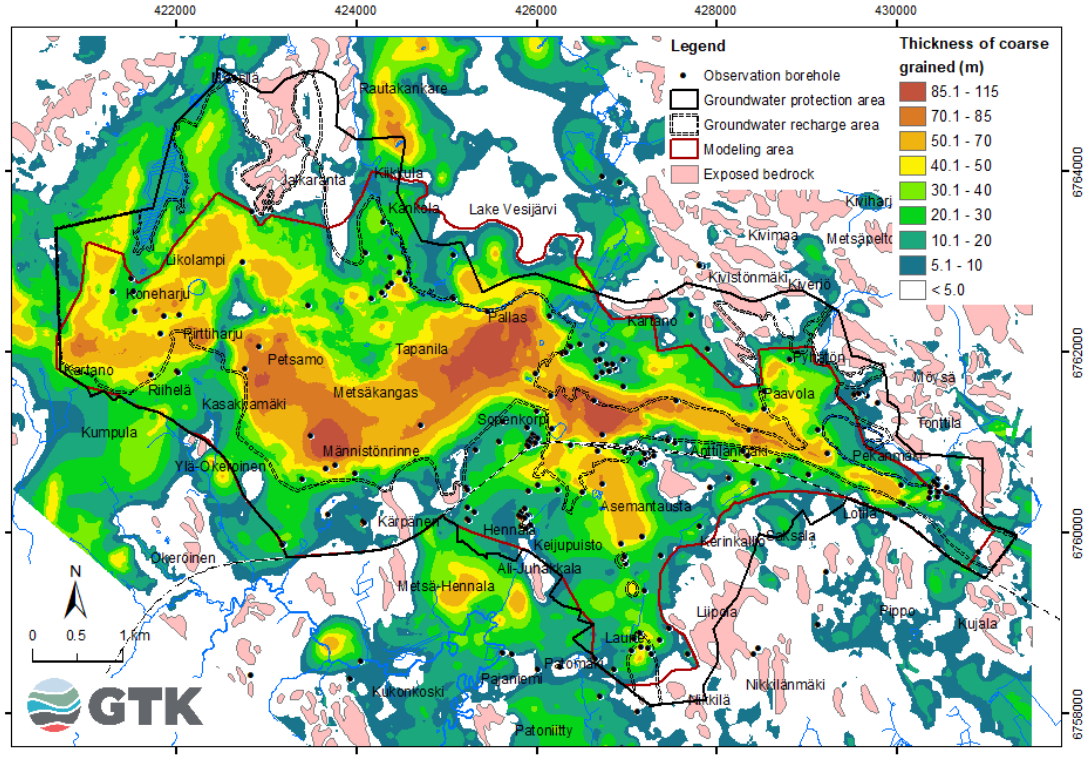

Fig. 15 Thickness map of the coarse-grained materials (sand, gravel, and coarse-grained till).

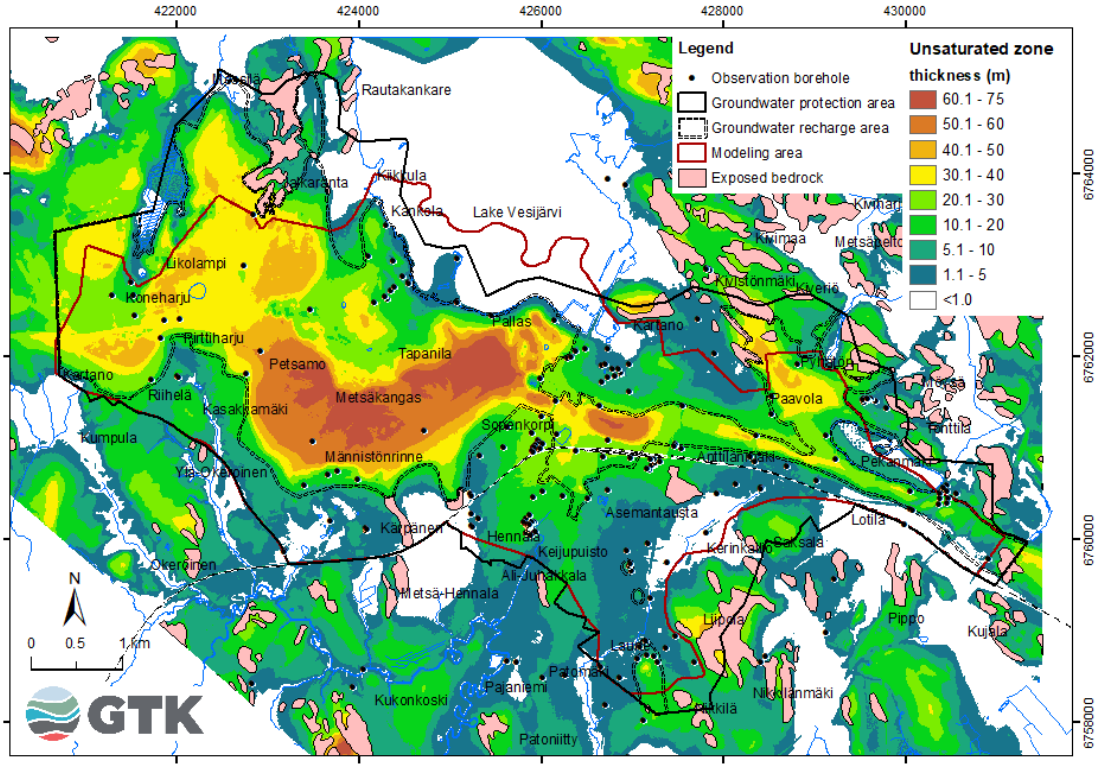

Fig. 16 Thickness of the unsaturated zone (LiDAR-DEM minus groundwater level).

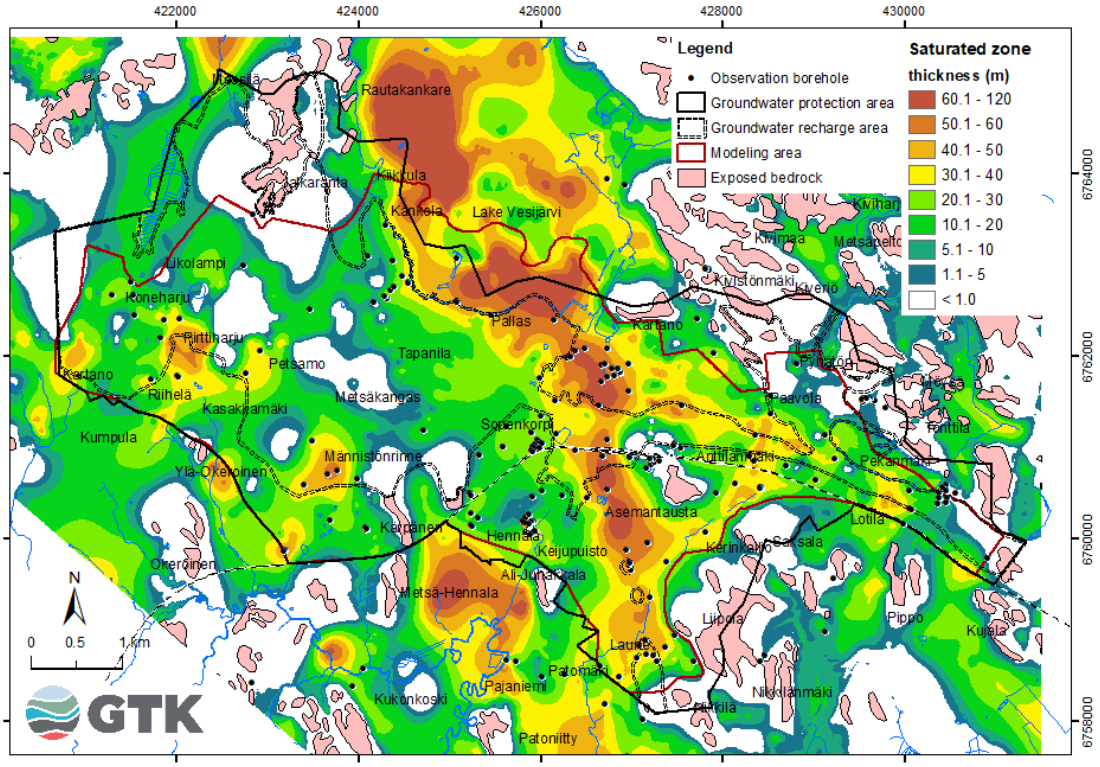

Fig. 17 Thickness of saturated zone (groundwater level minus top bedrock).

4.3.2 Conceptual model of the groundwater flow system

The shallow aquifer in the Lahti groundwater area consists of porous sand, gravel and coarse-grained till from the SSI ice-marginal deposit that extended approximately 300-900 m into the Lake Vesijärvi, where the aquifer was covered by thick glaciolacustrine rhythmite (silt and clay unit) and post-glacial lacustrine mud. These fine-grained units also cover large part of the groundwater area in the south. Consequently, the aquifers are confined or partially confined. The aquifer is characterized by a very thick unsaturated zone, especially in the western part of the groundwater area.

Groundwater flow directions follow the ground surface and the bedrock surface topography. Elevated bedrock surface divide groundwater into sub-areas. However, groundwater flow predominantly from north to south following the depression of bedrock surface that run from the Lake Vesijärvi in the north to Laune in the southern part of the aquifer area.

Groundwater recharges from two main sources: 1) the infiltration from the snowmelt and rainfall over the aquifer areas in the mainland, and 2) the lakebed infiltration from the Lake Vesijärvi. Based on the stable isotope data (Hendriksson, 2012), the proportions of surface water were found in the aquifer in the shoreline area of the Lake Vesijärvi. The highest values (85-90% of surface water) were found in the Jalkaranta water intake well area. 20% of surface water was found in the aquifer in Laune, in the south. The aquifer in Laune is in the bedrock depression area and approximately 3 km from the Lake Vesijärvi. The surface water could infiltrate from the Lake Vesijärvi and travel through the thick, porous aquifer in the depression of bedrock to Laune.

Lake Vesijärvi and the infiltration water received water from the snowmelt and rainfall that remain from the surface runoff and evaporation/evapotranspiration. However, the impervious surface in the urban area, the fine-grained layer that cover the aquifer area, and the thick unsaturated zone causes a reduction of the groundwater recharge. The infiltration may take longer time to flow through the root zone and transform into the soil moisture to full fill the soil capacity in the unsaturated zone, and only the excess water will arrive to the groundwater table at as a recharge. The previous infiltration water could be mixed with the newly arrival of the water or no recharge occur if insufficient water available at the ground surface.

Groundwater flow beneath the fine-grained layers and discharge to the low-lying areas to the spring, stream, and creeks. The spring discharge in the southern part of the groundwater area contribute a significant tributary to the Porvoonjoki River, that continue flowing through the southern part of Finland.

Fig. 18 presents the geological cross-sections along the lines A–A’ and B-B’, showing the sediments at the drilled boreholes, Lake Vesijärvi and mean groundwater levels along the cross-section lines. Locations of the cross-section lines and observation boreholes are presented in Fig. 20. Fig. 19 presents a simplified 3D visualization of Lake Vesijärvi, groundwater levels, observation boreholes and bedrock surface in the model domain area.

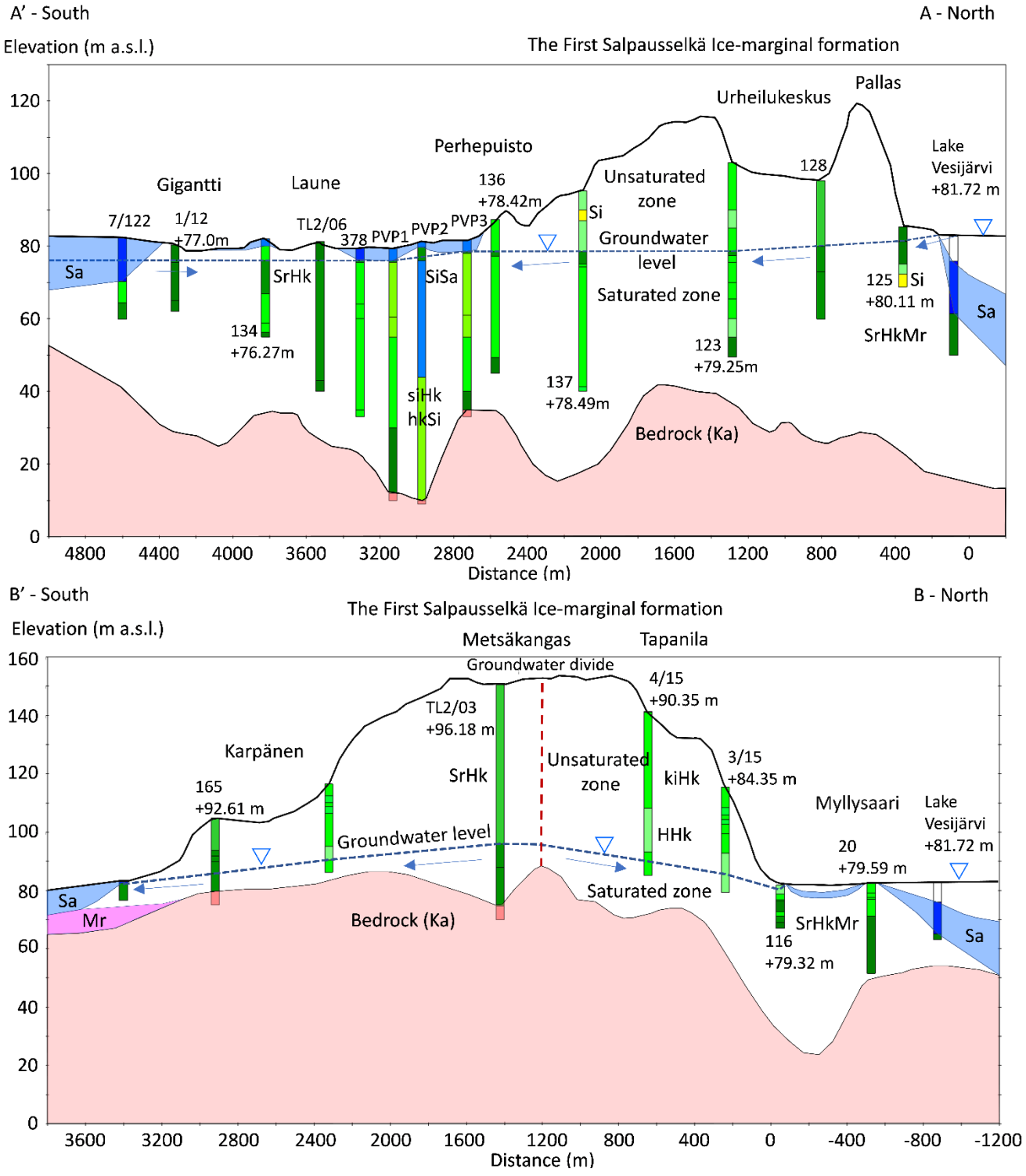

Fig. 18 Geological cross-sections along the lines A–A' and B-B', showing the sediments at the drilled boreholes, mean groundwater levels and Lake Vesijärvi. Explanation of symbols is shown in Fig. 19. Locations of the cross-section lines are shown in Fig. 20.

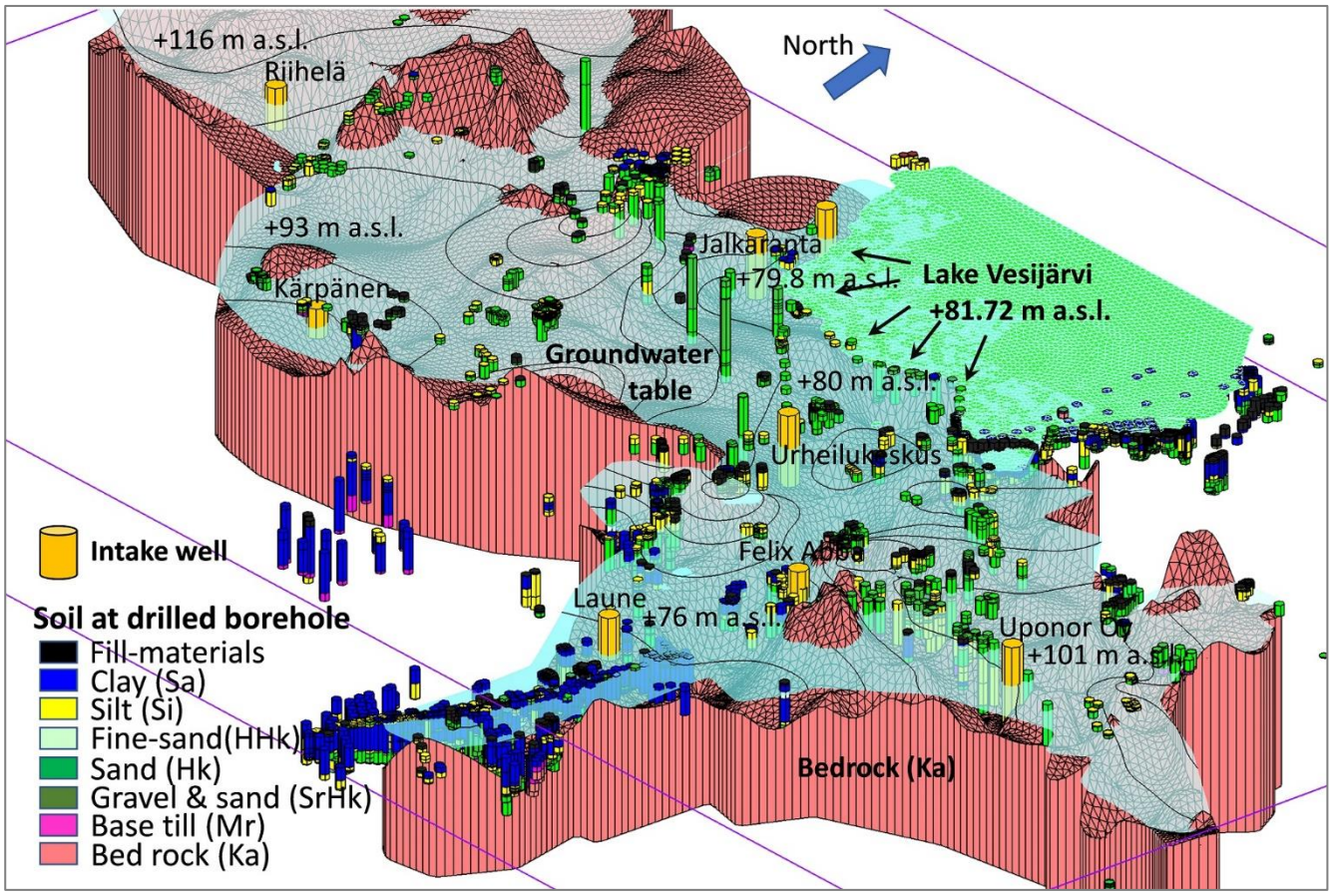

Fig. 19 Simplified 3D visualization of Lake Vesijärvi, groundwater levels, observation boreholes and bedrock surface in the model domain area.

4.4 Groundwater flow model

Groundwater flow model was performed for three phases:

1) the stead-state condition by using mean climate data (snowmelt and rainfall and PET) during 1961-2020 and constant pumping rate of 2002-2004. The calibration targets were mean groundwater levels during 2002-2004 and spring discharge rates. The calibrations were carried out by adjusting the Kh value, recharge, and lakebed conductance.
2) the transient state condition for 2000-2005 by using the initial head from the steady-state flow in phase 1 with a daily time step, daily climate data and lake level. The calibration targets were the monthly groundwater levels during 2002-2004 by adjusting the porosity and the specific yield (Sy), while the specific storage (Ss) was kept constant at 1E-05.
3) the transient state conditions of the current and scenarios data by using the calibrated model from phase 2 with the daily input of climate data for the three periods: 1979-2010; 2019-2050 and 2069-2100. The models were run without any further calibration. Additional two years data (1979-1980, 2019-2000 and 2069-2070) were needed for the warm-up process of the transient

simulation. The mean monthly of 30 years data for the periods 2021-2050 and 2071-2100 were compared with the historic data 1981-2010.

In the steady-state condition in phase 1, the sensitivity of groundwater levels and flow directions respond to the changes in pumping rates were simulated for the pumping and non-pumping conditions. The particle tracking following the groundwater flow path and capture zone were calculated for all water intake wells, as well as the flow paths and travel times from the groundwater risk areas.

4.4.1 Model discretization

Groundwater flow model was constructed by using MODFLOW-NWT code (Niswonger et al., 2011) and particle tracking for flow path was calculated by using MODPATH (Pollock, 1994) under the GMS graphic environment. MODFLOW-NWT is a Newton formulation of the MODFLOW-2005 (Harbaugh et al., 2017) that is designed for solving the problems of dry cells of the unconfined groundwater flow equation (Niswonger et al., 2011). Both MODFLOW-2005 and MODFLOW-NWT have been verified and are widely used for the numerical groundwater flow modeling. The model domain covers an area of 25.556 km^2 (Fig. 20) and is discretized into 100 m x 100 m grid size. The model domain was determined from the areas that contain the thickness of the coarse-grained materials greater than one meters.

In the northern boundary the model domain was extended approximately 300-900 meters into the lake area, covers an area of approximately 2 km^2, where the porous (sand and gravel, with thickness of 0-60 m and an average of 20 m) layer diminishes and was bounded by the clay and mud layers. Based on the seismic profile and drill logs data, the porous aquifer materials are draped by the fine-grained (silt, clay, and mud) layers with the thickness varies between 0-60 m and an average thickness of 19.6 m (Fig. 21). In the lakeshore area the fine-grained layers are thin or absent and the porous layer is exposed to the lake bottom and in direct contact with lake water.

To compromise the computational time with the daily stress period and the long simulation time of the climate scenario, the model is simplified in to a one-layer model with the thickness of the model varied from 1 to 120 m (an average of 22 m). The top layer is defined by the LiDAR-DEM for the land area, and the lake bottom defined by seismic profiles and drill logs for the lake area. The upper part of the bedrock surface normally contains fractures and weathered zones that is also important for the storage and movement of groundwater. Thus, the bottom layer is defined by 5 meters deep of the bedrock surface topography. The fine-grained (silt and clay) layer in the lake area was included in model and was simulated as a lakebed layer in the MODFLOW-RIVER (RIV) package. The fine-grained (silt and clay) layer in the south was considered as low permeable zone in the recharge estimation process.

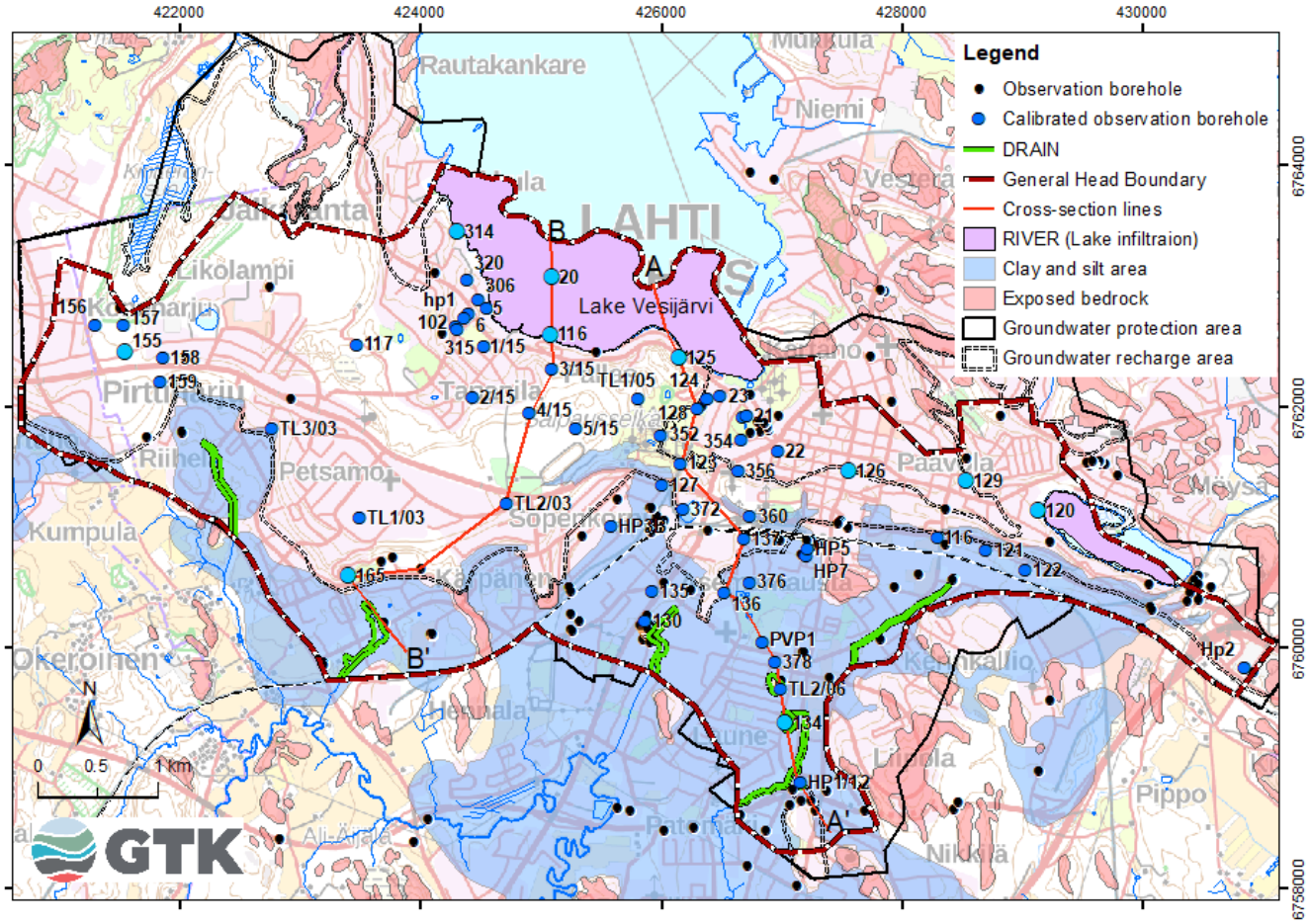

Fig. 20 Locations of the observation boreholes and cross-section lines A-A' and B'B', presented with the model domain and boundaries.

4.4.2 Model boundary conditions and input parameters

The MODFLOW processing packages applied in this study consists of the General Head Boundary (GHB), Well, and RIVER (RIV) packages (Fig. 20). Groundwater recharge and spring discharge (as a DRAIN boundary) were estimated via the UZF package. Details of each boundary condition described as follow:

General head boundary (GHB)

The GHB was assigned for most parts of the boundary areas, except the lake areas, where the fine-grained layer of the lakebed was assigned for the RIV package. GHB requires information of the head stages and the conductance of the aquifer materials at the boundary. The average groundwater level data during the period 2002-2004 was used as the head stage data. The low K value of 1.0E-06 m/d was used to calculate the conductance at the GHB.

Well

The constant pumping rates data from 2002-2004 (Insinööritoimisto Paavo Ristola Oy, 2004) were used for the entire simulations. The total daily pumping rate from seven main water intake wells and a

protective pumping well (north of the Felix Abba Oy Ab/Paasivaaran VO) is 24 410 m^3/d. The pumping rates of each water intake well are presented in Table 9.

Table 9 Lists of water intake wells and pumping rates used in this study.

Water intake well	Sub well	Screen top (m a.s.l.)	Screen bottom (m a.s.l.)	Screen length (m)	Pumping rate (m^3/d)	Pumping rate (m^3/d)
Jalkaranta	kaivo1	77.5	70.5	7.0	15 000	1 000
	kaivo3	75.0	60.5	14.5		1 600
	kaivo5	76.0	66.0	10.0		1 100
	kaivo6	76.0	67.0	9.0		1 600
	kaivo12	73.6	62.3	11.3		600
	kaivo11	70.1	59.6	10.5		1 000
	kaivo13	72.5	59.5	13.0		800
	kaivo10	71.2	61.2	10.0		1 600
	kaivo4	75.0	65.5	9.5		1 600
	kaivo7	68.4	57.9	10.5		1 200
	kaivo8	74.7	64.7	10.0		1 400
	kaivo9	74.3	63.3	11.0		1 500
Urheilukeskus	kaivo1	62.7	53.7	9.0	4 400	2 200
	kaivo2	60.1	48.6	11.5		2 200
Felix Abba Oy Ab (Paasivaaran VO)	kaivo1	68.1	63.1	5.0	260	260
Protective pumping well	Kaivo1				150	150
Laune	kaivo2	75.0	72.0	3.0	2 600	1 300
	kaivo3	77.0	72.0	5.0		1 300
Riihelä	kaivo1	101.0	92.5	8.5	1 150	575
	kaivo2	97.8	93.3	4.5		575
Kärpänen	kaivo1	90.6	80.6	10.0	600	600
Uponor Oy	kaivo1	68.0	58.0	10.0	250	250
				Total	24 410	24 410

RIVER (RIV)

Interactions between the lakes and the aquifer were estimated from the lake infiltration by using the RIVER (RIV) package. Leakages between lake and aquifer depend on the conductance of the lakebed (C), thickness of the lakebed and the head differences between the lake level (h_L) and the groundwater level (h_A). The conductance of the lakebed is calculated by the following equation:

$$C = (KLW)/T \qquad (16)$$

where

C lakebed conductance, in this case, conductance of the lakebed material (m^2/d)

K hydraulic conductivity of the lakebed material (silt and clay) (m/d)

L, W, T length, width, and thickness (m) of the lakebed.

Leakage (Q) through the lakebed or the flux of infiltration (m^3/d) is calculated by the following equation:

$$Q = \text{Conductance } (m^2/d) * \text{Head Difference } (m)$$
$$= (C)*(h_L-h_A) \qquad (17)$$

K values of the lakebed materials (silt and clay), approximately 1E-04-1E-10 m/d, were used initially from the literature and finalized by calibrating with the trail-and-error method until the simulated head and observed heads are in a good matched. A mean level during 1961-2021 of the Lake Vesijärvi of 81.72 m a.s.l. was used for the steady-state flow in simulation phase 1 and for the scenarios data in the simulation phase 3.

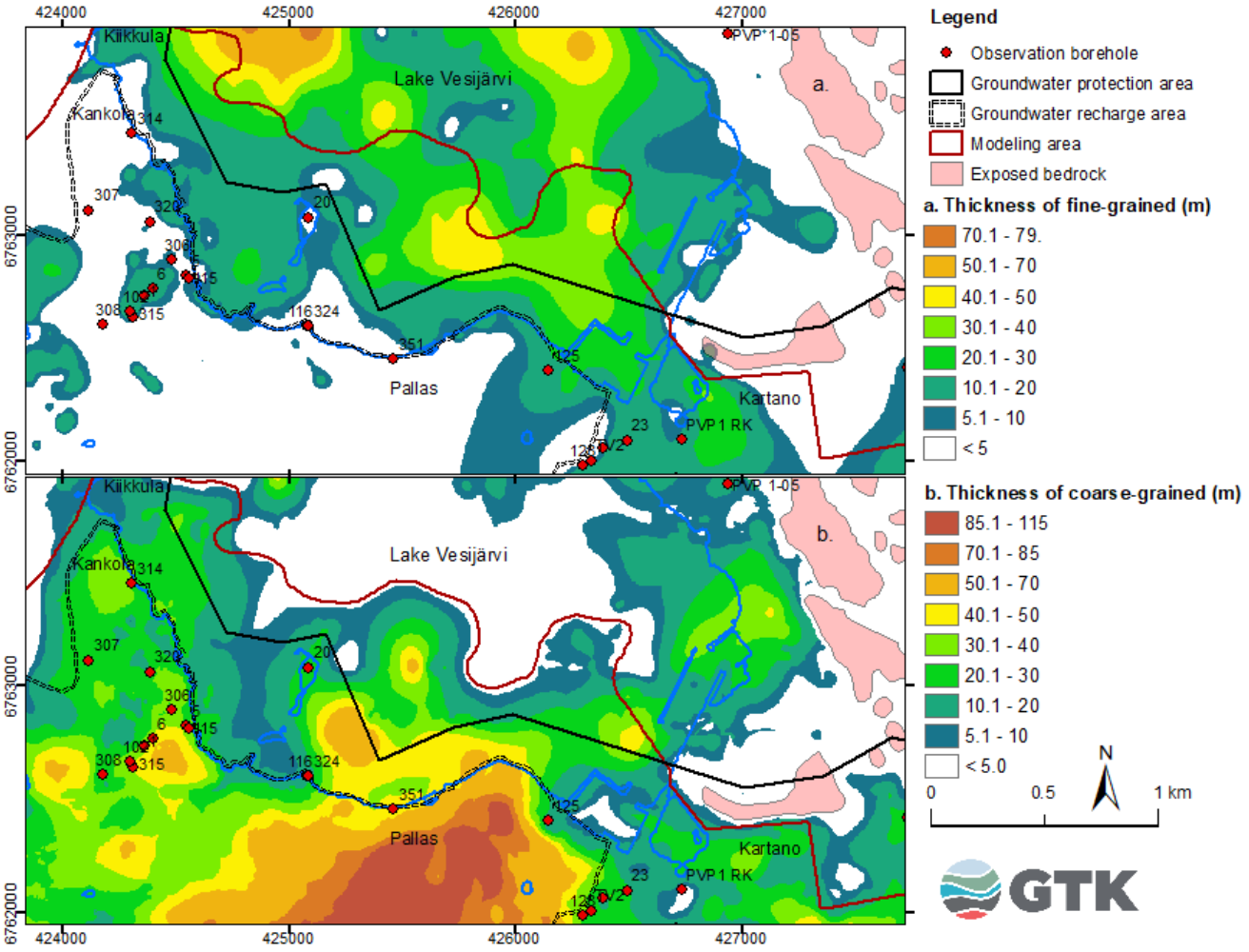

Fig. 21 Thickness maps of the fine-grained (silt and clay) layer (a.) and the coarse-grained layer (b.) in the Lake Vesijärvi in the model domain area.

Unsaturated zone flow (UZF)

The UZF Package was used to simulate vertical flow through the unsaturated zone between the ground surface, root zone, and the groundwater table using a 1D kinematic wave approximation to Richards' equation that ignores capillary forces (Niswonger et al., 2006). UZF can partition infiltrated water into evapotranspiration, unsaturated zone storage, and recharge to the groundwater level, where the 3D MODFLOW-NWT continues the simulation of the saturated zone flow. In the low-lying area where ground water levels rise above land surface, the surface leakage and groundwater discharge (DRAIN) will be calculated. The input parameters include the initial infiltration, the saturated soil water content (THTS), the saturated vertical hydraulic conductivity of the unsaturated zone (VKS), a Brooks-Corey epsilon or EPS variable that used to relate unsaturated hydraulic conductivity to soil water content, and the unsaturated zone thickness. The input parameters for the UZF simulation are listed in the Table 10.

Table 10 Parameters used for the UZF.

Name	Description	Value used in the model
FINF	Infiltration rate ((m/d)	Estimated by the snowmelt model
PET	ET demand rate (m/d)	Estimated by the PET model
EXTDP	Extinction depth (m)	0.1 - 1.5
EXTWC	Extinction water content	0.01
VKS	Saturated vertical hydraulic conductivity of the unsaturated zone (m/d)	1.0 - 1.4
EPS	Brook-Corey epsilon	3.0 - 4.0
THTS	Saturated water content	0.3
THTI	Initial water content	0.2
NUZTOP	Recharge/Discharge location	Highest active cell
IUZFOPT	Unsaturated zone Kv (m/d)	Kv from the LPF package
NTRAIL2	Number of trailing waves	10
NSET2	Number wave sets	20
n	Effective porosity	0.1 - 0.25
Sy	Specific yield	0.1 - 0.28
Ss	Specific storage (1/m)	1.00E-05

Hydraulic parameters

Hydraulic parameters, including horizontal saturated hydraulic conductivity (Kh), anisotropy (a ratio of horizontal (Kh) and vertical hydraulic conductivity (Kv)), specific storage (Ss), specific yield (Sy) and effective porosity, were initially assigned to the model layer based on the spatially distributions of the sediments in the model domain and were finally adjusted during the model calibration process. The initial Kh values were obtained from the soil analysis data and the slug test analyses performed in the HARA-aquifer mapping projects (Luoma & Ikonen, 2020; GTK-Lahde database, 2022). The estimated K-values corresponded to the stratigraphy, varying from 0.1-4.8 m/d in silty sand and fine sand, and 5-50 m/d in sand and gravel. The effective porosity values of between 0.1 and 0.25, a specific storage (Ss) value of 0.00001/m, and the specific yield (Sy) values between 0.1-0.28 were assigned to the model

domain area. In the bedrock area, the low Kh values of 0.001-1.0 m/d and low porosity of 0.01-0.1 were assigned.

4.4.3 Model calibration

For the steady-state flow model with the mean climate input data during 1961-2020, the calibration was carried out by using both PEST (Doherty, 2010) and manually trail-and-error methods. The parameters used for the calibrations consist of the Kh values, the initial infiltrations for UZF, and the lakebed conductance. The mean groundwater levels measured during 2002-2004 from 52 observation boreholes were used as the calibration targets. The calibration was performed until the discrepancy between the inflow and outflow less than 1% and the residual differences less than 0.5 m. The simulation performances were evaluated by using the mean error (ME), the mean absolute error (MAE) and the root mean square error (RMSE) equations as shown below:

$$ME = \frac{1}{n}\sum_{i=1}^{n}(h_{\mathrm{obs}} - h_{\mathrm{sim}}) \quad (18)$$

$$MAE = \frac{1}{n}\sum_{i=1}^{n}|h_{\mathrm{obs}} - h_{\mathrm{sim}}| \quad (19)$$

$$RMSE = \sqrt{\frac{1}{n}\sum_{i=1}^{n}(h_{\mathrm{obs}} - h_{\mathrm{sim}})^2} \quad (20)$$

where n, h_{obs}, and h_{sim} are the number of the observation, the observed head, and the simulated head, respectively.

The calibrated flow field obtained from the simulation was used to calculate the particle tracking groundwater path lines by using the MODPATH program (Pollock 1989).

For the transient flow during period 2000-2005, the calibration was carried out manually by adjusting the Sy values following the variations of the initial infiltrations and PET data, while the K values and the effective porosities were kept the same as in the steady-state flow. The monthly groundwater level data measured during 2002-2004 from 52 observation wells were used as the calibration targets.

For the transient flow with the climate scenario data during 1979-2100, the simulations were performed without any further calibrations.

5 RESULTS

5.1 Steady-state flow simulation

The comparison between the measured and the simulated heads and its residual are shown in Fig. 22. A summary table of the comparison is provided in Appendix 1. The water balance error (the difference between the inflow and outflow) is less than 0.1%, which is acceptable for the steady-state condition. The mean error (ME), the mean absolute error (MAE) and the root mean square error (RMSE) are 0.048, 2.2 and 0.32, respectively. High residuals (0.5-1.0 m) remain in some observation boreholes could cause by the complex hydrogeology of the area and the simple one-layer model may not represent the hydraulic conditions of those area.

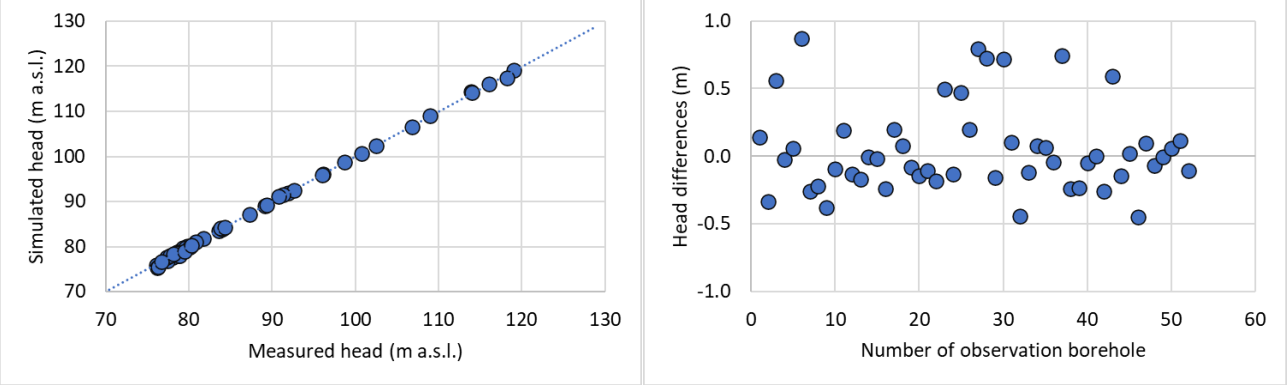

Fig. 22 Calibrations and residuals (head differences) between simulated and observed heads of the steady-state condition during 1961-2020.

Figs. 23-30 present the distribution maps of the calibrated Kh value, recharge, porosity, specific yield, simulated groundwater levels, the difference of heads between the pumping and non-pumping conditions and lake infiltrations. The water budgets of the model domain from the steady-state simulation for pumping and non-pumping conditions are presented in Table 11.

In non-pumping condition the mean groundwater level increase approximately 0.2-4 m compared with pumping condition. With no pumping takes place in the Jalkaranta water intake well area, groundwater level increase and discharge into the lake and no lake infiltration occurs.

Table 11. Comparison of water budgets from the steady-state flow simulations during 1961-2020 between the pumping and non-pumping conditions. Unit in m^3/d.

Component	Pumping condition		Non-pumping condition	
	Inflow	Outflow	Inflow	Outflow
Well	0.0	24 410.0	0.0	0.0
Stream discharge	0.0	3 167.2	0.0	6 923.1
Lake infiltration	9 387.5	1.0	0.0	11 267.7
Recharge	18 190.7	0.0	18 190.7	0.0
Total	27 578.2	27 578.2	18 190.7	18 190.7

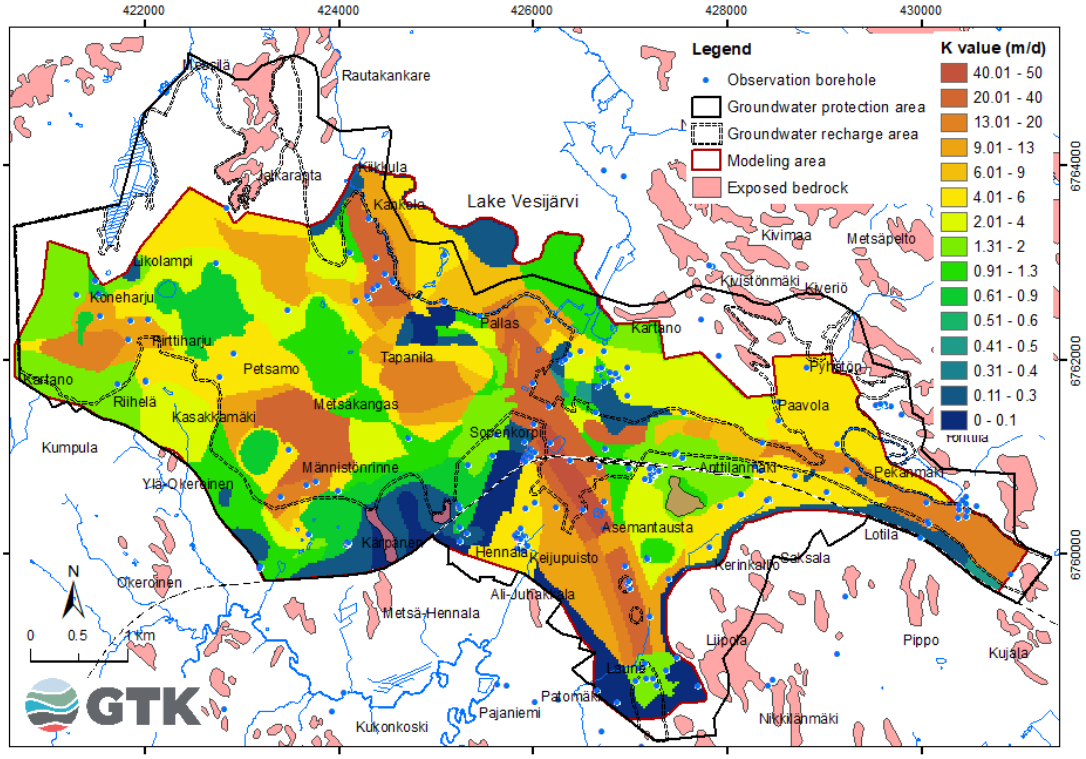

Fig. 23 Distribution map of the calibrated Kh value.

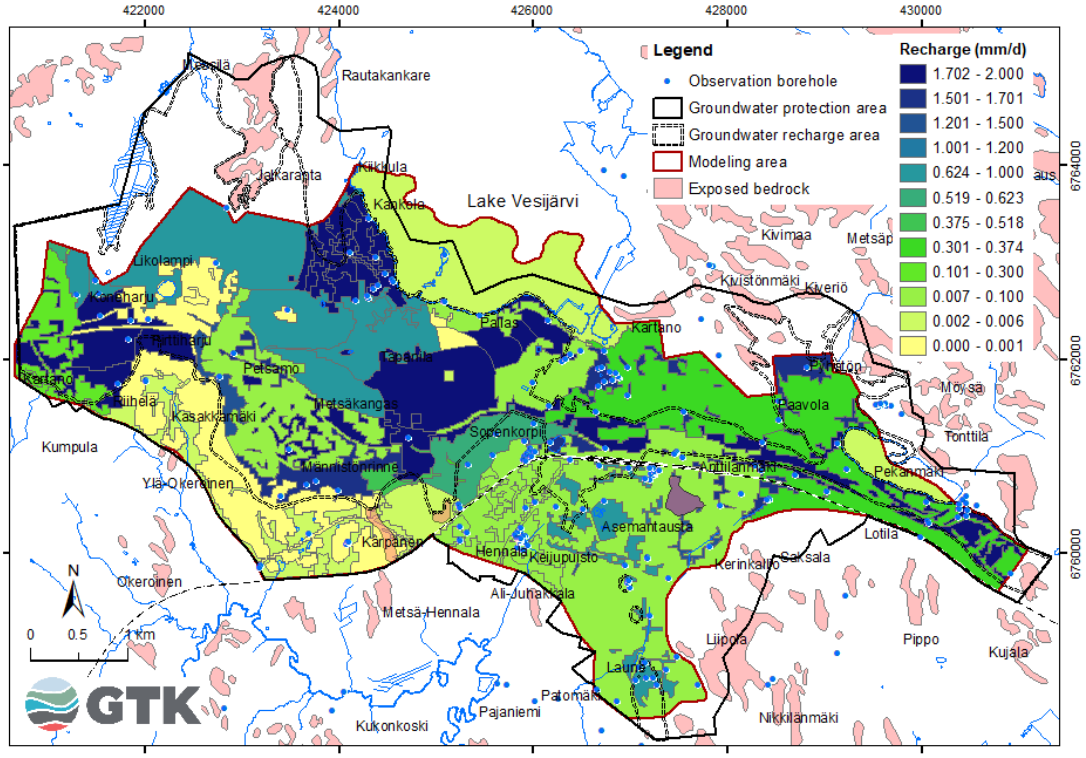

Fig. 24 Distribution map of calibrated recharge of the steady-state condition during 1961-2020.

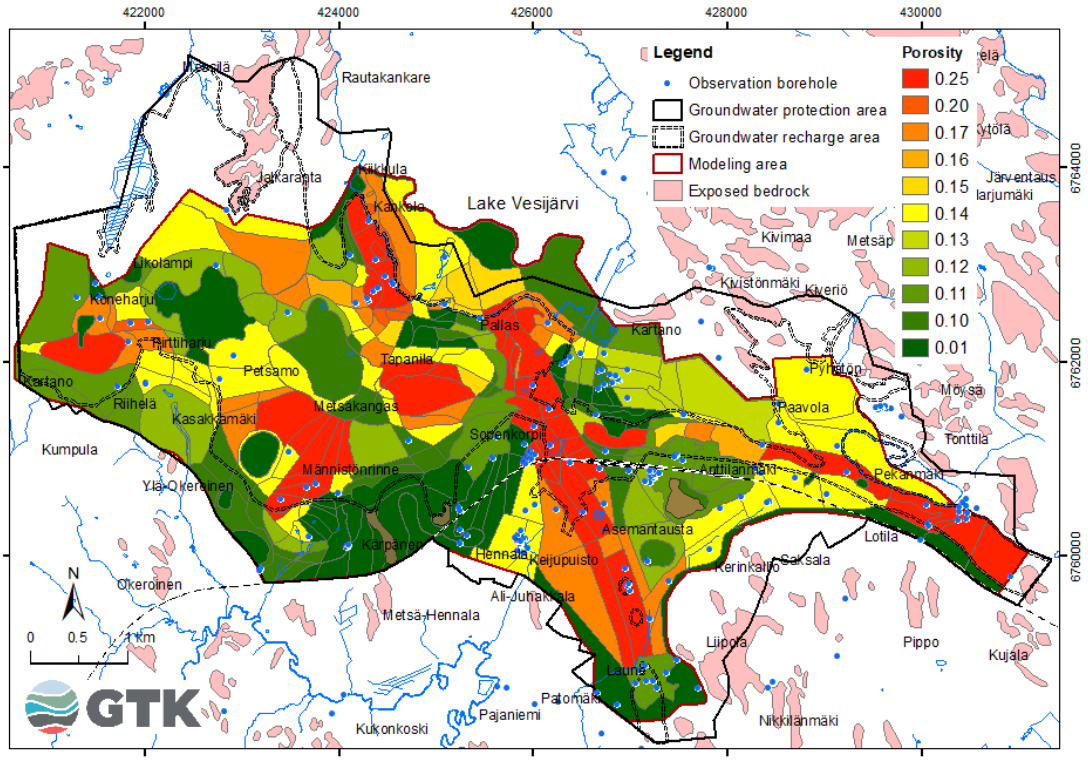

Fig. 25 Distribution map of applied effective porosity.

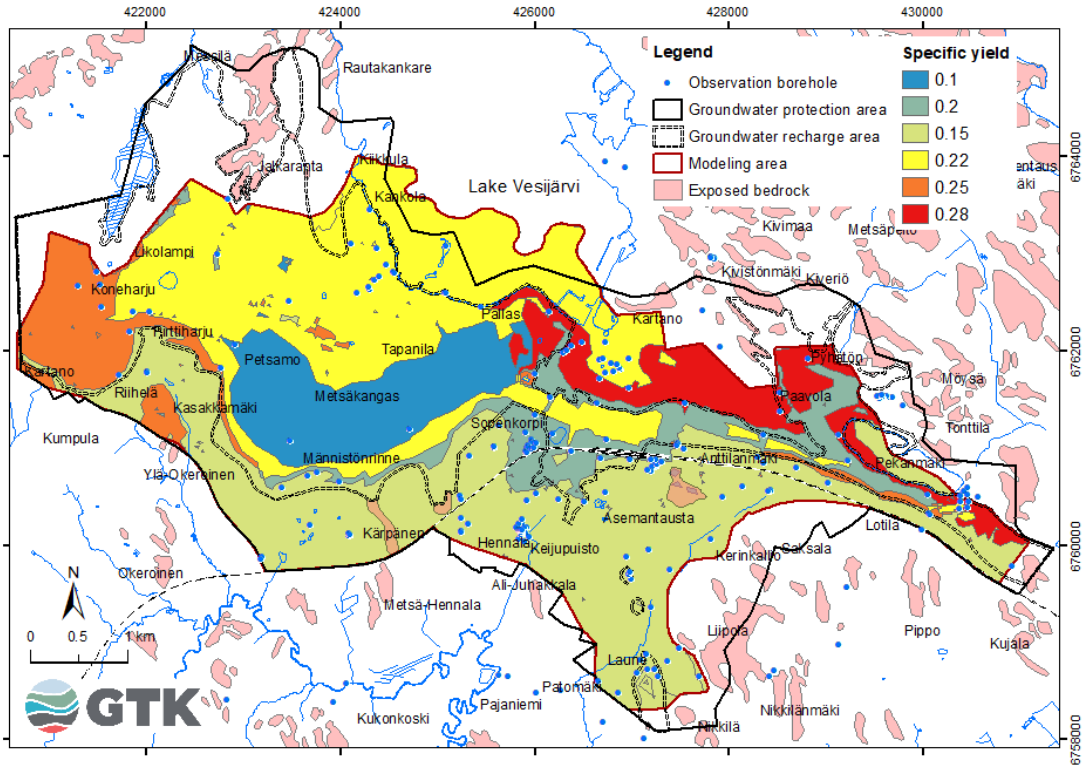

Fig. 26 Distribution map of calibrated specific yield (Sy).

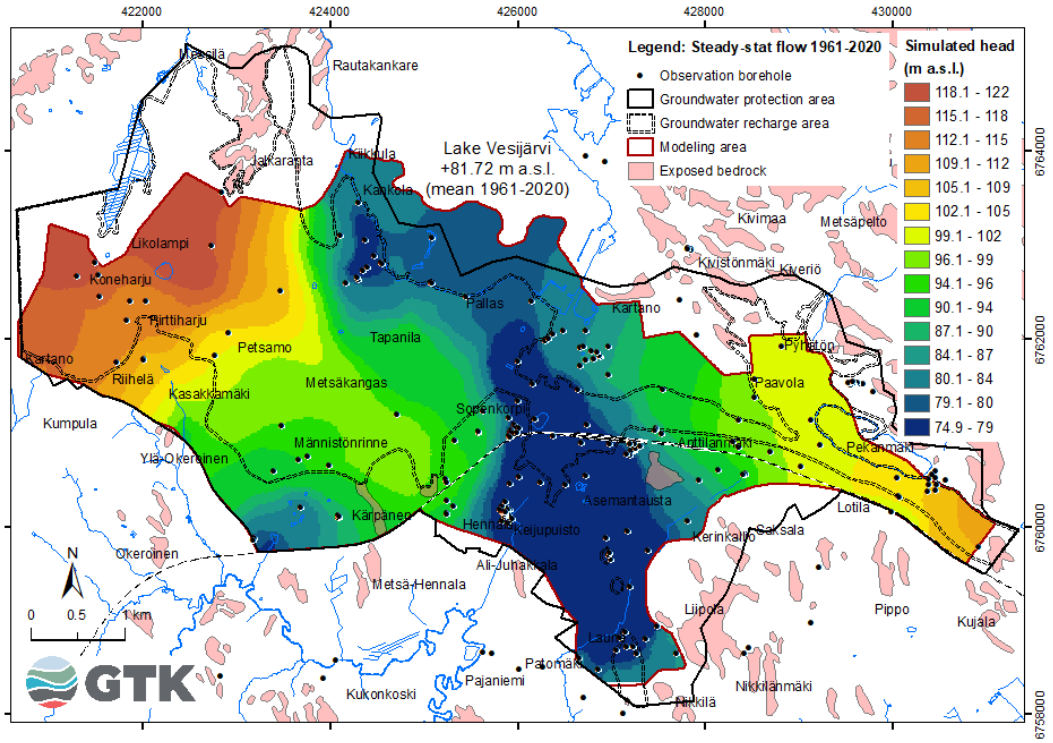

Fig. 27 Distribution map of simulated groundwater level with pumping condition of the steady-state simulation during 1961-2020.

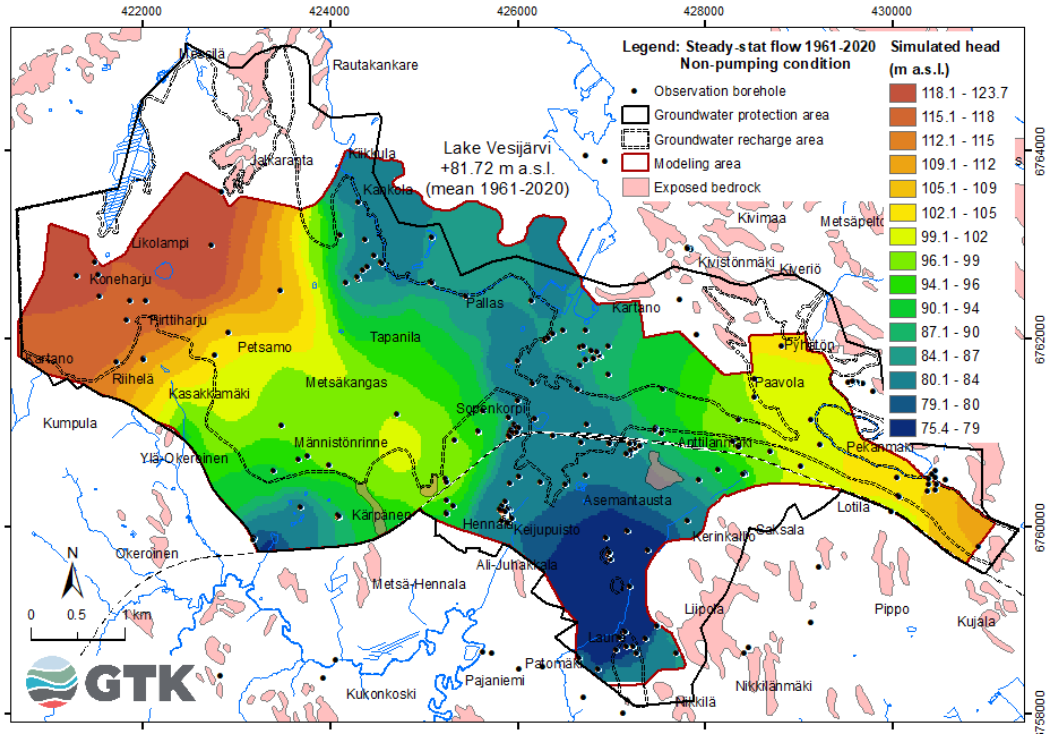

Fig. 28 Distribution map of simulated groundwater level with non-pumping condition of the steady-state simulation during 1961-2020.

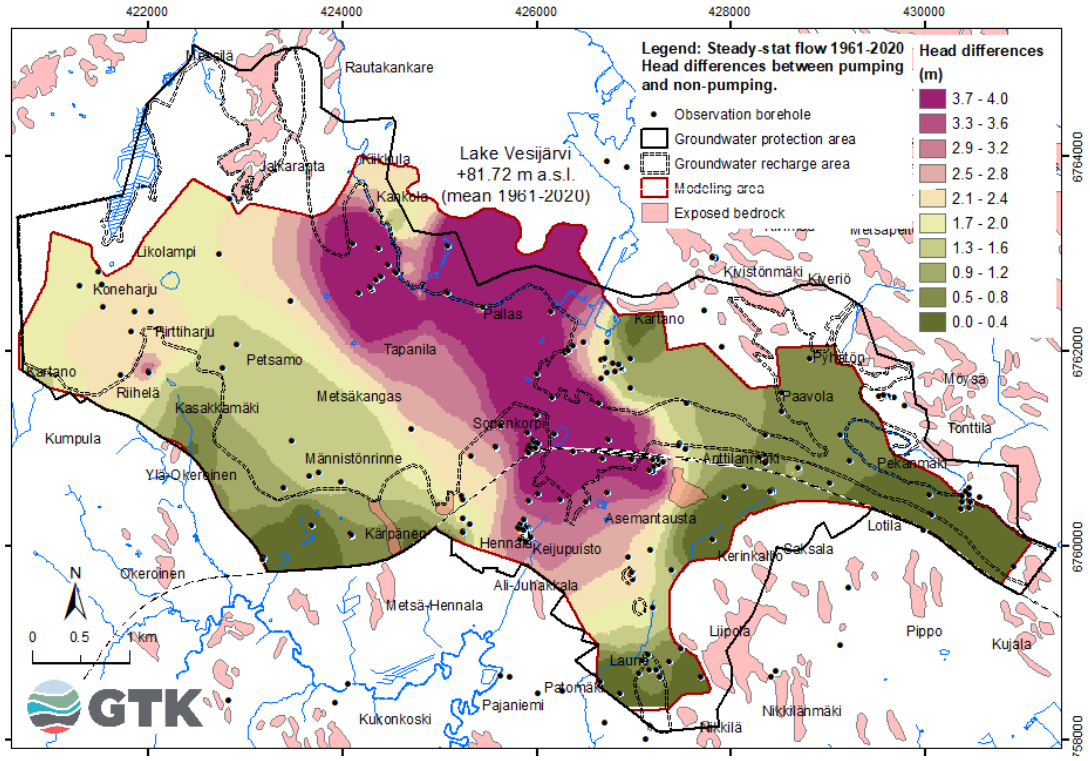

Fig. 29 Head differences between pumping and non-pumping conditions of the steady-state simulation during 1961-2020.

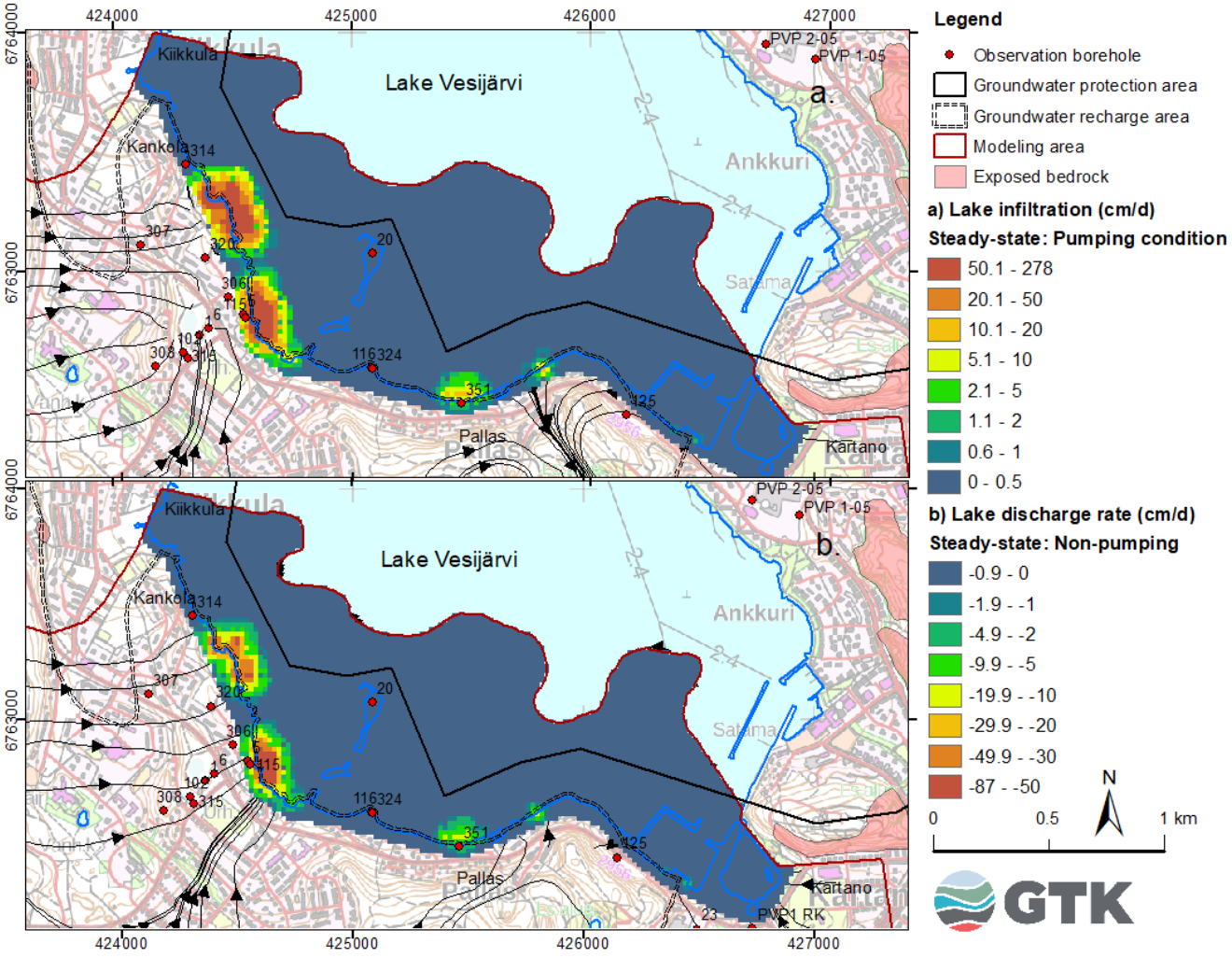

Fig. 30 Comparison of lake infiltrations for the pumping and non-pumping conditions. During the pumping condition lake infiltration occurs mainly along the lake shoreline and the water intake wells. During natural condition with no pumping, groundwater levels rise and discharge into the lake. Negative value represents outflow or discharge from the aquifer into the lake.

5.2 Transient flow simulation during 2000-2005

Fig. 31 presents the comparisons of the transient simulated heads and observed heads during 2002-2004 of the selected observation boreholes located in different parts of the aquifer area: HP314, HP20, HP116, HP125, HP126, HP134, HP120, HP129, HP155 and HP165. Locations of those observation boreholes are presented in Fig. 20. There are some discrepancies between the simulated and observed heads, which could be due to the limits of some parameters, e.g., constant pumping rates applied in the simulation and the complexity of the geological background of the aquifer. However, for the assessments of the climate change impact, this calibrated model version is acceptable and can be used for the simulation of the climate change impacts scenarios.

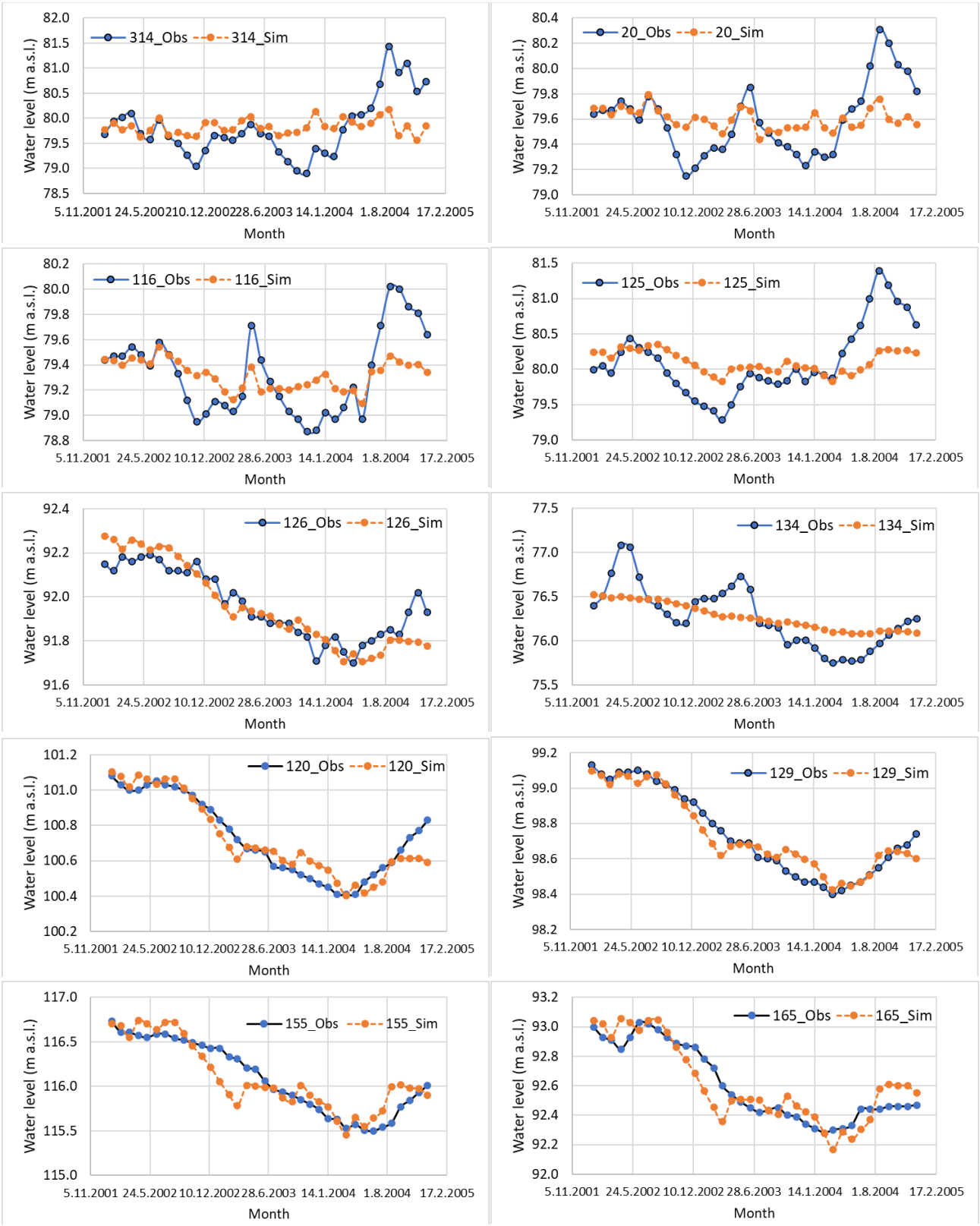

Fig. 31 Comparisons of the transient simulated heads and observed heads of the selected observation boreholes during 2002-2004 (see Fig. 20 for the locations of the observation boreholes).

Fig. 32 presents the simulation results of the infiltration from the root zone and the simulated recharge at the water table after routing through the unsaturated zone during 2000-2005 from the selected aquifer areas. Due to the spatial variability of the unsaturated zone and the initial infiltration conditions, the amount of recharge and lag times between infiltration from the root zone and recharge at the water table also show spatial and temporal variabilities. Less lag times were found in the porous aquifer area with shallow groundwater level such as in Jalkaranta (time lags of 33-46 days). While longer lag times were found in thick unsaturated zones e.g., in the porous aquifer areas in Pallas, Radiomäki (time lags of 139-176 days) or in the finer-grained aquifer with poor infiltration capacity from impervious land cover in the urban areas, e.g., Sopenkorpi (time lags of 223-244 days).

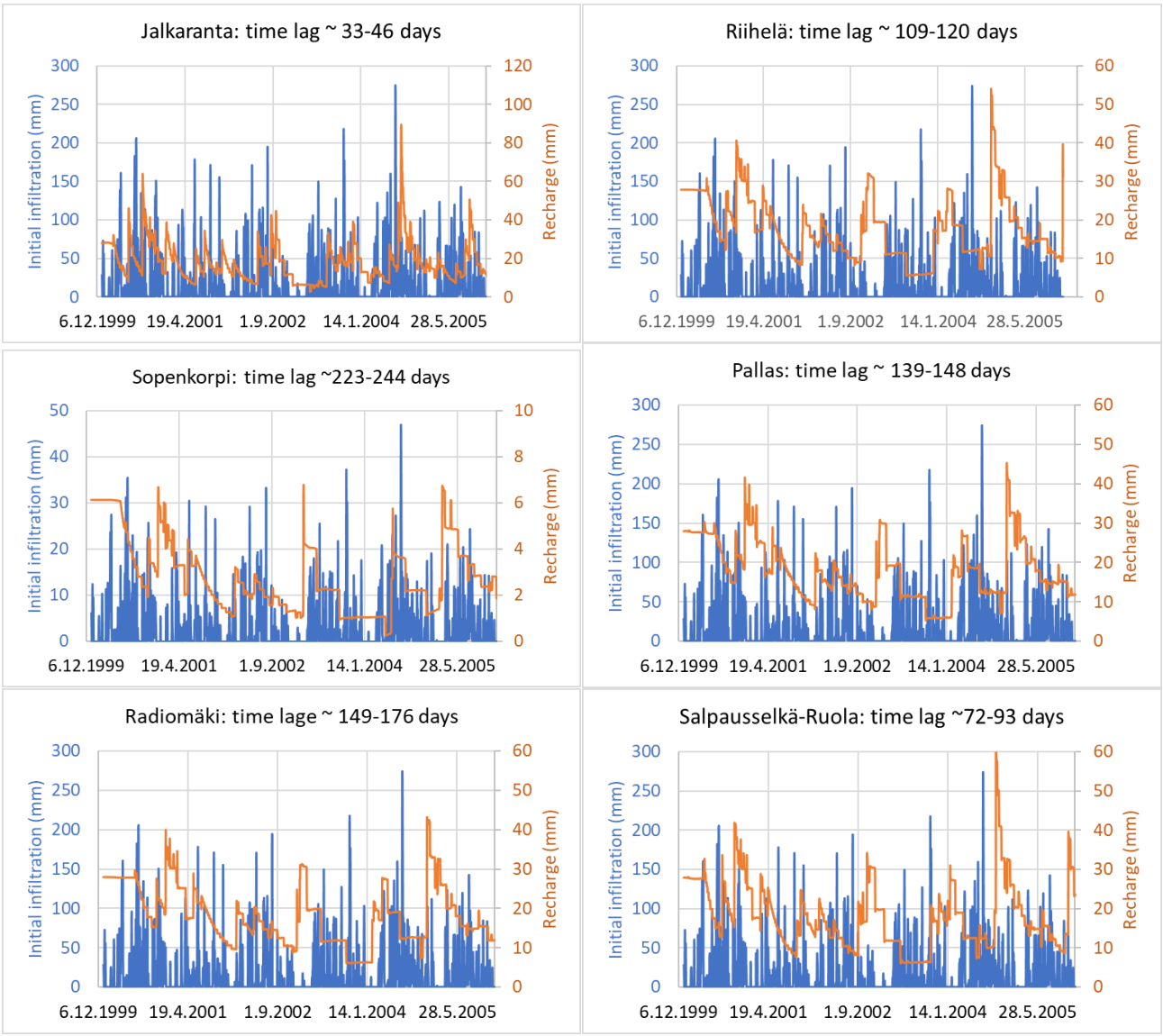

Fig. 32 Simulation results of the infiltration from the root zone (blue line) and the simulated recharge (brown line) at the water table after routing through the unsaturated zone and lag times between those values from the selected aquifer areas.

5.3 Transient flow with the scenarios data

5.3.1 Recharge, lake infiltration and runoff

Monthly mean 30-year simulated infiltration in the unsaturated zone, recharge, lake infiltration, and surface runoff (mm/month) during the periods 1981-2010, 2021-2050 and 2071-2100 and changes of the scenarios data (%) compared with the current data (1981-2010) are resented in Fig. 33. and Tables 12-15. At current condition (1981-2010), the annual mean infiltration is 287.9 mm (42% of snowmelt and rainfall, Fig. 13), the annual mean recharge is 188.9 mm (27.7 % of snowmelt and rainfall), the annual mean runoff is 312 mm (45.7% of snowmelt and rainfall, and the annual mean lake infiltration is 177.5 mm.

Annual mean infiltration of the scenario data increase 12.8% and 33.7% for the periods 2021-2050 and 2071-2100, respectively, compared with the current condition. Like the snowmelt and rainfall, the infiltrations show seasonal variabilities. The significant changes in infiltration patterns occur in winter and spring in both periods, where snowmelt and infiltration take place earlier in winter, due to the relatively increase in temperature. The high peak of infiltration during spring (April) in current condition does not exist in the scenarios data. High infiltrations are also observed in autumn in both periods, while in summer the infiltrations show slightly increase compare with the current condition.

Annual mean recharge of the scenario data increase 10.8% and 30.1% for the periods 2021-2050 and 2071-2100, respectively, compared with the current condition. At current condition (1981-2010), snowmelt reached the highest value in April (Fig. 13), however, the mean recharge shows a time lag between the infiltration from the root zone and the groundwater table with the highest peak in August (Fig. 33) (approximately 4 months lag time).

Annual mean runoff shows the similar pattern as the snowmelt and rainfall. At current condition, the highest runoff occurs in spring (April) after the snow melted and the lowest runoff is in winter, where the ground is frozen. Annual mean runoff of the scenario data increase 67.4% and 153.5% for the periods 2021-2050 and 2071-2100, respectively, compared with the current condition. The most significant increase in runoff is found in winter.

Lake infiltrations show slightly decreases (less than 13%) from the current condition. With the recharge increase, groundwater level also increases and reduce the lake infiltration rate. However, the variabilities of lake infiltrations are also low. The main reason for this could come from the same input of lake levels (81.72 m a.s.l.) applied to all scenarios.

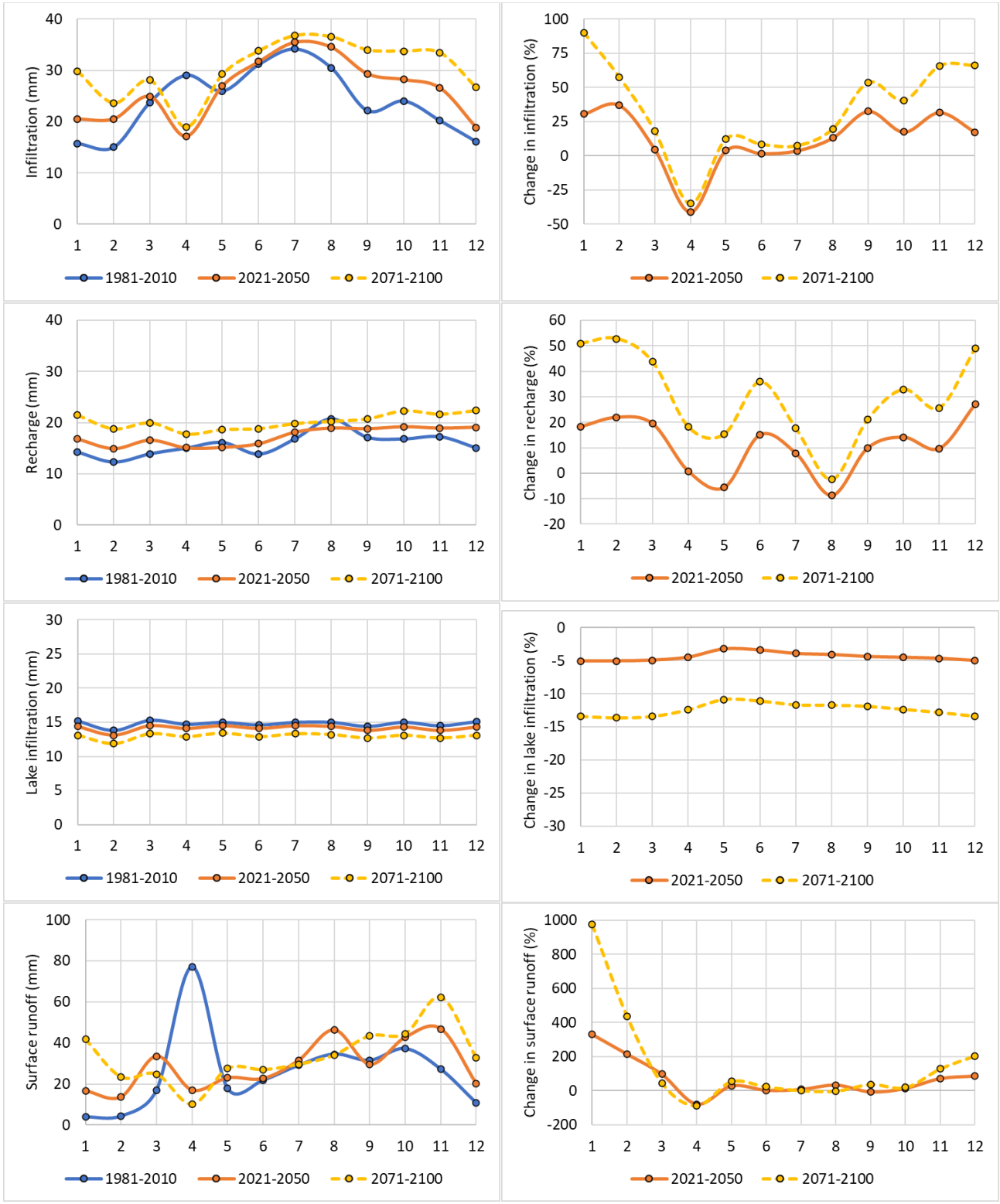

Fig. 33 Monthly mean infiltration, recharge, lake infiltration, and surface runoff (mm/month), and changes (%) of the scenario data (2021-2050 and 2071-2100) compared with the current condition (1981-2010).

Table 12 Initial infiltration (mm) and change in infiltration (%)

Month	Infiltration	(mm)		Change in infiltration (%)	
	1981-2010	2021-2050	2071-2100	2021-2050	2071-2100
1	15.7	20.5	29.8	30.7	90.0
2	15.0	20.6	23.6	37.1	57.6
3	23.8	24.9	28.1	4.8	18.1
4	29.1	17.2	18.9	-41.0	-34.9
5	26.0	27.0	29.2	4.0	12.5
6	31.2	31.7	33.8	1.7	8.4
7	34.2	35.5	36.8	3.8	7.5
8	30.5	34.5	36.5	13.2	19.8
9	22.1	29.4	34.0	32.6	53.6
10	24.0	28.2	33.8	17.4	40.4
11	20.2	26.6	33.4	31.7	65.7
12	16.1	18.9	26.7	17.4	66.0
Mean	24.0	26.2	30.4	12.8	33.7
Sum	287.9	314.9	364.7		

Table 13 Recharge (mm) and change in recharge (%).

Month	Recharge	(mm)		Change in recharge (%)	
	1981-2010	2021-2050	2071-2100	2021-2050	2071-2100
1	14.2	16.8	21.4	18.3	50.9
2	12.3	15.0	18.7	22.0	52.8
3	13.9	16.6	19.9	19.5	43.7
4	15.0	15.1	17.7	0.7	18.2
5	16.1	15.2	18.6	-5.7	15.4
6	13.8	15.9	18.8	15.1	35.9
7	16.8	18.1	19.8	7.8	17.6
8	20.7	18.9	20.2	-8.8	-2.3
9	17.1	18.8	20.7	9.9	21.2
10	16.8	19.2	22.3	14.2	32.9
11	17.2	18.9	21.6	9.7	25.7
12	15.0	19.1	22.4	27.0	48.9
Mean	15.7	17.3	20.2	10.8	30.1
Sum	188.9	207.5	242.2		

Table 14 Lake infiltration (RIV) (mm) and change in lake infiltration (%).

Month	Lake infiltration (RIV) (mm)			Change in RIV (%)	
	1981-2010	2021-2050	2071-2100	2021-2050	2071-2100
1	15.2	14.4	13.1	-5.1	-13.4
2	13.8	13.1	11.9	-5.1	-13.6
3	15.3	14.5	13.3	-4.9	-13.4
4	14.7	14.1	12.9	-4.5	-12.4
5	15.0	14.5	13.4	-3.2	-10.9
6	14.6	14.1	12.9	-3.4	-11.1
7	15.0	14.5	13.3	-3.9	-11.7
8	15.0	14.4	13.2	-4.1	-11.7
9	14.4	13.8	12.7	-4.4	-11.9
10	15.0	14.3	13.1	-4.5	-12.4
11	14.5	13.8	12.7	-4.7	-12.8
12	15.1	14.3	13.1	-5.0	-13.4
Mean	14.8	14.2	13.0	-4.4	-12.4
Sum	177.5	169.8	155.6		

Table 15 Surface runoff and change in surface runoff (%).

Month	Surface runoff (mm)			Change in runoff (%)	
	1981-2010	2021-2050	2071-2100	2021-2050	2071-2100
1	3.9	16.7	41.7	330.4	975.4
2	4.4	13.7	23.4	215.5	437.8
3	17.0	33.5	24.8	97.0	45.9
4	77.0	17.0	10.0	-77.9	-87.0
5	17.8	23.0	27.5	29.2	54.7
6	21.9	22.6	26.9	3.6	23.3
7	29.1	31.5	29.6	8.4	1.8
8	34.5	46.3	34.1	34.1	-1.4
9	31.5	29.6	43.5	-6.1	37.9
10	37.2	42.7	44.4	14.7	19.3
11	27.2	46.8	62.3	72.3	129.3
12	10.7	20.1	32.7	87.1	205.1
Mean	26.0	28.6	33.4	67.4	153.5
Sum	312.1	343.6	401.0		

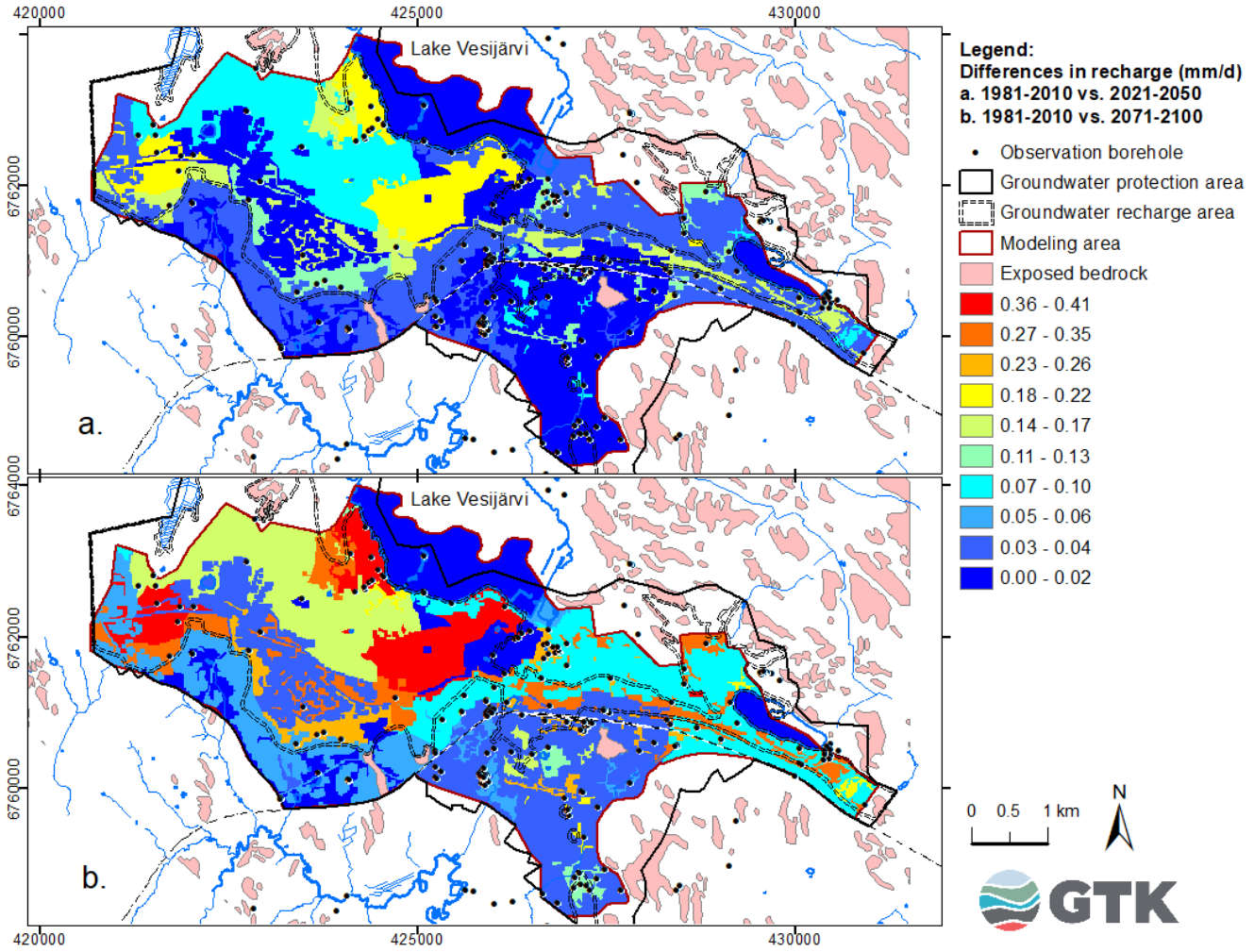

Fig. 34 Maps of changes in monthly mean 30-year recharge during 2021-2050 and 2071-2100 compared with 1981-2010. Less differences in recharge are found in the urban area over the scenarios data.

5.3.2 Groundwater levels

Fig. 35 presents the monthly mean simulated groundwater levels extracted from the selected observation boreholes, and Fig. 36, change of groundwater levels of those wells over the scenario data compared with the current condition. The historic groundwater levels of these boreholes are presented in the transient flow calibration in section 5.2 (Fig. 31). The monthly groundwater levels during 2002-2004 show recharge vary spatially and temporally. In the thick unsaturated zone area, recharge may occur many months after the infiltration started at the soil zone. However, the monthly mean 30-year groundwater levels show low seasonal variability. Monthly mean groundwater levels increase between 0.03-1.32 m (mean of 0.79 m) and 0.21-2.81 m (mean of 1.78 m) in 2021-2050 and 2071-2100, respectively.

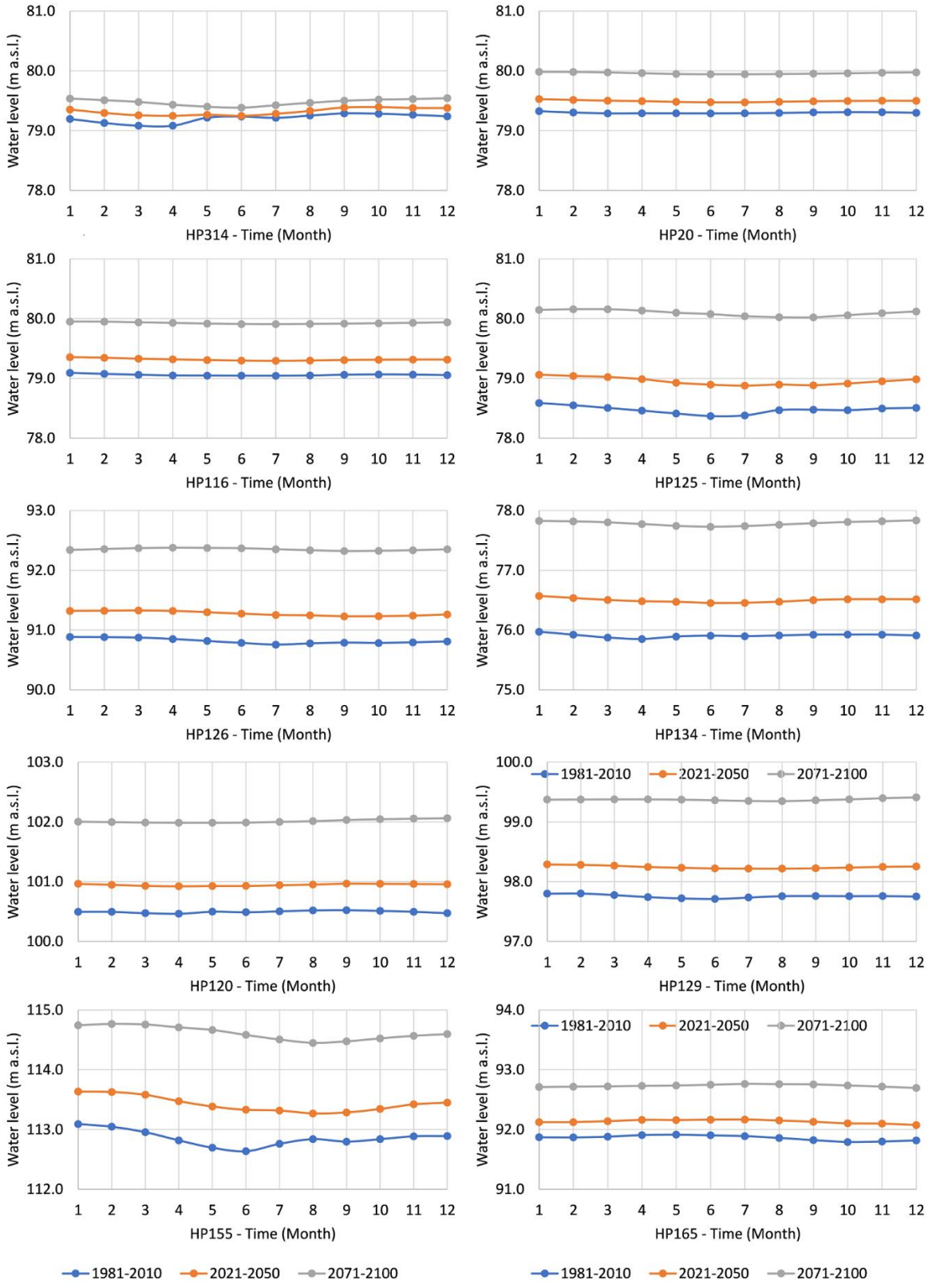

Fig. 35 Monthly mean of the 30-year simulated groundwater levels of the selected boreholes for the current condition (1981-2010) and the scenario data during 2021-2050 and 2071-2100.

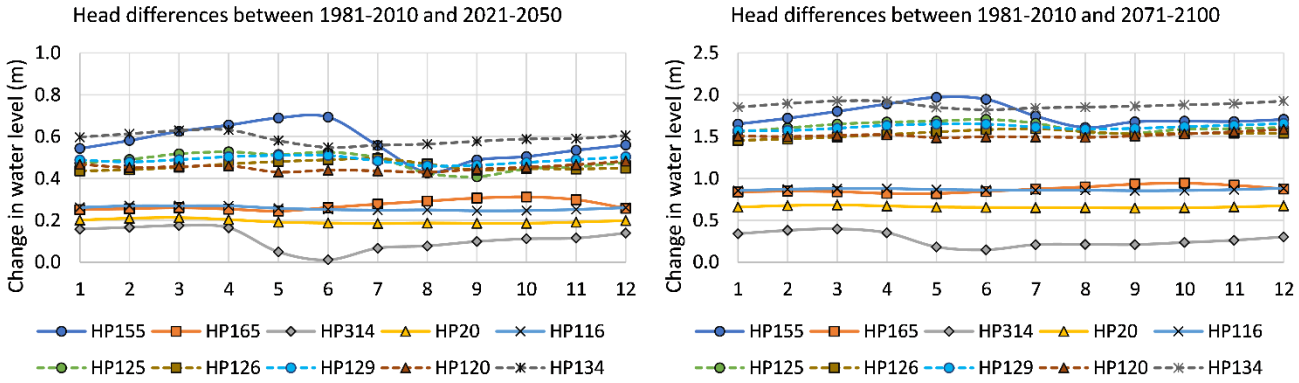

Fig. 36 Changes of groundwater levels during 1981-2010 compared with during 2021-2050 and 2071-2100. Locations of the observation boreholes are presented in Fig. 20.

5.3.3 Water budget

The main components of water budget based on the water balance between inflow and outflow consist of recharge, lake infiltration, drains (stream discharge). The flux rates (m^3/d) of those components within the model domain (area of 25.556 km^2) are summarized in the Appendix 2 and are presented in Fig. 37. The constant pumping rate of 24 410 m^3/d was omitted in the summary.

At current condition (1981-2010) the inflow and outflow rates in the model domain vary between 32 860 – 37 460 m^3/d with the mean value of 34 357 m^3/d. The annual mean flow rates are predicted to increase 2.4 and 7.4% during 2021-2050 and 2071-2100, respectively. The recharge flux rates vary between 11 190 - 17 080 m^3/d with the mean value of 13 212 m^3/d. The lake infiltration flux rates, which mainly occur in the lakeshore nearby the water intake wells, vary between 12 300 – 12 620 m^3/d with the mean value of 12 432 m^3/d. The mean recharge increases 9.9 and 28.4%, while the mean lake infiltration decreases 4.4 and 12.4% during 2021-2050 and 2071-2100, respectively. The main outflow consists of pumping rate and drain (stream discharge). The mean discharge rate at current condition is 2 330 – 2 380 m^3/d with the mean value of 2 352 m^3/d. The discharge rate is predicted to increase 10 and 27% from present during 2021-2050 and 2071-2100, respectively.

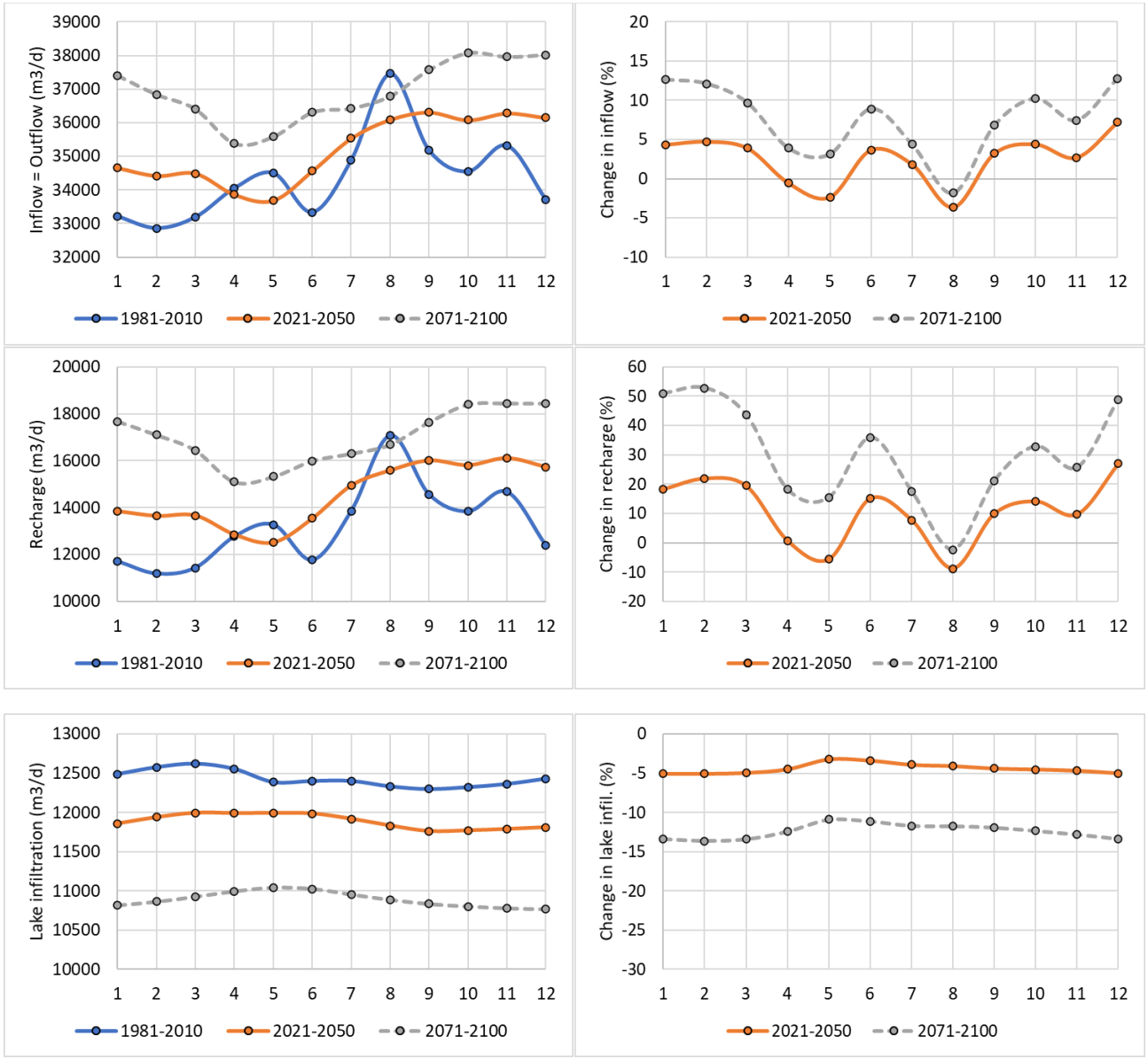

Fig. 37 Variability of the flow flux rate, recharge and lake infiltration, and changes of those values during 2021-2050 and 2071-2100, compared with the current condition 1981-2010.

5.4 Model limitations

The model was developed with sparse data; thus, some limitations and uncertainties remain as described in the following:

- A single layer model for a complex aquifer setting. Base on the intensive drill logs data the aquifer is complex and high heterogeneity, e.g., interbedded between fine-grained and coarse-grained layers or the existing of the perched groundwater in some areas. The objective of this modeling was to evaluate the sensitivity of the aquifer under climate change scenarios by using

the flow model as an evaluation tool. The simulation of the infiltration of an aquifer needs to be done on a daily time step basis to represent the flow process from the ground surface through the soil zone, unsaturated zone and to the aquifer. This created a tremendous data file. To compromise between the computational capacity, the model was simplified into a single layer. This may not represent the real hydrogeological condition in some complex aquifer areas.

- A thick unsaturated zone. The aquifer is characterized by a very thick unsaturated zone which adds more challenges for the recharge estimation. Depend on the amount of the infiltration water that is available on the ground surface. The infiltration may take longer time to flow through the root zone and transform into the soil moisture to full fill the soil capacity in the unsaturated zone, and only the excess water will arrive to the groundwater table at the aquifer as a recharge. The previous infiltration water could be mixed with the newly arrival of the water or no recharge occur if insufficient water available at the ground surface. This cause high uncertainty in recharge estimation. Therefore, the recharge estimation in the thick unsaturated zone aquifer should be evaluated by using multiple methods, e.g., water balance method, to reduce uncertainty and support the interpretation of the numerical simulation.

- A set of constant input parameters. The model was run and calibrated successfully by using the constant input parameters. These include the pumping rate in each water intake well, the lake level, the one-time measured spring data available for the calibrations and the same land use pattern. The simulation will represent purely the results of the climate variables (temperature and precipitation), but no impacts from those constant input parameters. Additional data at current and future conditions are needed for the simulation of climate scenarios.

6 DISCUSSION

6.1 Recharge, lake infiltration and runoff

Although the main part of the aquifer material consists of porous materials (sand and gravel), the largest part of the groundwater area is the urban area (51%) which is covered by the impervious surface. The impervious surface could prevent the infiltration capacity and promote the surface runoff. The simulation results show the annual mean infiltration and runoff are 42% and 45.7% of the snowmelt and rainfall (or 45.1% and 48.8% of total precipitation), respectively. Valtanen (2015) reported the surface runoff in Lahti urban areas vary between 48-68% of the total precipitations. The infiltration capacity is limited by the impervious surfaces, and with the increase in precipitation from the scenario data, only the small portions of the water will infiltrate through the impervious surface and the excess water will overflow as runoff or evaporate back to the atmosphere. Under the scenario data, the snowmelt and rainfall are predicted to increase, especially in the winter, due to the increase in temperature, and the increase in runoff is also expected. The infiltration capacity of the aquifer is limited by the impervious surface in the urban area. With the increase in the snowmelt and rainfall in the scenario data, the large part of the excess water will contribute to the runoff. This could induce more the potential stormwater flood risk in the future.

The aquifer is characterized by the very thick unsaturated zone. This causes the long lag time between the infiltration from the root zone and the groundwater table and the reduction of the recharge as some parts of the infiltrated water will fill up the soil water content in the unsaturated zone. Thus, only the excess water will percolate and arrive to the groundwater table as the recharge. At current condition, the annual mean recharge is about 28% of snowmelt and rainfall with the average lag time of 4 months. However, the lag time would increase (and so decrease in recharge) in the finer-grained aquifer area.

This study clarified the characteristics of the aquifer in the Lake Vesijärvi area and the potential infiltration area. Based on the calibration, lake infiltrations occur mainly in the lake shore areas, where the fine-grained layer is thin or absent. The highest infiltration takes place in the Jalkaranta water intake well area. In this area, the stable isotope data indicates the influences of lake water up to 90% into the aquifer. Based on the simulation with non-pumping rate case, the groundwater level in the Jalkaranta increases approximately 3-4 m and discharges into the lake. The lake infiltration rates in this area are affected by the pumping activities of the water intake wells along the lake shore. Aquifer in area nearby the Myllysaari is covered thinner fine-grained layer of the glaciolacustrine rhythmically alternating (varved) silt and clay and postglacial lacustrine poorly bedded mud. These fine-grained sediments contain very poor hydraulic conductivity. However, due to the thin layer in this area, any activity that could remove this clay layer, could allow more lake infiltration in this area.

Based on the water budget balance, the main total inflow is obtained from the recharge and the lake infiltration. At current and over the scenario conditions, the simulation results show that the amount of recharge alone (up to 19 000 m^3/d) is not sufficient to meet with the pumping rate of 24 410 m^3/d. To maintain the sustainable water resources and water supply, the infiltration and recharge areas should be preserved and enhance correspond to future climate change variability and water demand. For more accurate recharge estimation, the additional field investigations are needed for the hydraulic properties of the unsaturated zone flow and detailed groundwater and lake water interactions along the lake infiltration area.

6.2 Groundwater level and water budget

Based on the simulated recharge and the calibration, the monthly mean groundwater levels are predicted to increase approximately 0.79 and 1.78 m in 2021-2050 and 2071-2100, respectively. The highest increase of groundwater levels of 1.32 and 2.81 m in 2021-2050 and 2071-2100, respectively, is found in the observation boreholes 155 in Riihelä in the west and 314 in Laune. The sediments in these areas are complex. However, the modelled high groundwater level could also be due to the inappropriate input parameters, e.g., K value. Site investigation and additional data in this area are needed. The long-term monthly measured groundwater levels indicated that groundwater recharge occur slowly and long lag time between the infiltration and the recharge takes place. However, the monthly mean 30-year water levels revealed a relatively uniform or low seasonal variability of groundwater levels, particularly in the thick unsaturated zone areas. Thick unsaturated zone aquifer could provide more stable of the groundwater level variability compared with the shallow groundwater level.

6.3 Implication for vulnerability assessment of the aquifer

The calibrated simulation of the steady-state condition (1961-2020) was used to calculate the particle tracking and advective travel time (based on the groundwater flow velocity). The capture zones in each time frame around the water intake wells and the travel time from the groundwater risk areas along the flow paths were calculated as presented in Figs. 38-41 and Appendix 3. Many parts of the aquifer areas contain thick unsaturated zone and are covered by thick fine-grained layers, especially in the southern part of the groundwater area. This provides the protective layer for the aquifer from the contaminants on the ground surface. However, there are some observation boreholes that show the possible connections between the perched groundwater and the main groundwater. The contamination route could transport from sources to the main aquifer via the perched groundwater. Further investigations could clarify the role of perched groundwater in the connectivity with the main groundwater. As well as the bedrock exposed in the groundwater area, where the fractures could provide the preferential pathways for the infiltration and the solute transport.

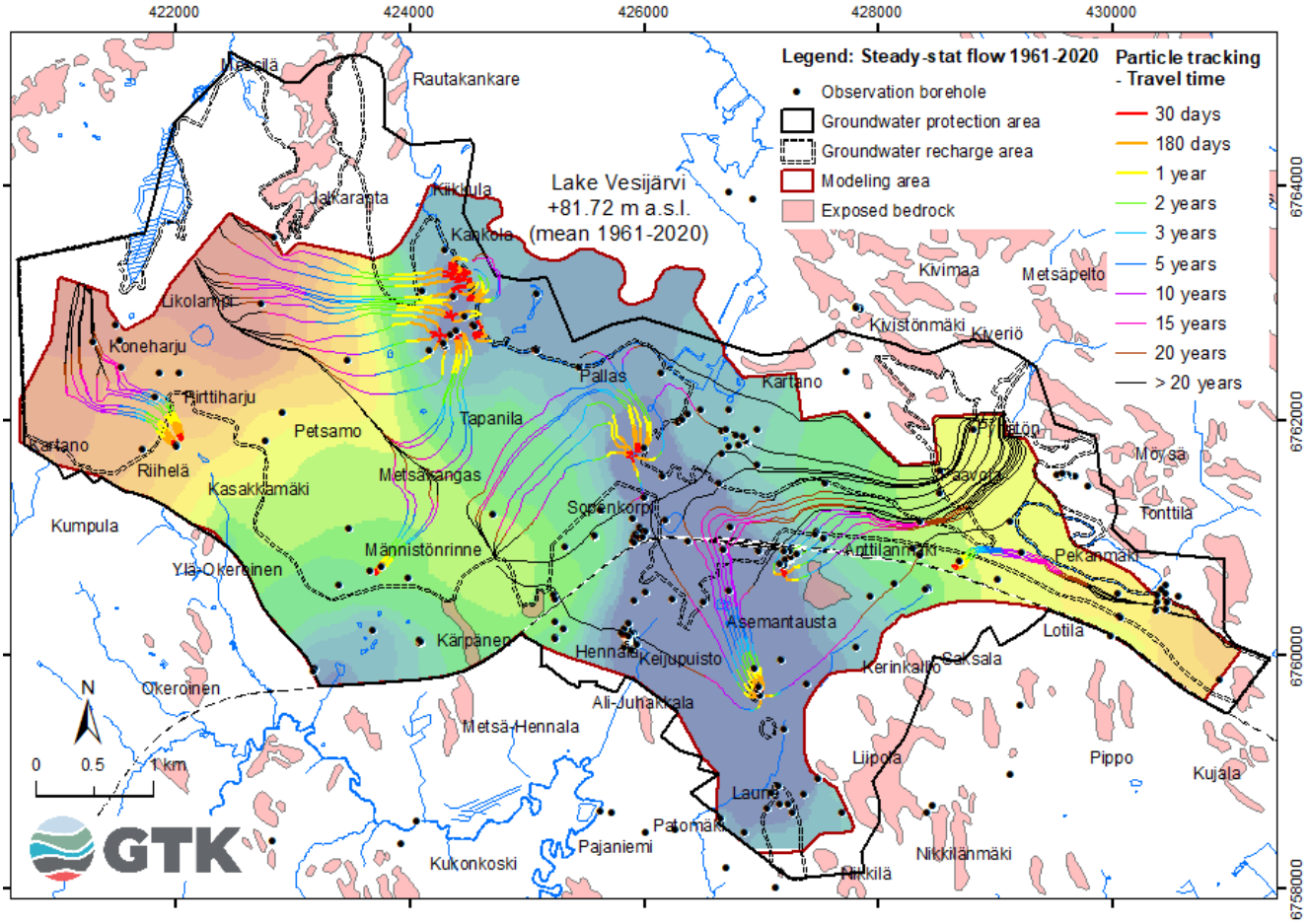

Fig. 38 Flow paths and travel times to the water intake wells based on the steady-state flow 1961-2020.

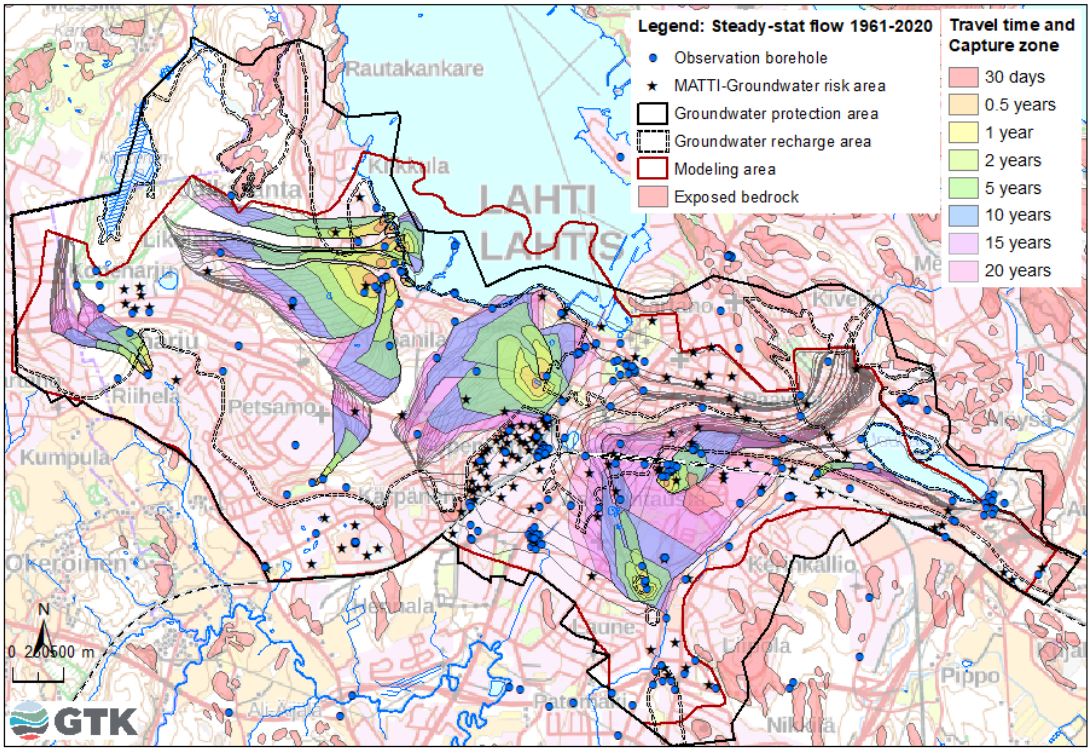

Fig. 39 Capture zones around the water intake wells based on the steady-state flow 1961-2020.

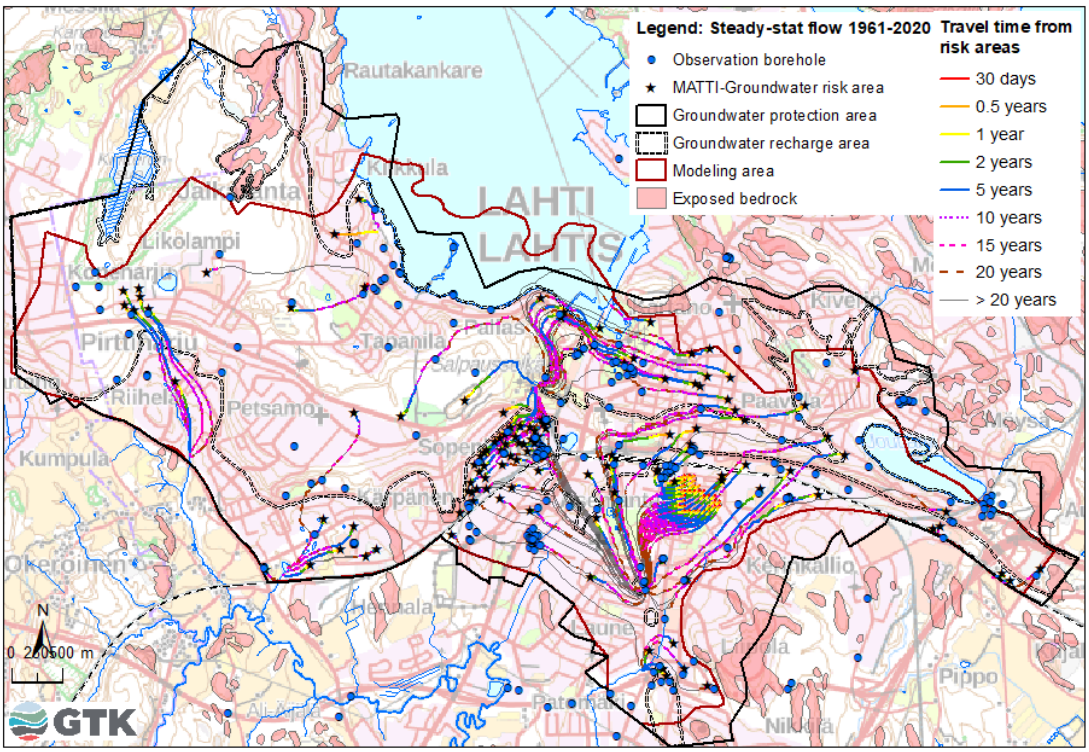

Fig. 40 Travel times from groundwater risk areas based on the steady-state flow 1961-2020.

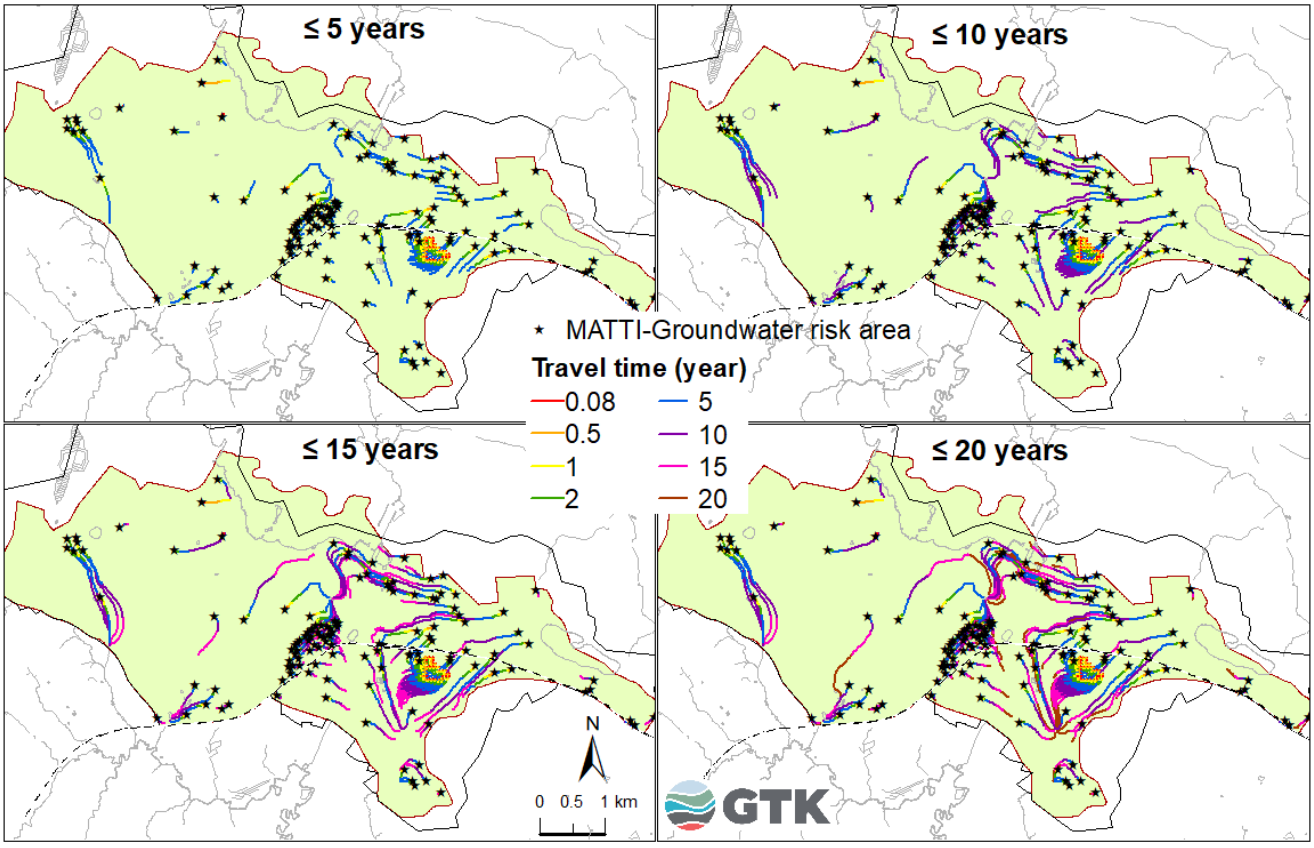

Fig. 41 Particle tracking and travel times from the groundwater risk areas based on the steady-state flow 1961-2020.

7 CONCLUSIONS AND RECOMMENDATIONS

This study investigated the impacts of climate change on groundwater resources in the shallow groundwater area in the city of Lahti, southern Finland by using the groundwater flow model as an evaluation tool. The flow model was developed by using the unsaturated zone flow (UZF) coupled with the saturated zone flow MODFLOW-NWT, to simulate the flow from the ground surface through unsaturated zone to the aquifer. Lake infiltration and surface water - groundwater interactions were simulated by using the RIVER package, where the infiltration rate depends on the lakebed conductance and the head differences between lake stage and groundwater level. The snowmelt model was used to calculate the snowmelt and rainfall, which then was integrated to the infiltration factors to provide the initial infiltration water for the UZF model. The infiltration factors include land use, runoff, soil type and vegetation. 51% of the study area belongs to the urban area with high impervious surface, e.g., asphalt and concrete (up to 89% of impervious). The impervious surface prevents infiltration to the soil zone, induces more runoff, especially in the high slope area, and consequently, reduces recharge.

The flow models were performed in 3 phases: first, the steady-state model of the mean climate data during 1961-2020 to provide the initial head for the transient flow model was made. Second, the daily time step transient flow model of climate data during 2000-2005 was made to evaluate the seasonal

variability of groundwater by calibrating with the measured groundwater level during 2002-2004. Then, the calibrated model was used to simulate the potential impacts of climate scenario data. Temperature and precipitation data from the high-emissions scenario RCP 8.5 from the SMHI for the period 2021-2100 were used for the simulation. The scenario data was performed for the bias correction and calibration with the historic data by using the Delta-change approach. To evaluate the impacts of climate change, the monthly mean 30-year of the simulation results during the periods 2021-2050 and 2071-2100 were compared with the current condition during the period 1981-2010.

The aquifer in the Lake Vesijärvi area is covered by thick fine-grained layer that has a very poor hydraulic conductivity. The lake infiltration mainly occurs in the lake shoreline where the fine-grained layer is thin or absent. The main infiltration rate occurs around the water intake well in the Jalkaranta area. The sensitivity analysis of the steady-state simulation shows that with non-pumping condition, the mean groundwater level rise to 1-4 m compared with pumping condition. In the rise of water level, groundwater discharge into the lake and streams and no lake infiltration is observed in the water intake well area. The particle tracking and capture zones, that performed in the steady-state flow with pumping condition, indicated the different groundwater capture zones within the model domain. The most distinct sub-zones and groundwater divides are in the western side of the model domain in the Riihelä, Käipänen and Jalkaranta water intake well areas. While the capture zones in the central of the model domain showed contributions of water from various directions, including from the Lake Vesijärvi following the bedrock depression/esker area in the north-south direction, and from the first Salpausselkä formation in the east. The particle tracking from the bedrock exposed in the south-eastern of the Paasivaara (Felix Abba Oy Ab) water intake well, showed groundwater flows toward the south-western direction to the Laune water intake well. In the southern of the study area, the aquifer is covered by the fine-grained layer, which prevent the infiltration but also protect the groundwater from the contamination on the ground surface. Groundwater flows beneath this fine-grained layer and discharge in the low-lying areas, e.g., stream or creek. However, the bedrock exposed area could act as a conduit and preferential pathway for the recharge and the contaminations from the ground surface into the aquifer.

The results of transient flow show that at current condition (1981-2010), the annual mean infiltration is 287.9 mm (42% of snowmelt and rainfall), the annual mean recharge is 188.9 mm (27.7 % of snowmelt and rainfall), the annual mean runoff is 312 mm (45.7% of snowmelt and rainfall), and the annual mean lake infiltration is 177.5 mm. Impervious surface in the urban area cause the reduction of the infiltration from the snowmelt and rainfall and promote more the surface runoff. Moreover, thick unsaturated zone causes a longer lag time between the infiltration from the soil zone and the groundwater table and a reduction of the recharge. At current condition, snowmelt reached the highest value in April, while the highest mean recharge is presented in August.

Under the scenario data, the annual mean temperature is predicted to increase 1.6 and 4.2 ^{o}C during 2021-2050 and 2071-2100, respectively, compare with the current condition. The highest increase in mean temperature is 6.1 ^{o}C in winter during 2071-2100. The annual mean precipitation is predicted to increase 10.4% and 30.9% during 2021-2050 and 2071-2100, respectively. While the annual mean snowmelt and rainfall is predicted to increase 26.4% and 60.8% during 2021-2050 and 2071-2100, respectively, compare with the current condition. The highest increase in the snowmelt is found in winter during 2071-2100 due to the highest increase in temperature in this period.

Annual mean infiltration of the scenario data increase 12.8% and 33.7% for the periods 2021-2050 and 2071-2100, respectively, compared with the current condition. The significant changes in infiltration patterns occur in winter and spring in both periods, where snowmelt and infiltration take place earlier in winter. The high infiltration during spring (April) in current condition does not exist in the scenario data. Annual mean recharge of the scenario data increase 10.8% and 30.1% for the periods 2021-2050 and 2071-2100, respectively. The recharge patterns show less seasonal variability over the scenario data. On the opposite, the annual mean lake infiltrations show slightly decreases 4.4% and 12.4% for the periods 2021-2050 and 2071-2100, respectively, compared with the current condition. With the recharge increase, groundwater level also increases and reduce the lake infiltration rate. Annual mean runoff shows the similar pattern as the snowmelt and rainfall. At current condition, the highest runoff occurs in spring (April) after the snow melted and the lowest runoff is in winter, where the ground is frozen. Annual mean runoff of the scenario data increase 67.4% and 153.5% for the periods 2021-2050 and 2071-2100, respectively. The most tremendous increase in runoff is found in winter during 2071-2100. The infiltration capacity of the aquifer is limited by the impervious surface in the urban area. With the increase in the snowmelt and rainfall in the scenario data, the large part of the excess water will contribute to the runoff. This could induce more the potential stormwater flood risk from the snowmelt.

At current condition (1981-2010), the inflow and outflow rates in the model domain vary between 32 860 – 37 460 m^3/d with the mean value of 34 357 m^3/d. The annual mean flow rates are predicted to increase 2.4% and 7.4% during 2021-2050 and 2071-2100, respectively. The recharge flux rates vary between 11 190 - 17 080 m^3/d with the mean value of 13 212 m^3/d. The lake infiltration flux rates, which mainly occur in the lakeshore nearby the water intake wells, vary between 12 300 – 12 620 m^3/d with the mean value of 12 432 m^3/d. The mean recharge increases 9.9% and 28.4%, while the mean lake infiltration decreases 4.4% and 12.4% during 2021-2050 and 2071-2100, respectively. The main outflow consists of pumping rate and stream discharge. The mean discharge rate at current condition is 2 330 – 2 380 m^3/d with the mean value of 2 352 m^3/d. The discharge rate is predicted to increase 10 and 27% from present during 2021-2050 and 2071-2100, respectively. The main total inflow is obtained from the recharge and the lake infiltration. At current and over the scenario conditions, the simulation results show that the recharge alone (up to 19 000 m^3/d) does not sufficient to meet with the pumping rate of 24 410 m^3/d. The infiltration and recharge areas should be preserved and incorporated into the future land use planning.

The simulations were run and calibrated successfully with the current input parameters. However, additional data from site investigations and monitoring are needed for the enhancement of the modeling. These data include:

- Long term daily groundwater level monitoring of the observation boreholes for the minimum of 2-3 years (based on the simulated lag time data). Daily groundwater abstraction and stream discharge data of the same period are also needed. These data can be calibrated with the daily climate data from FMI and the daily lake level from SYKE.

- Soil-water content monitoring in the soil zone, especially in the main recharge area, to provide information of the unsaturated zone flow such as the vertical hydraulic conductivity of the unsaturated zone.

- Detailed hydrogeological distributions of the aquifer materials and the roles of perched groundwater and fractured bedrock in the groundwater area.
- Validation of flow simulation and flow path by using the solute transport of the tracers, e.g., chloride, isotope, and geochemistry of groundwater.
- The impacts of evaporation and evapotranspiration on the lake water level, and groundwater and lake water interactions.

Acknowledgements

This work resulted from the RAINMAN project (Towards higher adaptive capacity in urban water management) is implemented with the support of the South-East Finland – Russia CBC 2014-2020 programme funded by the European Union and the Republic of Finland. Additional funding was received from the Hydrogeology and the Global Change (HYGLO) development program (WP1: 5040002321) of the Geological Survey of Finland (GTK). The authors thank Lahti City for providing background reports and data from the previous studies in this area.

References

American Society of Civil Engineers. 1970. Design and construction of sanitary and storm sewers. Manuals and Reports of Engineering Practice No. 37. American Society of Civil Engineers, New York.

Anderson, M.P., Woessner, W.W., & Hunt, R.J. 2015. Applied Groundwater Modeling (Second Edition), Academic Press, 2015, ISBN 9780120581030. https://doi.org/10.1016/B978-0-08-091638-5.00019-5

Cisneros, J.B.E., Oki, T., Arnell, N.W., Benito, G., Cogley, J.G., Döll, P., Jiang, T. & Mwakalila, S.S. 2014. Freshwater resources. *In*: Climate Change 2014: Impacts, Adaptation, and Vulnerability. Part A: Global and Sectoral Aspects. Contribution of Working Group II to the Fifth Assessment Report of the Intergovernmental Panel on Climate Change [Field, C.B., Barros, V.R., Dokken, D.J., Mach, K.J., Mastrandrea, M.D., Bilir, T.E., Chatterjee, M., Ebi, K.L., Estrada, Y.O., Genova, R.C., Girma, B., Kissel, E.S., Levy, A.N., MacCracken, S., Mastrandrea, P.R. & White, L.L. (eds.)]. Cambridge University Press, Cambridge, United Kingdom and New York, NY, USA, pp. 229-269. https://www.ipcc.ch/site/assets/uploads/2018/02/WGIIAR5-Chap3_FINAL.pdf

Doherty, J. 2010. PEST—Model-independent parameter estimation user manual (5th ed.), and addendum: Brisbane, Queensland, Australia, Watermark Numerical Computing.

Erickson, A.J., Weiss, P.T., & Gulliver, J.S. 2013. Optimizing Stormwater Treatment Practices - A Handbook of Assessment and Maintenance. https://link.springer.com/book/10.1007/978-1-4614-4624-8

Fyfe, G.J. 1990. The effect of water depth on ice-proximal glaciolacustrine sedimentation: Salpausselka I, southern Finland. Boreas 19:147–164. https://doi.org/10.1111/j.1502-3885.1990.tb00576.x

FMI. 2021. Finnish Meteorological Institute - Download observations. https://en.ilmatieteenlaitos.fi/download-observations#!/

Freeze, R.A. & Cherry, J.A. 1979. Groundwater: Upper Saddle River, N.J., Prentice-Hall Inc., 604 p.

Gilbert, R.O. 1987. Statistical methods for environmental pollution monitoring. Van Nostrand Reinhold, New York.

GTK-Lahde database, 2022. Lahde - geological and groundwater database. Geological Survey of Finland. https://lahde.gtk.fi.

GTK - Pohjatutkimus database 2022: http://gtkdata.gtk.fi/Pohjatutkimukset/index.html

Hämäläinen, J. 2018. Vesijärven sedimenttitutkimukset kaikuluotaamalla (Shallow reflection seismic survey for the study of sediments in the Lake Vesijärvi). Geological Survey of Finland, Espoo.

Hamon, R.W. 1963. Computational of Direct Runoff Amounts from Storm Rainfall, vol. 63. International Association of Scientific Hydrology Publication, Wallinford, Oxon., UK. 52–62.

Harbaugh, A.W., Langevin, C.D., Hughes, J.D., Niswonger, R.N., & Konikow, L. F. 2017. MODFLOW-2005 version 1.12.00, the U.S. Geological Survey modular groundwater model: U.S. Geological Survey Software Release, 03 February 2017, http://dx.doi.org/10.5066/F7RF5S7G

Hendriksson, N., 2012. Isotooppitutkimus Lahden pohjavedenottoalueilla (Stable isotopes of groundwater from the water intake wells areas in Lahti). Investigation report for the Lahti Aqua Oy 27.6.2012. Unpublished report.

Insinööritoimisto Paavo Ristola Oy., 2004. Lahden ja Hollolan pohjavedenvirtausmalli raportti 16459 (Groundwater flow model of the Lahti and Hollola areas). Unpublished report.

Jarva, J. (ed.), Klein, J. (ed.), Akentyeva, E., Eskelinen, A., Fasolko, D., Gvozdev, V., Ignatchik, V., Kautto, N., Kesäniemi, O., Kostenko, I., Mamaeva, M., Parry, M., Pasonen, H., Rautio, J. & Zadonskaya, O. 2022. The RAINMAN project. General recommendations on adapting water management practices to climate change impacts in eastern and southern Finland and St. Petersburg. Geological Survey of Finland, Open File Research Report 6/2022.

Jokinen, P., Pirinen, P., Kaukoranta, J.P., Kangas, A., Alenius, P., Eriksson, P., Johansson, M., & Wilkman, S. 2021. Climatological and oceanographic statistics of Finland 1991–2020. Finnish Meteorological Institute. http://hdl.handle.net/10138/336063

Jyrkama, I.M. & Sykes, J.F. 2007. The impact of climate change on spatially varying groundwater recharge in the Grand River watershed (Ontario). J. Hydrol. 338, 237–250.

Klein, J. & Luoma, S. 2020. Regional Climate Change Scenarios for the Water Management in Lahti and Mikkeli. GTK Open File Work Report. https://tupa.gtk.fi/raportti/arkisto/61_2019.pdf

Kokkonen, T., Jakeman, A.J., Koivusalo, H. & Norton, J.P. 2006. Computational Methods for Water Resources Assessments: An Exercise Kit. Available from: https://www.iemss.org/wp-content/uploads/CMWRA_Text.pdf

Kottek, M., Grieser, J., Beck, C., Rudolf, B. & Rubel, F. 2006. World Map of the Köppen-Geiger climate classification updated. Meteorologische Zeitschrift, Vol. 15, No. 3, 259-263. doi: 10.1127/0941-2948/2006/0130 https://opus.bibliothek.uni-augsburg.de/opus4/frontdoor/deliver/index/docId/40083/file/metz_Vol_15_No_3_p259-263_World_Map_of_the_Koppen_Geiger_climate_classification_updated_55034.pdf

Kuusisto, E., 1984. Snow Accumulation and Snow Melt in Finland. Publications of the Water Research, Institute, vol. 55, Helsinki, Finland, National Board of Waters.

City of Lahti. 2022. The city of Lahti. https://www.lahti.fi/en/

Luoma, S. & Ikonen, J. 2020. Vulnerability assessment of the shallow groundwater in Finland. GTK Open File Work Report: Contribution to the HOVER - WP7, Deliverable D.7-2 report. https://tupa.gtk.fi/raportti/arkisto/35_2020.pdf

Luoma, S. & Okkonen, J. 2014. Impacts of Future Climate Change and Baltic Sea Level Rise on Groundwater Recharge, Groundwater Levels, and Surface Leakage in the Hanko Aquifer in Southern Finland. Water, 6(12), 3671-3700, https://doi.org/10.3390/w6123671

Mäkinen, R., Orvomaa, M., Veijalainen, N., & Huttunen, I. 2016. The climate change and groundwater regimes in Finland. *In*: Watershed and River Basin Management. Fehér, J. (ed.). Trivent Publishing, Budapest. 111-120.
https://oszkdk.oszk.hu/storage/00/02/59/05/dd/1/2__Watershed_and_River_Basin_Management.pdf#page=116

Male, D.H. & Gray, D.M. 1981. Snow cover ablation and runoff. In: Gray, D.M., Male, D.H. (Eds.), Handbook of Snow Principles, Processes, Management and Use. Pergamon Press, Toronto. 360–436.

Nash, J.E. & Sutcliffe, J.V. 1970. River Flow Forecasting through Conceptual Model. Part 1 - A Discussion of Principles. Journal of Hydrology, 10, 282-290.

http://dx.doi.org/10.1016/0022-1694(70)90255-6

Niswonger, R.G., Prudic, D.E. & Regan, R.S. 2006. Documentation of the Unsaturated-Zone Flow (UZF1) Package for modeling unsaturated flow between the land surface and the water table with MODFLOW-2005: U.S. Geological Survey Techniques and Methods 6-A19, 62 p.

Niswonger, R.G., Panday, S. & Ibaraki, M. 2011. MODFLOW–NWT, A Newton formulation for MODFLOW–2005: U.S. Geological Survey Techniques and Methods 6–A37, 44 p. https://pubs.usgs.gov/tm/tm6a37/

NSL. 2021. National Land Survey of Finland (NLS) - Based map and LiDAR-DEM data. https://www.maanmittauslaitos.fi/en

Nuottimäki, K. & Jarva, J. 2015. A qualitative approach for identifying areas prone to urban floods with the support of LiDAR, GFF, 137:4, 373-382, DOI: 10.1080/11035897.2015.1055512

Okkonen, J. & Kløve, B. 2010. A conceptual and statistical approach for the analysis of climate impact on ground water table fluctuation patterns in cold conditions. Journal of Hydrology. 388 (1-2), 1-12.

Pirinen, P., Simola, H., Aalto, J., Kaukoranta, J-P., Karlsson, P., & Ruuhela, R. 2010. Climatological statistics of Finland 1981–2010. Finnish Meteorological Institute, Helsinki, Finland. https://helda.helsinki.fi/handle/10138/35880

Pollock, D.W. 1994. User's guide for MODPATH/MODPATH-PLOT, Version3—A particle tracking post-processing package for MODFLOW, the U.S. Geological Survey finite-difference ground-water flow model: U.S. Geological Survey Open-File Report 94–464, 249 p.

Hunt, R.J., Prudic, D.E., Walker, J.F. & Anderson, M.P. 2008. Importance of Unsaturated Zone Flow for Simulating Recharge in a Humid Climate. Vol. 46, No. 4—GROUND WATER—July–August 2008. 551–560.

Saarnisto, M., & Saarinen, T. 2001. Deglaciation chronology of the Scandinavian Ice Sheet from the Lake Onega Basin to the Salpausselkä End Moraines. Glob Planet Chang 31:387–405. https://doi.org/10.1016/S0921-8181(01)00131-X

Salmi, T., Määtä, A., Anttila, P. Ruoho-Airola, T. & Amnell, T. 2002. Detecting Trends of Annual Values of Atmospheric Pollutants by the Mann-Kendall Test and Sen's Slope Estimates the Excel Template Application MAKESENS. Finnish Meteorological Institute. https://en.ilmatieteenlaitos.fi/makesens

Sauramo, M. 1923. Studies on the Quaternary varve sediments in southern Finland. Comm Géol Fin Bull 60:1–164.

SMHI. 2017. CORDEX EUR-11 SMHI RCA4. World Data Center for Climate (WDCC) at DKRZ. http://cera-www.dkrz.de/WDCC/ui/Compact.jsp?acronym=CXEU11SMRCA4

Statistic of Finland, 2022. Statistic of Finland – Population: https://www.stat.fi/til/vrm_en.html

Suomi, J. 2018. Extreme temperature differences in the city of Lahti, southern Finland: Intensity, seasonality and environmental drivers. Weather and Climate Extremes 19, 20–28. https://doi.org/10.1016/j.wace.2017.12.001

Suomi, J & Käyhkö, J. 2012. The impact of environmental factors on urban temperature variability in the coastal city of Turku, SW Finland. International Journal of Climatology 32: 451–463. DOI:10.1002/joc.2277

SYKE. 2020. Finnish Environment Institute - POVET-database for groundwater levels and monitoring: http://www.syke.fi/fi-FI/Avoin_tieto/Ymparistotietojarjestelmat

SYKE. 2021. Finnish Environment Institute - Hydrological database. https://www.vesi.fi/

SYKE 2022. Finnish Environment Institute - Groundwater in Finland. https://www.ymparisto.fi/en-US/Waters/Protection_of_waters/Groundwater_protection/Groundwater_in_Finland

Valjus, T. 2019. Kallionpinnan tason määritys painovoimamittauksia käyttäen Lahden pohjavesialueella No. 0439801 (Gravimetric survey for the determination of the bedrock surface in the Lahti groundwater area). Geological Survey of Finland, Espoo.

Valtanen, M. 2015. Effects of urbanization on seasonal runoff generation and pollutant transport under cold climate. Thesis. Department of Environmental Sciences Faculty of Biological and Environmental Sciences, University of Helsinki. https://helda.helsinki.fi/handle/10138/153832

Vehviläinen, B. 1992. Snow Cover Models in Operational Watershed Forecasting. Publications of the Water Research, Institute, vol. 11, National Board of Waters, 149 pp.

Virtasalo, J.J., Kotilainen, A.T., Räsänen, M.E., & Ojala, A.E.K. 2007. Late-glacial and post-glacial deposition in a large, low relief, epicontinental basin: the northern Baltic Sea. Sedimentology 54:1323–1344. https://doi.org/10.1111/j.1365-3091.2007.00883.x

Virtasalo, J.J., Hämäläinen, J., Kotilainen, A.T. 2014. Toward a standard stratigraphical classification practice for the Baltic Sea sediments: the CUAL approach. Boreas 43:924–938. https://doi.org/10.1111/bor.12076

WDCC. 2017. World Data Center for Climate. https://cera-www.dkrz.de/WDCC/ui/cerasearch/

Appendix 1 Residuals-heads differences between measured heads and simulated heads (Sim.) for steady-state flow with pumping and non-pumping conditions. Locations of the observation boreholes are presented in Fig. 20.

Observation borehole	X	Y	Measured head (m a.s.l.)	Pumping condition		Non-pumping	
				Sim. Head (m a.s.l.)	Residual (m)	Sim. head (m a.s.l.)	Residual (m)
117	423473.00	6762517.00	106.78	106.64	0.14	108.96	-2.18
314	424304.00	6763451.00	79.81	80.14	-0.33	83.02	-3.21
320	424384.00	6763058.00	78.81	78.25	0.56	83.89	-5.08
306	424481.00	6762892.00	78.81	78.83	-0.02	83.55	-4.74
5	424546.00	6762822.00	78.82	78.76	0.06	83.23	-4.41
6	424399.00	6762765.00	78.81	77.94	0.87	84.57	-5.76
102	424294.00	6762663.00	78.57	78.83	-0.26	85.76	-7.19
315	424311.00	6762636.00	78.95	79.17	-0.22	85.71	-6.76
116	425081.00	6762599.00	79.32	79.70	-0.38	83.87	-4.55
20	425087.00	6763077.00	79.60	79.69	-0.09	83.87	-4.27
125	426148.00	6762402.00	80.11	79.91	0.20	83.86	-3.75
23	426493.00	6762092.00	81.77	81.90	-0.13	84.49	-2.72
128	426297.00	6761983.00	80.84	81.01	-0.17	84.48	-3.64
353	426674.00	6761911.00	83.57	83.58	-0.01	85.51	-1.94
21	426712.00	6761925.00	83.98	84.00	-0.02	85.67	-1.69
354	426667.00	6761723.00	83.79	84.03	-0.24	86.17	-2.38
22	426972.00	6761628.00	87.30	87.10	0.20	88.29	-0.99
126	427555.00	6761463.00	91.96	91.88	0.08	93.09	-1.13
352	426002.00	6761766.00	77.48	77.56	-0.08	83.35	-5.87
123	426161.00	6761521.00	77.48	77.63	-0.15	82.94	-5.46
127	426012.00	6761345.00	77.50	77.61	-0.11	82.80	-5.30
356	426646.00	6761465.00	78.62	78.81	-0.19	82.98	-4.36
372	426184.00	6761150.00	78.09	77.60	0.49	82.31	-4.22
360	426742.00	6761092.00	78.42	78.55	-0.13	82.54	-4.12
136	426520.00	6760458.00	77.39	76.92	0.47	80.27	-2.88
378	426950.00	6759883.00	76.11	75.91	0.20	78.33	-2.22
31	427000.00	6759653.00	76.19	75.39	0.80	77.87	-1.68
134	427024.78	6759375.71	76.27	75.55	0.72	77.43	-1.16
156	421303.00	6762676.00	119.04	119.20	-0.16	121.14	-2.10
157	421537.00	6762681.00	118.19	117.47	0.72	119.50	-1.31
155	421547.00	6762451.00	116.10	116.00	0.10	118.08	-1.98
158	421864.00	6762404.00	113.89	114.33	-0.44	116.50	-2.61
159	421834.00	6762208.00	114.04	114.16	-0.12	116.33	-2.29
165	423403.00	6760594.00	92.61	92.53	0.08	93.57	-0.96
120	429135.00	6761138.00	100.73	100.67	0.06	101.22	-0.49
129	428533.00	6761379.00	98.74	98.78	-0.04	99.49	-0.75

Appendix 1 (Cont') Residuals-heads differences between measured heads and simulated heads (Sim.) for steady-state flow with pumping and non-pumping conditions. Locations of the observation boreholes are presented in Fig. 20.

Observation borehole	X	Y	Measured head (m a.s.l.)	Pumping condition		Non-pumping	
				Sim. Head (m a.s.l.)	Residual (m)	Sim. head (m a.s.l.)	Residual (m)
hp1	424360.00	6762733.00	78.84	78.09	0.75	85.02	-6.18
130	425871.00	6760225.00	77.35	77.59	-0.24	80.69	-3.34
135	425923.00	6760470.00	77.72	77.96	-0.24	81.42	-3.70
TL2/03	424712.80	6761197.70	96.10	96.15	-0.05	98.42	-2.32
HP1/12	427161.38	6758880.43	76.69	76.69	0.00	77.42	-0.73
HP7_Felix	427204.41	6760765.75	78.20	78.46	-0.26	82.97	-4.77
TL1/05	425810.64	6762059.99	79.53	78.94	0.59	83.86	-4.33
HP3B	425589.00	6761012.01	91.33	91.47	-0.14	94.33	-3.00
hp5/15	425295.20	6761821.10	89.10	89.08	0.02	92.39	-3.29
hp4/15	424904.60	6761948.00	90.76	91.21	-0.45	94.25	-3.49
hp2/15	424431.50	6762073.30	89.36	89.26	0.10	92.71	-3.35
hp1/15	424523.30	6762497.80	80.31	80.38	-0.07	85.15	-4.84
hp3/15	425088.50	6762310.10	84.32	84.32	0.00	88.16	-3.84
TL1/03	423491.00	6761082.00	96.00	95.94	0.06	97.30	-1.30
TL3/03	422771.10	6761822.10	102.51	102.39	0.12	103.73	-1.22
Hp2	430846.79	6759831.91	109.00	109.10	-0.10	109.13	-0.13
				n	36.0		36.0
				ME	0.05		-3.19
				MAE	2.20		0.24
				RMS	0.33		3.63

.

Appendix 2 Water budget components within the model domain (area of 25.556 km^2) and percentage change in the scenarios data compared with the current condition. Negative values represent decreasing:

Table A2.1 Total inflow flux rate and change in the inflow.

Month	Total inflow = Total outflow (m^3/d)			% Change	
	1981-2010	2021-2050	2071-2100	2021-2050	2071-2100
1	33211	34655	37407	4.4	12.6
2	32860	34420	36845	4.7	12.1
3	33193	34489	36409	3.9	9.7
4	34056	33859	35387	-0.6	3.9
5	34505	33686	35590	-2.4	3.1
6	33337	34561	36313	3.7	8.9
7	34892	35535	36431	1.8	4.4
8	37460	36093	36793	-3.7	-1.8
9	35180	36311	37572	3.2	6.8
10	34554	36080	38077	4.4	10.2
11	35326	36282	37962	2.7	7.5
12	33712	36147	38022	7.2	12.8
Mean	34357	35177	36901	2.5	7.5

Table A2.2 Recharge flux rate and change in recharge flux.

Month	Recharge (m^3/d)			% Change	
	1981-2010	2021-2050	2071-2100	2021-2050	2071-2100
1	11707	13849	17671	18.3	50.9
2	11190	13649	17097	22.0	52.8
3	11437	13663	16435	19.5	43.7
4	12769	12858	15092	0.7	18.2
5	13276	12525	15321	-5.7	15.4
6	11765	13541	15990	15.1	35.9
7	13861	14939	16302	7.8	17.6
8	17080	15582	16682	-8.8	-2.3
9	14561	16002	17641	9.9	21.2
10	13842	15801	18394	14.2	32.9
11	14675	16101	18441	9.7	25.7
12	12382	15725	18441	27.0	48.9
Mean	13212	14519	16959	10.8	30.1

Table A2.3 Lake infiltration and change in lake infiltration.

Month	Lake infiltration (m^3/d)			% Change	
	1981-2010	2021-2050	2071-2100	2021-2050	2071-2100
1	12490	11857	10817	-5.1	-13.4
2	12576	11939	10862	-5.1	-13.6
3	12620	11995	10925	-5.0	-13.4
4	12553	11990	10993	-4.5	-12.4
5	12388	11992	11040	-3.2	-10.9
6	12402	11985	11024	-3.4	-11.1
7	12402	11918	10953	-3.9	-11.7
8	12333	11831	10886	-4.1	-11.7
9	12300	11760	10834	-4.4	-11.9
10	12325	11769	10802	-4.5	-12.4
11	12364	11787	10779	-4.7	-12.8
12	12432	11810	10767	-5.0	-13.4
Mean	12432	11886	10890	-4.4	-12.4

Table A2.4 Stream discharge (Drain) and change in stream discharge.

Month	Stream discharge (m^3/d)			% Change	
	1981-2010	2021-2050	2071-2100	2021-2050	2071-2100
1	2346	2582	2977	10.1	26.9
2	2338	2576	2970	10.2	27.0
3	2340	2579	2966	10.2	26.8
4	2373	2583	2958	8.9	24.7
5	2364	2582	2962	9.2	25.3
6	2361	2588	2975	9.6	26.0
7	2364	2596	2986	9.8	26.3
8	2363	2604	2994	10.2	26.7
9	2352	2596	2996	10.4	27.4
10	2343	2589	2991	10.5	27.6
11	2337	2588	2996	10.7	28.2
12	2329	2573	2982	10.5	28.1
Mean	2351	2586	2980	10.0	26.7

Appendix 3 Travel times and capture zones in the different water intake areas.

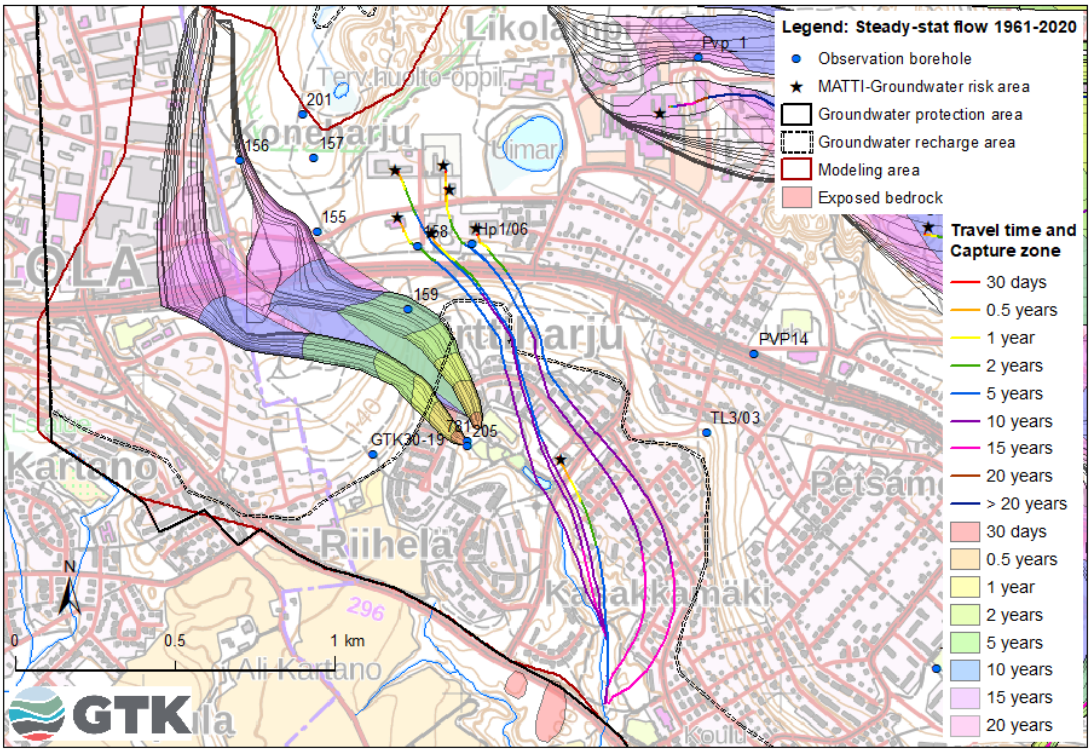

Fig. A3.1 Travel times and capture zones in Riihelä area.

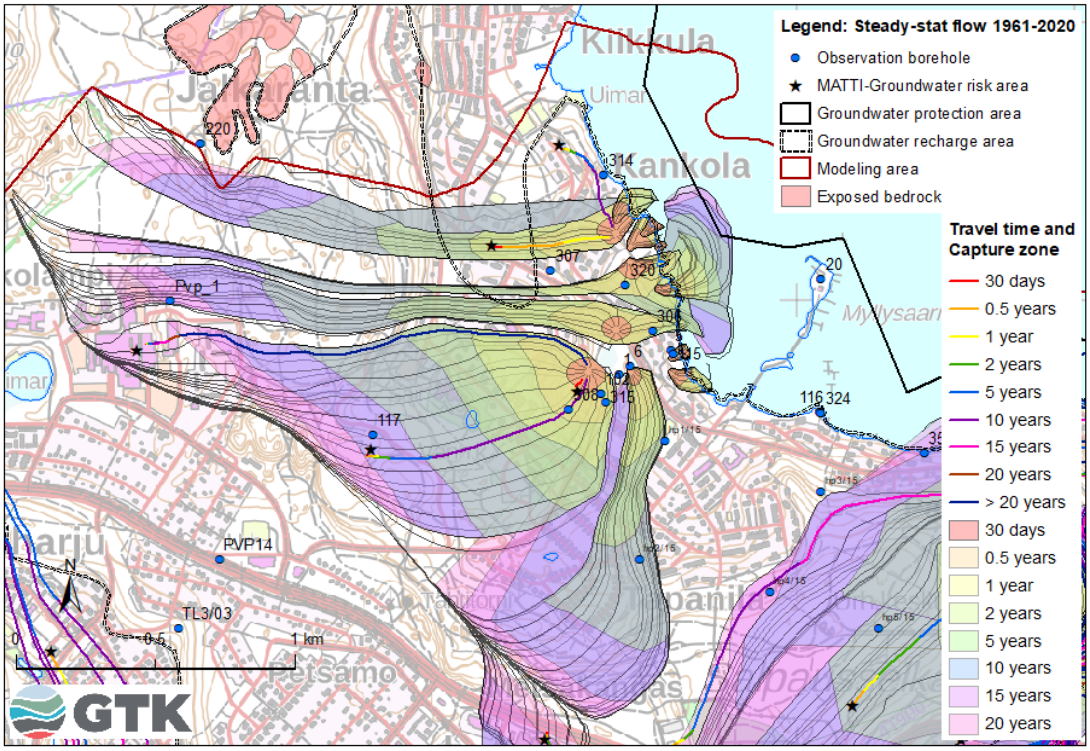

Fig. A3.2 Travel times and capture zones in Jalkaranta area.

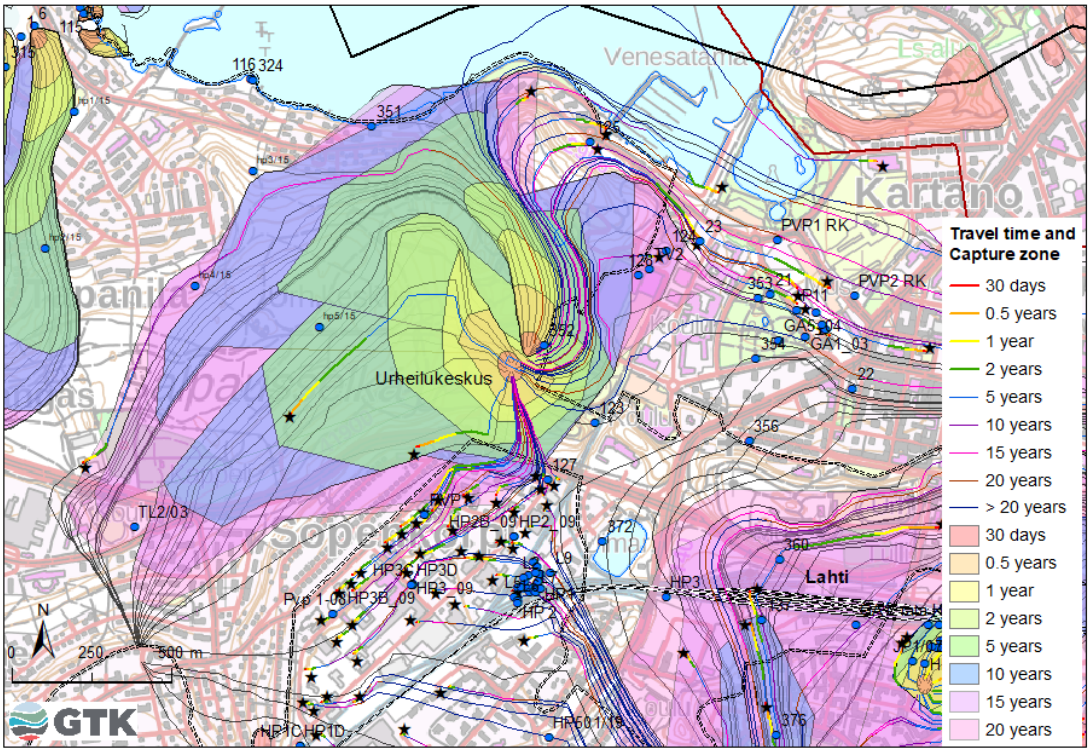

Fig. A3.3 Travel times and capture zones in Urheilukeskus area.

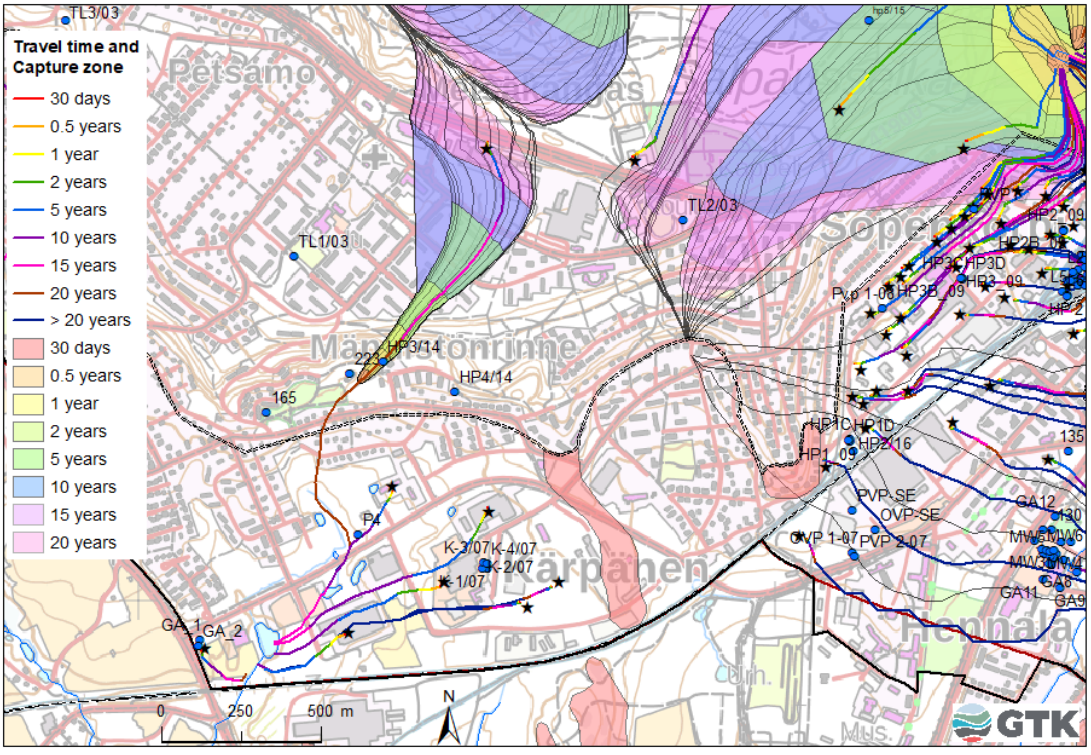

Fig. A3.4 Travel times and capture zones in Kärpänen area.

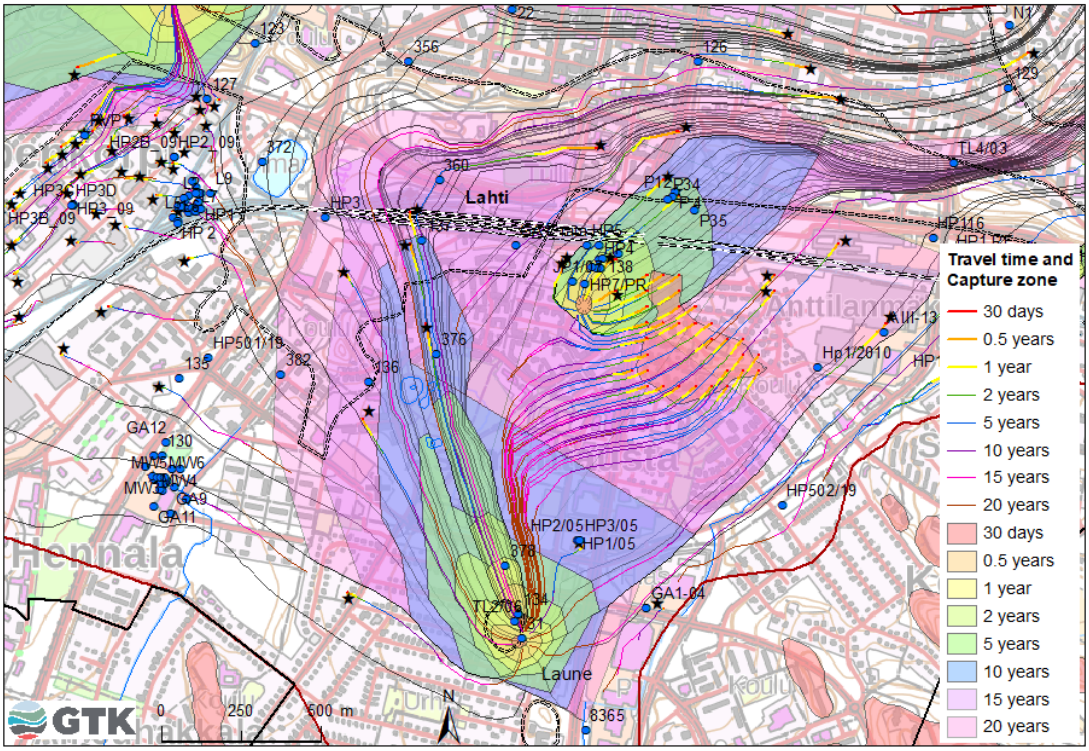

Fig. A3.5 Travel times and capture zones in Laune, Paasivaara, and railway station areas.

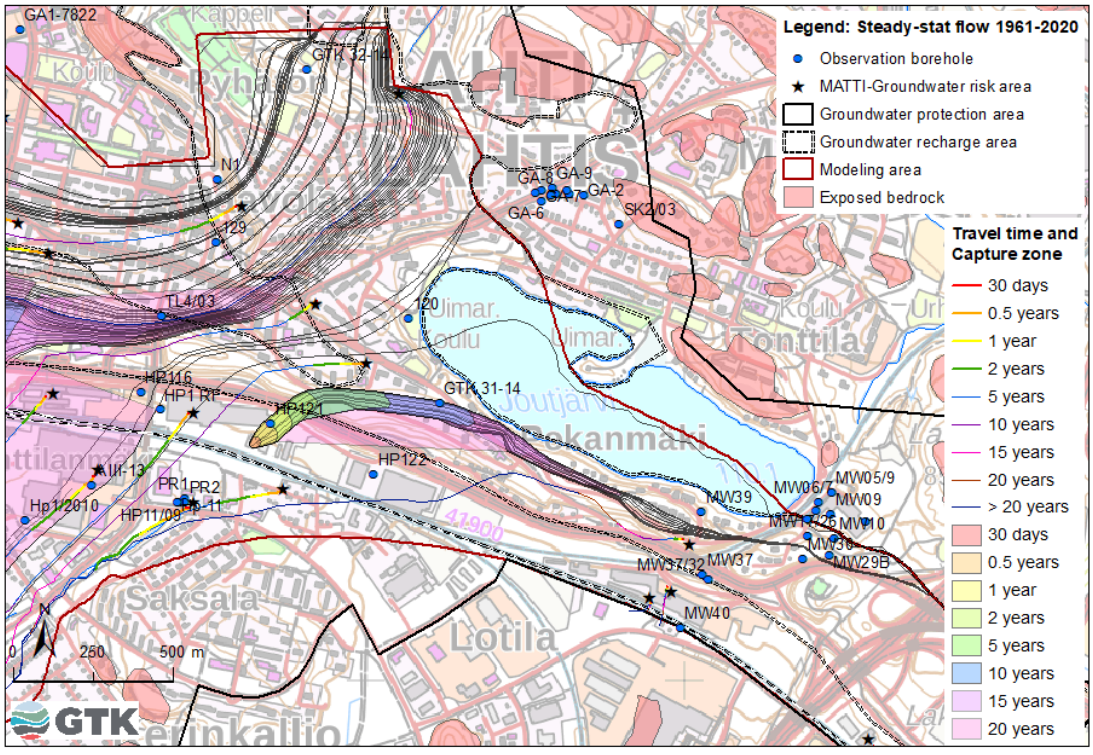

Fig. A3.6 Travel times and capture zones in Joutjärvi areas.